

FAST BLOOD VESSEL SEGMENTATION FOR SURGICAL AND INTERVENTIONAL PLANNING AND NAVIGATION

Rahul Prasanna Kumar

September 26, 2014

Department of Informatics
Faculty of Mathematics and Natural Science
University of Oslo
Oslo, Norway

The Intervention Centre
Oslo University Hospital, Rikshospitalet
Faculty of Medicine
University of Oslo
Oslo, Norway

A thesis submitted for the degree of Doctor of Philosophy

© **Rahul Prasanna Kumar, 2014**

*Series of dissertations submitted to the
Faculty of Mathematics and Natural Sciences, University of Oslo
No. 1574*

ISSN 1501-7710

All rights reserved. No part of this publication may be
reproduced or transmitted, in any form or by any means, without permission.

Cover: Hanne Baadsgaard Utigard.
Printed in Norway: AIT Oslo AS.

Produced in co-operation with Akademika Publishing.
The thesis is produced by Akademika Publishing merely in connection with the
thesis defence. Kindly direct all inquiries regarding the thesis to the copyright
holder or the unit which grants the doctorate.

Abstract

A fast segmentation of tubular tree structures like vessel systems in volumetric datasets is of vital interest for many medical applications. This is especially valid for planning and navigation in catheter based interventions and liver resection surgical procedures. For catheter based navigation, blood vessel segmentation helps in planning the placement of stents and valves, and also in navigating to the desired location. For liver resection, a good visualisation of the blood vessels in relation to tumours provides better information about spatial relationship, which is very important in planning an optimal resection plane. Also a fast blood vessel segmentation will make it feasible to update the models intra-operatively.

In this thesis, we have developed a couple of methods for fast and user-friendly blood vessel segmentation. The methods work from a user-initiated seed, by tracking and segmenting the blood vessels to the ends of the vessel tree using a local structure analysis approach. To perform the structure analysis, we propose novel *multiscale modified vesselness* and *circleness* filters. The bifurcation cross-sections of the blood vessel were found by either detecting multiple peaks in the filtering output, or by estimating the sudden change in radius of the bifurcation, or by estimating significant change in the compactness and radius variance of the vessel cross-section. The novelty in our final algorithm is in performing the whole blood vessel segmentation by use of only 2D analysis on the blood vessel cross-sections, which makes it faster than performing a 3D image analysis.

Our methods were validated using synthetic as well as medical images, and also by clinically testing the method on liver hepatic and portal vein segmentation. The results have shown that the methods work in just seconds for images related to catheter navigation and in a couple of minutes for liver resection planning images. On medical validation of the liver blood vessel segmentation, our method detected 100% of blood vessels at and above 3mm radius and 80% at 2.5mm radius, which are the most clinically relevant blood vessels for liver resection planning.

Preface

This thesis is submitted to the University of Oslo for the degree of Doctor of Philosophy. The research work for the thesis was carried out at The Intervention Centre, Oslo University Hospital, and was supervised by Associate Professor Ole Jakob Elle PhD (OUS/UiO), Professor Fritz Albrechtsen (UiO/OUS), Professor Bjørn Edwin MD PhD (OUS/UiO), Thomas Langø PhD (SINTEF) and Professor Martin Reimers PhD (UiO). The research has received funding from the European Community's Seventh Framework Programme (FP7/2007-2013) under grant agreement number 238802 (IIIOS project) and also, received top-up financing from Norwegian Research Council.

Acknowledgements

I would like to thank a number of people who helped me through the duration of my PhD work. Foremost, I would like to express my profound gratitude to my main supervisor Associate Professor Ole Jakob Elle for believing in me and choosing me from the pool of candidates that had applied for this PhD position. His knowledge and expertise in the field of image-guided interventions always helped me keep my goals on track. Also, his continuous support, motivation and patience had constantly helped me in improving myself. I would like to thank him for giving me the freedom and resources to work and innovate with my ideas.

Beside my main supervisor, I had the privilege to have four other prominent scientists as co-supervisors, Professor Fritz Albregtsen, Professor Bjørn Edwin, Thomas Langø and Professor Martin Reimers, who had given their guidance at every step of my PhD. I greatly appreciate all my supervisors for regularly giving feedback, checking my progress and having fruitful discussion at all our meetings.

My sincere thanks to Professor Fritz Albregtsen, for being my go to person for any and all technical queries, and for promptly giving his comments and critics on all the work even when he was on holidays. I would like to also thank him for helping me understand and focus better for a research career path. I would like to thank Professor Bjørn Edwin for helping me comprehend the clinical aspects of the project and directing me towards the clinical needs. I also deeply thank him for letting me be at his surgeries and for explaining the procedures. I would like to thank Professor Martin Reimers for always taking time to be at every meeting to discuss and provide suggestions on improving my research work. My thanks to Thomas Langø for sharing his knowledge and experience with me. I wish I could continue collaborating with all of them during my future endeavours.

I would like to thank all the other co-authors, Erik-Jan Rijkhorst, Oliver Geier, Dean Barratt and Leonid Barkhatov, for their help in making the papers. I thank Erik-Jan Rijkhorst and Dean Barratt, also for their guidance during my Master's degree, which solidified my interest in the field of medical image analysis.

I would like to thank Rafael Palomar for our discussions we had related to the setting and improving of the HepaNavi platform for the liver resection planning, and also for proofreading many of my work. I jointly thank Kim Mathiassen and Rafael Palomar for introducing me to GIT and Latex, without which my PhD work will not have reached to the current extent. Also, I would like to thank all my colleagues (clinicians, technologists and physicists) at The Intervention Centre who created a friendly environment and worthwhile discussions of all kind. Especially, I want to thank Abubakr Eldirdiri, Anna Kim, Dilla Handini, Hugues Fontenelle, Kim Mathiassen, Quoc Phuong, Rafael Palomar, Raul Chavez, Wassim Zahid and Sergio Caccamo, for our leisure activities and lunch-time off-work discussions, which brought fun into my

PhD work life. Also, I would like to thank Marianne Berg, who is the soul of The Intervention Centre, for helping me at many occasions related to administrative paperworks.

I am thankful for being part of the IIIOS project as a Marie Curie Early Stage Researcher. My thanks to all the Early Stage Researchers, Experienced Researchers, Professors and administrative staff of the IIIOS project for all their support and collaboration in my project, and also for the constructive and fun-filled time we had at all our get-togethers.

I would like to express my wholehearted thanks to my parents, Jyothi Prasanna Kumar and Prasanna Kumar, for giving birth to me in the first place, and for encouraging me to learn and for giving me opportunities to do so, throughout my life. They have been constantly supportive during my PhD work.

Last but not least, my heartfelt thanks to my wife, Nayana Geetha Ravi, for the support she have given me during final stages of my PhD. She also have helped me by giving feedback on my thesis and my papers. I love her and cannot thank her enough for understanding and enduring with me through all the paper submissions, deadlines and thesis writing.

Rahul Prasanna Kumar
Oslo, September 2014

List of Thesis Papers

1. Rahul Prasanna Kumar, Fritz Albregtsen, Martin Reimers, Thomas Langø, Bjørn Edwin, and Ole Jakob Elle. "*3D multiscale vessel enhancement based centerline extraction of blood vessels.*" In SPIE Medical Imaging, pages 86691X-86691X-9. International Society for Optics and Photonics, 2013.
2. Rahul Prasanna Kumar, Erik-Jan Rijkhorst, Oliver Geier, Dean Barratt, and Ole Jakob Elle. "*Study on liver blood vessel movement during breathing cycle.*" In Colour and Visual Computing Symposium (CVCS), 2013, pages 1-5. IEEE, 2013.
3. Rahul Prasanna Kumar, Fritz Albregtsen, Martin Reimers, Bjørn Edwin, Thomas Langø, and Ole Jakob Elle. "*Blood vessel segmentation and centerline tracking using local structure analysis.*" In 6th European Conference of the International Federation for Medical and Biological Engineering, pages 122-125. Springer International Publishing, 2015.
4. Rahul Prasanna Kumar, Fritz Albregtsen, Martin Reimers, Bjørn Edwin, Thomas Langø, and Ole Jakob Elle. "*Three-dimensional blood vessel segmentation and centerline extraction based on two-dimensional cross-section analysis.*" Annals of Biomedical Engineering, accepted for publication, 2014.
5. Rahul Prasanna Kumar, Leonid Barkhatov, Bjørn Edwin, Fritz Albregtsen, and Ole Jakob Elle. "*Hepatic and portal vein segmentation for liver surgery.*" Minimally Invasive Therapy and Allied Technologies, under review, 2014.

Contents

Abstract	iii
Preface	v
Acknowledgements	vii
List of Thesis Papers	ix
1 Aim of the Thesis	1
2 Blood Vessel Segmentation Methods : A Survey	5
2.1 Vessel Enhancement	5
2.2 Thresholding	10
2.3 Region Growing	11
2.4 Deformable Models	12
2.5 Centreline Tracking	16
2.6 Validation	18
3 Vessel Segmentation in Clinical Practice	23
3.1 Catheter Navigation	23
3.2 Liver Resection Planning and Navigation	26
4 Summary of the Papers	31
4.1 Overview	31
4.2 Paper I	33
4.3 Paper II	34
4.4 Paper III	35
4.5 Paper IV	37
4.6 Paper V	39
5 Discussion	41
6 Conclusion and Future Work	45
References	47

Papers	59
I 3D multiscale vessel enhancement based centerline extraction of blood vessels .	61
II Study on liver blood vessel movement during breathing cycle	73
III Blood vessel segmentation and centerline tracking using local structure analysis	81
IV Three-dimensional blood vessel segmentation and centerline extraction based on two-dimensional cross-section analysis	87
V Hepatic and portal vein segmentation for liver surgery	125

Chapter 1

Aim of the Thesis

Motivation

Visualisation of blood vessels is crucial for many clinical procedures. The planning and navigation during catheterisation and liver resection, requires a good knowledge of the blood vessels, centrelines and diameters at different cross-sections of the blood vessels.

For catheter navigation, a segmentation and visualisation of blood vessels in 3D will help the interventionist to guide the catheter through the blood vessel to the desired region. Thus helping in the better placement of valves and stents. With the introduction of Magnetic Resonance (MR) into the interventional imaging, a 3D visualisation of blood vessels for catheter navigation has only become more important, as explained in Chapter 3. With additional information such as the centreline and radius of the blood vessel, the interventionists will be able to better decide on choosing the right size of stent and valves that would better fit for the specific patient.

For liver resection as well, segmentation and visualisation of hepatic and portal vein is vital for planning the resection. A good spatial knowledge of the blood vessel, tumour and liver surface is important for estimating the optimal resection plane for the liver resection. Fig 1.1 show visualisations of blood vessels, tumour and classified liver surface, which provide an easy way to estimate the resectable region of the liver. The figure also shows liver surface classified according to the branching of blood vessels, which will provide extra information to a surgeon in understanding liver region to be resected for maintaining inflow and outflow of blood in the remaining part of the liver. Currently, the methods for liver blood vessel segmentations are either performed by an external company or in-house technician, where in both cases the doctors do not get the freedom to visualise the data themselves. Also, longer processing time is required for getting the segmentation output as explained in Chapter 3.

A fast blood vessel segmentation is also important for intra-operative use. This will include catheter navigation, and also navigation in liver resection if an intra-operative update of the blood vessels are required. In liver resection for example, the surgeon will be able to wait only a couple of minutes during surgery for getting a new update of blood vessels.

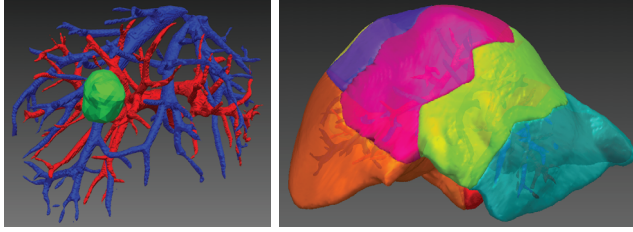


Figure 1.1: Left: A visualisation of hepatic veins, portal veins and tumour in liver. Right: Visualisation of classified liver surface, where the hepatic and portal veins can be seen through the surface. From [39]

General Aim

Among the blood vessel segmentation methods that are currently available in the literature, centreline tracking methods are found to be most computationally efficient, as explained in Chapter 2. However, many of these methods require a multi-scale vessel enhancement step which is usually applied to the whole image, making the process time consuming. Therefore, the main part of this academic thesis work is to introduce a novel, fast and user-friendly blood vessel segmentation method based on centreline tracking with only locally applied vessel enhancement, for applications to pre-operative and intra-operative interventional planning and navigation. The focus will also be on developing a single start point method, where the user needs to provide only one start position to segment the whole connected blood vessel structure.

For achieving the goal, we aim to investigate novel ways to process the vessel structure information that would provide a fast blood vessel segmentation. The novel methods are to produce the blood vessel segmentation output in less than a minute for images for catheter navigation, and in a couple of minutes for images for live resection. The final segmentation results are to be validated by computing overlap measures with ground-truth synthetic blood vessels, and percentage of detection of blood vessels by the proposed method for medical images.

Specific Aims

- Develop a modified multi-scale vesselness filter incorporating the advantages of both the Frangi *et al.* [53] and Erdt *et al.* [45] approaches.
- Develop a seed based centreline tracking of blood vessels.
- Develop a circle enhancement filter for easy centre point detection of 2D circular structure.
- Develop a fast blood vessel segmentation method with tracking by 2D cross-sectional analysis at vessel trunks and 3D vesselness at vessel bifurcations.
- Develop an alternate blood vessel segmentation method with tracking by 2D cross-sectional analysis at both trunks and bifurcations.

- Test the clinical use of a fast and user-friendly blood vessel segmentation for liver resection planning and validate the percentage of detection of blood vessels by our method against manual ground-truth.

Chapter 2

Blood Vessel Segmentation Methods : A Survey

In the past two decades, a wide range of blood vessel segmentation methods have been developed, aimed at various medical imaging techniques. However, there is no single blood vessel segmentation technique that works for all kinds of images. Reviews by Kirbas and Quek [69], and Lesage *et al.* [82], and thesis work by Lathen [77] and Dreshler [35], provide a good insight into the blood vessel segmentation methods in the literature.

Here, we present a survey into some of the blood vessel segmentation approaches that are currently in the literature. As part of the survey, we classified the various blood vessel segmentation techniques into vessel enhancement, thresholding, region growing, deformable models and centreline tracking. The vessel enhancement step is usually used as a preprocessing step in many methods to enhance the vessel structures in the image, and the other methods are mostly used for extraction of these vessel structures. Our final subsection is on validation, where we describe the state of art methods used for validating the results of blood vessel segmentation methods.

2.1 Vessel Enhancement

Vessel enhancement approaches deal with filters that enhance tubular or vessel-like structures in the image. Vessel enhancement is a widely used technique in the literature, mainly as a preprocessing technique, before extraction methods could be used to extract the vascular regions.

The vessel enhancement techniques that are most common, use the Hessian matrix based on the second order derivatives of a Gaussian. Such methods are developed by Sato *et al.* [107], Frangi *et al.* [53] and Erdt *et al.* [45]. These methods are also known as *vesselness* filters, as they measure the likelihood of a voxel belonging to a vessel. The Hessian matrix of 3D image $I(X)$ is given by

$$H(X; \sigma) = \begin{bmatrix} I_{xx}(X; \sigma) & I_{xy}(X; \sigma) & I_{xz}(X; \sigma) \\ I_{yx}(X; \sigma) & I_{yy}(X; \sigma) & I_{yz}(X; \sigma) \\ I_{zx}(X; \sigma) & I_{zy}(X; \sigma) & I_{zz}(X; \sigma) \end{bmatrix} \quad (2.1)$$

where $X = (x, y, z)$, $I_{xx}(X; \sigma) = \left\{ \frac{d^2}{dx^2} G(\sigma) \right\} * I(X)$, $I_{xy}(X; \sigma) = \left\{ \frac{d^2}{dxdy} G(\sigma) \right\} * I(X)$, etc.

Let eigenvalues of H be λ_1 , λ_2 and λ_3 and their corresponding eigenvectors be \vec{v}_1 , \vec{v}_2 and \vec{v}_3 . On sorting the eigenvalues ($|\lambda_1| \leq |\lambda_2| \leq |\lambda_3|$), \vec{v}_1 represents the direction along which the second derivative is maximum i.e. the direction of the tube. The eigenvectors \vec{v}_2 and \vec{v}_3 correspond to the tube cross-section directions. An illustration of this is shown in Fig. 2.1.

Based on the tube model, Sato *et al.* [107] proposed a line enhancement filter function given by

$$f = \begin{cases} e^{-\frac{\lambda_1^2}{2(\alpha_1 \lambda_c)^2} \lambda_c} & \lambda_1 \leq 0, \lambda_c \neq 0 \\ e^{-\frac{\lambda_1^2}{2(\alpha_2 \lambda_c)^2} \lambda_c} & \lambda_1 > 0, \lambda_c \neq 0 \\ 0 & \lambda_c = 0 \end{cases} \quad (2.2)$$

where $\alpha_1 < \alpha_2$ and $\lambda_c = \min(-\lambda_2, -\lambda_3)$. Here, the eigenvalues are sorted as $\lambda_1 \geq \lambda_2 \geq \lambda_3$.

Frangi *et al.* [53] used the geometrical aspect of the eigenvalues as a second order ellipsoidal model to distinguish plate-like, blob-like and tubular structures. The eigenvalues are sorted as $|\lambda_1| \leq |\lambda_2| \leq |\lambda_3|$. The deviation from a blob-like structure is given by the ratio

$$R_b = \frac{|\lambda_1|}{\sqrt{|\lambda_2 \lambda_3|}} \quad (2.3)$$

and another ratio distinguishes between plate-like and tubular structures, given by

$$R_a = \frac{|\lambda_2|}{|\lambda_3|} \quad (2.4)$$

The filter also makes use of the Frobenius matrix norm to reduce the influence of noise.

$$S = \sqrt{\lambda_1^2 + \lambda_2^2 + \lambda_3^2} \quad (2.5)$$

The final filter is given by

$$f = \begin{cases} 0 & \lambda_2 > 0, \lambda_3 > 0 \\ (1 - e^{-\frac{R_a^2}{2a^2}}) e^{-\frac{R_b^2}{2b^2}} (1 - e^{-\frac{S^2}{2c^2}}) & \end{cases} \quad (2.6)$$

where a , b and c are thresholds which control the sensitivity of the line filter to the measures R_a , R_b and S .

Erdt *et al.* [45] used a parameterless anatomical approach to construct the filter

$$f = (1 - \frac{||\lambda_2| - |\lambda_3||}{|\lambda_2| + |\lambda_3|}) (\frac{2}{3} \lambda_1 - \lambda_2 - \lambda_3) \quad (2.7)$$

where the eigenvalues are sorted as $\lambda_1 \geq \lambda_2 \geq \lambda_3$. The first term is an isotropy factor to avoid detection of plate-like structures, and the second term is the vessel signal.

The method of Erdt *et al.* has the advantage of being parameterless. According to a com-

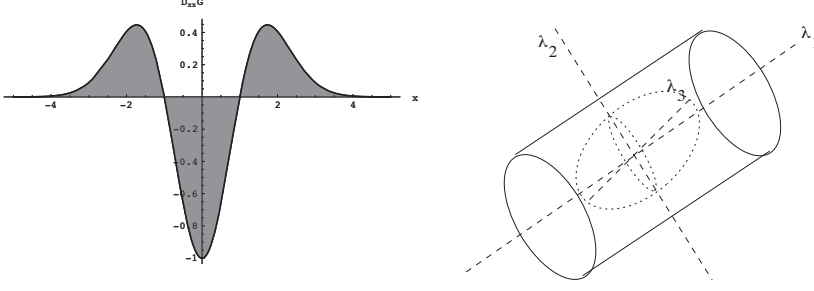


Figure 2.1: Left: The second order derivative of a Gaussian kernel probes inside/outside contrast of the range $(-s, s)$. In this example $s = 1$. Right: The second order ellipsoid describes the local principal directions of curvature. From [53]

parison done by Drechsler and Laura [36], the methods of Erdt *et al.* and Sato *et al.* have the advantage of detecting properly connected vessels, whereas the Frangi *et al.* method has its strength in the suppression of background noise.

The Hessian based methods make use of linear Gaussian scale space for computation of the spatial derivatives. This may result in an undesired diffusion of nearby structures into one another and this leads to problems such as detection of two tangenting tubes as one single tube. To avoid this problem, Bauer and Bischof [9] introduced a new method where the multi-scale computation of the gradient vectors is replaced by the Gradient Vector Flow (GVF), because it allows an edge-preserving diffusion of gradient information.

Apart from the vesselness filters, there are also *medialness* filters that measure the likelihood of a voxel being at the medial position of the tube. Krissian *et al.* [72,73] proposed a medialness response by taking the relationship between the radius of the structure and the scale at which it is detected. The response function is locally maximal at the centre of the vessel, given by

$$R_\sigma(\bar{x}) = \frac{1}{N} \sum_{i=0}^{N-1} -\nabla_\sigma I_0(\bar{x} + \tau\sqrt{\sigma}\vec{v}_\alpha) \cdot \vec{v}_\alpha \quad (2.8)$$

where $N = \text{int}(2\pi\sqrt{\sigma} + 1)$, $\alpha = 2\pi/N$, \vec{v}_α is the radial direction and $-\nabla_\sigma I_0$ is the gradient vector of the initial image, computed at the scale σ .

The medialness of Krissian *et al.* also produces a response for other edges and non-tube-like structures. An improved medialness response was proposed by Pock *et al.* [101], that takes the symmetry property criteria of the object into account.

$$R_\sigma(\bar{x}) = \frac{1}{N} \sum_{i=0}^{N-1} w(b_i)b_i \quad (2.9)$$

where $w(b_i) = e^{\frac{1}{2} \frac{(1 - \frac{b_i}{R_0^+})^2}{\sigma_w^2}}$, with $b_i = -\nabla_\sigma I_0(\bar{x} + \tau\sqrt{\sigma}\vec{v}_\alpha) \cdot \vec{v}_\alpha$ and $R_0^+ = \frac{1}{N} \sum_{i=0}^{N-1} b_i$.

Later, Foruzan *et al.* [49] proposed a medial-axis enhancement filter where the isotropic

coefficient introduced by Pock *et al.* was used to reduce the response of the filter for asymmetric cross-sections. Fig. 2.2 shows the difference in output between Pock's method and Foruzan's method.

Apart from Hessian based vessel enhancement filters, many other filters are also being developed. The traditional Hessian-related vessel filters often suffer from detecting complex structures like bifurcations due to an over-simplified cylindrical model. To overcome this drawback, a strain energy 3D vessel enhancement filter was proposed by Xiao *et al.* [123]. Here, the Hessian matrix is considered as the stress tensor and the orthogonal tensor invariants can be expressed as interns of eigenvalues. The final vessel shape discriminating function is given by

$$V(x) = \begin{cases} \sqrt{FA} & FA < 1 \\ \frac{1}{2}[mode(x) + 1], & otherwise \end{cases} \quad (2.10)$$

where FA is fractional anisotropy expressed in eigenvalues and,

$$mode(x) = \sqrt{2} \frac{\frac{1}{3} \sum_{i=1}^3 (\lambda_i - \bar{\lambda})^3}{(\frac{1}{3} \sum_{i=1}^3 (\lambda_i - \bar{\lambda})^2)^{3/2}} \quad (2.11)$$

where $\bar{\lambda}$ is the average eigenvalue.

Quadrature filtering that was successfully applied by Granlund and Knutsson [59] for local structure estimation, was proposed for use in vessel segmentation by Lathen *et al.* [78, 79]. The filter combines directions and scales to produce a multi-scale filter response which captures lines and edges with high precision.

Morphological filters, such as variants of top-hat operators, were also proposed as vessel enhancement filters, especially for 2D retinal image analysis. Zana and Klein [127] proposed an algorithm that combines morphological filters and cross-curvature evaluation to segment vessel-like patterns. The vessel filter is modelled according to its morphological descriptions such as linearity, connectivity and vessel width, and also related to calculation of parameters such as the curve of the Gaussian profile and its variation along the crest lines. Rossant *et al.* [106] also used morphological top-hat operator with a disc-shaped structuring element slightly larger than the thickest vessel to remove background areas. Fig. 2.3 demonstrates the use of a morphological top-hat operator for vessel enhancement.

Law and Chung [80] proposed a curvilinear structure detector, called the Optimally Oriented Flux (*OOP*). The oriented flux encodes directional information by projecting the image gradient along some axes, prior to measuring the amount of the projected gradient that flows in or out of a local spherical region, and *OOP* discovers the structure direction by finding an optimal projection axis which minimises the oriented flux. This method focuses on the detection of intensity discontinuities occurring at the object boundaries of curvilinear structures. Benmansour and Cohen [11] proposed a link between *OOP* and Hessian based vessel enhancement, where the method exploits the orientation of the vessels by using the optimally oriented flux to

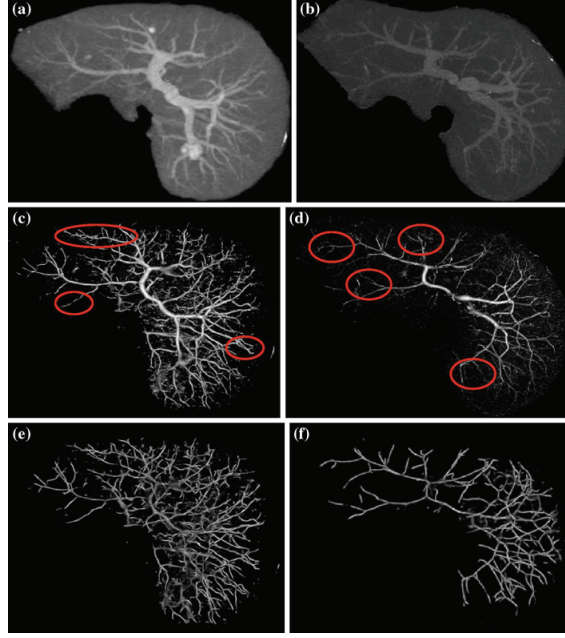


Figure 2.2: Enhancement of medial-axes of portal veins in the second phase of two CT datasets. (a),(b) Original images. (c),(d) The output of Pock's method. (e),(f) The output of Foruzan's method. The red circles show the regions where the Foruzan's method outperformed Pock's method. From [49]

construct a multi-resolution anisotropic metric that extracts the local geometry from the image and describes the vessels orientation and scales.

Reuze *et al.* [104] introduced the use of 3D geometrical moments for blood vessel segmentation. The method was later used for liver blood vessel segmentation by Esneault *et al.* [46], where a geometrical moment based cylinder detector is applied at every voxel of the image.

Tyrrell *et al.* [118] proposed using cylindrical superellipsoids to model complex 3D vasculature. Superellipsoids are restricted to cylindrical forms that model a range of shapes from a simple ellipsoid to an elliptical cylinder. This model allows for joint robust estimation of the vessel boundary and centrelines.

Though many filters are explained here that are not based on Hessian, Hessian based filter are still the most used method in the literature. Also, many of the vessel enhancement filters are based on a scale-space approach, and a multi scale integration is essential for detecting vessels of varying widths, as shown in Fig. 2.4. The most commonly used multi scale integration is done by finding the maximum over the covered scale-space [45,53,107,123]. A variation to this technique was introduced by Lathen *et al.* [78] and Drechsler and Laura [37], using weighted additives of scale responses. An additive of the scales focusses on enhancement of the vessel around its centre, shown in Fig. 2.5.

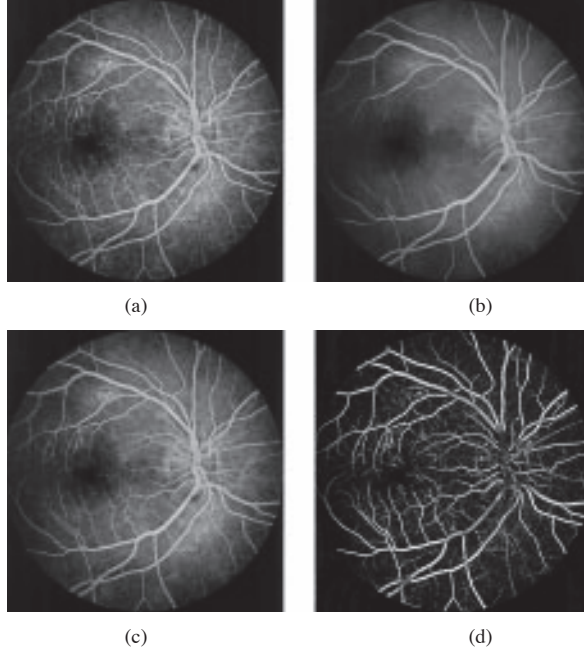


Figure 2.3: Steps of the morphological treatment: (a) initial image, (b) supremum of opening, (c) reconstruction, and (d) sum of top-hats. From [127]

2.2 Thresholding

Thresholding is a basic segmentation step to classify the images into foreground and background. It is a common step to binarize vessels after vessel enhancement filtering and could also be used to limit the application of a global method. In bi-level thresholding, the histogram of the image is usually assumed to have one valley between two peaks, the peaks representing background and objects respectively. The segmentation by thresholding is given by

$$I_B(x) = \begin{cases} 1 & I(x) > threshold \\ 0 & otherwise \end{cases} \quad (2.12)$$

The parameter of threshold can be selected manually or automatically. The threshold parameter can be manually set by either visually inspecting the image or checking the histogram of the image. Though a number of automatic thresholding algorithms are proposed in the literature [3, 4, 110], the most commonly used algorithm is given by Otsu [97]. However, analysis by Albregtsen [4] on thresholding error versus object area, shows that the Kittler and Illingworth method [71] and a method by Kapur *et al.* [65] perform better than the Otsu method, when the object to background ratio is low. The finding was also confirmed by quantitative performance evaluation of thresholding techniques by Sezgin and Sankur [110].

The method of Kittler and Illingworth is based on obtaining a minimum classification error from continuously updated estimates of the distribution parameters. The method of Kapur *et*

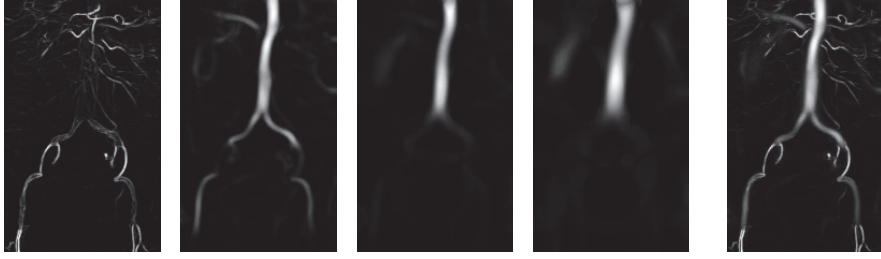


Figure 2.4: The first four images show the vesselness obtained at increasing scales. The last image is the result after multiscale integration. From [53]

al. is a thresholding algorithm based on entropy. Here, the image foreground and background are considered as two different signal sources, so that when the sum of the two class entropies reaches its maximum, the image is said to be optimally thresholded.

Hysteresis thresholding is another thresholding method with the use of two thresholds. The image is first segmented by a ‘hard’ threshold which yields only high confidence object pixels. A second threshold operation, this time with a ‘weak’ threshold, returns then the entire object together with many background pixels. Using prior knowledge with respect to object connectivity, the segmentation is achieved by choosing from among the object pixels selected by the ‘weak’ threshold only those pixels connected to a high confidence one. Hysteresis thresholding was used for blood vessel segmentation by Condurache and Aach [98], where the two thresholds were computed by a fast percentile rule.

2.3 Region Growing

Region growing is a simple region based segmentation method, where the neighbouring pixels to a seed are added into the region if they satisfy some specified criteria. The process is iterated until all the pixels satisfying the criteria are added into the region. The final region will be a connected region. Region growing and its variants are widely used as an extraction step for blood vessel segmentation.

Boskamp *et al.* [14] and Martinez *et al.* [89] used classic region growing for extracting the blood vessels. Boskamp *et al.* uses region growing based vessel segmentation where the user provides one or more seed points, and neighbouring pixels are added into the region on certain criteria. The criteria include lower grey level intensity, adaptive upper grey level intensity and gradient threshold. Martinez *et al.* uses an 8-neighbourhood pixel region growing after scale space analysis for vessel extraction.

Masutani *et al.* [90] proposed a shape-based region growing algorithm. Here, the region-growing is processed in the space limited by the initial shape and the structural information of the shape is simultaneously obtained. The region grows while avoiding non-vessel regions and keeps its local smoothness based on math-morphological information and local shape processing.

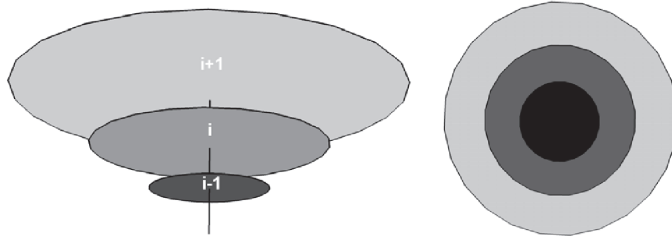


Figure 2.5: Left: Vesselness filtered scale space representation of a tubular structure. Right: Result after adding the vesselness measures of each scale. Darker colors represent higher values. From [37]

Eiho *et al.* [42] proposed a branch based region growing technique for blood vessels. In this method, region growing is performed branch by branch and if the growing point reaches a branch bifurcation part, it is let to go into only one side of the branches. When the growing point reaches an edge of the vessel, the growing stops, and then it starts again from the latest branch bifurcation point. A similar region growing is wavefront propagation by Kirbas and Quek [70]. Fig. 2.6 illustrates the wavefront propagation through a tube.

Selle *et al.* [108] proposed a threshold based region growing, where the threshold is automatically suggested. Here, after each iteration of the region growing, the output is set as new seeds. The region growing is then contained with reduced threshold. The process continues until the newly added voxels are completely outside the vessel limits.

Another threshold based region growing is proposed by Erdt *et al.* [45]. Here the values of pixels detected as foreground is compared to the mean intensity of the image. If 80% of the pixels are above the mean intensity, then the threshold is lowered and the procedure is applied anew. This automatic approach allows the continuous segmentation of vessels that are disconnected in the original dataset while preventing the segmentation of noisy structures.

Dehmeshki *et al.* [32] proposed sphericity oriented region growing. The region growing is weighted according to the strength of connectivity in the connectivity map of each point neighbouring the current region. This is so that neighbouring points with higher connectivity are added to the region before neighbouring points with lower connectivity.

Zhan-Peng *et al.* [128] proposed a 3D hierarchical seeded region growing. The algorithm uses 3D sub-blocks instead of single pixels and allows the image to be represented in multiple resolutions. The seeded region growing does the region merging at a lower resolution with a bigger sub-block size. Then a higher resolution with a smaller sub-block is used to continue to enlarge over the specified area of the image.

2.4 Deformable Models

Deformable models are techniques where models are deformed to best fit the object. Active contours are popular image segmentation tools that evolve a contour through external and internal forces. The external force is an image derived force to expand the contour towards the

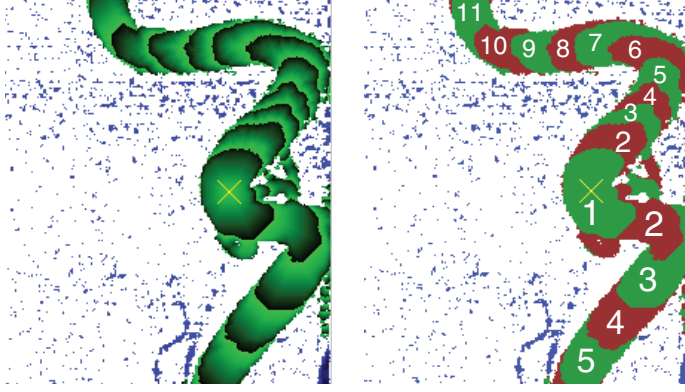


Figure 2.6: Left: Wave propagation. Right: Wave count images through an angiogram segment. From [70]

object border and the internal force is based on the assigned model that restrain the contour from free movement. This approach is widely used for vessel segmentations as the forces could be modelled according to different parameters that fit a vessel-like structure.

The snakes method proposed by Kass *et al.* [66] is considered the fundamental segmentation method using active contours. It is an energy minimising spline guided by external constraint forces and influenced by image forces that pull it toward features such as lines and edges. By representing the position of the snake parametrically by $v(s) = (x(s), y(s))$, its energy can be written as

$$E = \int_0^1 \frac{1}{2} [\alpha |v'(s)|^2 + \beta |v''(s)|^2] + E_{ext}(v(s)) ds \quad (2.13)$$

where α and β are weighting parameters that control tension and rigidity of the snakes, and $v'(s)$ and $v''(s)$ are first and second derivatives of $v(s)$ with respect to s . The external energy function $E_{ext}(v(s))$ is derived from the image. Given a graylevel image $I(x, y)$, the external energy designed to lead an active contour toward step edges is

$$E_{ext}(x, y) = -|\nabla I(x, y)|^2 \quad (2.14)$$

Xu and Prince [124] proposed the GVF-snakes method, which uses the Gradient Vector Flow (GVF) as its external energy function. The GVF energy function is calculated by applying a generalised diffusion equation to both components of the gradient of an image edge map, and thus extend far away from the object. This allows the snake to start far from the object, and still draws it towards the object. As explained earlier, GVF is also used for vessel enhancement.

A variation to the snakes algorithm was proposed by Toledo *et al.* [116], called eigensnake. The eigensnake learns an optimal object description and searches for such image feature in the target image. This is achieved by applying principal component analysis on image responses of a bank of Gaussian derivative filters. The external energy of the snake is defined as a function of the Mahalanobis distance of the projected image features to the centre of the learned cluster.

Another snake algorithm was proposed by McInerney and Terzopoulos [92], called topology adaptive snakes or T-snakes. Their approach exploits an affine cell decomposition of the image domain (ACID), which allows the T-snakes to segment and reconstruct objects with significant protrusions, tubular objects, or objects with bifurcations. The ACID divides the image domain into a collection of convex polytopes. Using the ACID framework, contour evolution is performed by tracking and recording the interior region of a T-snake as it expands or contracts under the influence of pressure forces. The strength of these pressure forces can be directly linked to the local or global statistics of the image pixel intensity values of the target object. These statistical constraints allow ACID-based models to behave as active region growing models that can effectively integrate edge information with region-based information.

Many deformable models have been implemented using the level-set based numerical algorithms [109]. The advantage of the level set method is that numerical computations involving curves and surfaces can be performed on a fixed Cartesian grid without having to parameterise these objects. The level set method amounts to represent a closed curve Γ using an auxiliary function φ , called the level set function. Γ is represented as the zero level set of φ by

$$\Gamma = \{(x, y) | \varphi(x, y) = 0\} \quad (2.15)$$

and the level set method manipulates Γ implicitly, through the function φ . This function φ is assumed to take positive values inside the region delimited by the curve Γ and negative values outside [47, 109].

Fei and Park [48] used the level-set method for liver blood vessel segmentation. They segmented the liver automatically using morphological filtering and an improved Otsu's threshold method, and then the liver boundary was used as the level set initialisation. Lathen *et al.* [78] also used level-set for front propagation after applying their quadrature filter.

Lorigo *et al.* [85] developed the CURVES system which models the object boundary as a manifold that evolves iteratively to minimise an energy criterion. This energy criterion is based both on intensity values in the image and on local smoothness properties of the vessel wall.

A model based quantification of vessel morphology was proposed by Frangi *et al.* [51, 52], where linear vessel segments are modelled with a central vessel axis curve coupled to a vessel wall surface. The method consists of a central vessel axis computation and a 3D boundary model which is then initialised and fitted to the image data using a boundary criterion. Initially a rough central vessel axis is approximated from user initiated seeds joined by a geodesic curve along the iso-surface. Then the central vessel axis is approximated using a B-spline curve and fitted into the image data using the vesselness calculated at each voxel of the image. Finally the vessel wall is modelled using a tensor product of a B-spline that fits to the boundaries of the underlying vessel. Fig. 2.7 illustrates the working of the method.

Biesdorf *et al.* [12] proposed segmentation of the aortic arch using a joint 3D model-based segmentation and elastic registration. The approach is based on an energy-minimising func-

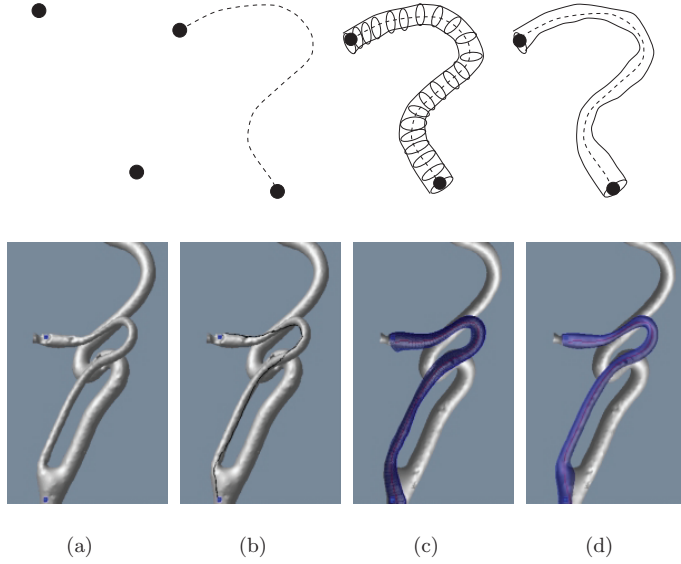


Figure 2.7: (a) A user initializes two (or more) points on the surface. (b) From these seeds, a geodesic path is computed. (c) The geodesic path is deformed until the central vessel axis is determined. Using the distance between the newly obtained vessel axis and the original geodesic path, a circular cross-section is swept along the axis to generate an initialization of the vessel wall model. (d) Vessel wall and central vessel axis. From [51, 52]

tional J_k corresponding to a vessel segment k , and consists of two terms:

$$J_k(p_k, u_k) = J_M(g_M, g_{I,k}^{roi}, p_k) + J_R(g_{I,k}^{roi}, g_{M,k}^{roi}, p_k) \quad (2.16)$$

The first term J_M denotes an intensity similarity measure between a 3D cylindrical intensity model g_M with parameters p_k and the intensities $g_{I,k}^{roi}$ within a 3D ROI of a tomographic image g_I . The second term J_R denotes an energy-minimising functional for elastic registration of $g_{I,k}^{roi}$ with an image $g_{M,k}^{roi}$ generated from the 3D intensity model g_M . The result of the elastic registration is represented by the deformation field u_k . By minimising the overall functional J_k , the segmentation result from the 3D model fitting is used to increase the registration accuracy, while at the same time the registration result is used to improve the 3D model fitting. After fitting the aortic arch at vessel segment k , a Kalman filter is used to predict the parameters p_{k+1} for the next segment.

A fast energy minimisation function, called graph cuts was proposed by Boykov *et al.* [15–17]. The graph cut algorithm works on the principle that a globally optimal segmentation satisfying hard constraints can be computed efficiently in low-order polynomial time using max-flow/min-cut algorithms on graphs. The algorithm works by making a directional graph, which starts from setting two terminal nodes, the object terminal S and background terminal T . All the intermediate voxels in the image between the terminal nodes are set as intermediate nodes and

directed weighted links connect the nodes. Two kinds of links are identified: t-links connecting voxel to the terminals S and T , and n-links between a pair of intermediate nodes. The energy function for graph cut method is given by

$$E = E_{region} + E_{boundary} \quad (2.17)$$

where a data term E_{region} is an energy coding the probability that a voxel belongs to the class ‘object’ or ‘background’ set on t-links, and a smoothing term $E_{boundary}$ is an energy coding the local discontinuity between a pair of voxels represented by the n-links. Once the graph is built with the correct weight assigned to each link, a min-cut/max-flow combinatorial optimisation algorithm is applied to the graph giving the segmentation result, as illustrated in Fig. 2.8.

Graph cut is being widely used in blood vessel segmentation [46, 54]. Freiman *et al.* [54] proposed a segmentation of carotid arteries using a graph min-cut method based on a new edge weights function that adaptively couples the voxel intensity, the intensity prior, and geometric vesselness shape priors. Esneault *et al.* [46] proposed a method for liver vessel segmentation by introducing a 3-D geometrical moment-based detector of cylindrical shapes within the minimum-cut/maximum-flow energy minimisation framework.

2.5 Centreline Tracking

Centreline tracking methods are based on tracking/tracing from a user initiated seed to the ends of the vessel by calculating the centreline. These methods are considered computationally efficient when the computations are performed only locally. However, many of these methods require whole image analysis to get filtered images to perform smooth tracking of the centreline.

Aylward and Bullitt [6] proposed a seed initiated method, where the centreline is found by transversing through the ridge. Ridge methods operate by considering an N-dimensional image to be a surface in an N+1 dimensional space by mapping intensity to height; tubular object centrelines will exist as one-dimensional (1-D) height ridges on that surface. Here the ridge is calculated through computation the eigenvalues and eigenvectors of Hessian matrix. The eigenvalues are sorted as $\lambda_1 \leq \lambda_2 \leq \lambda_3$ and the eigenvector corresponding to λ_3 is the direction of tracking.

Krissian *et al.* [73] proposed centreline tracking and vessel reconstruction by using an adaptive medialness measure. Again centreline tracking is done using the local eigenvector corresponding to vessel direction. They compute the multiscale response from responses at a discrete set of scales, then extract the local maxima in this multiscale response in order to estimate the vessel centrelines. The medialness response used here is explained in Eq. 2.8, and the local maxima are characterised as

$$(\bar{x}; t_i) \text{ is local maximal} \iff R_{t_i}^n(\bar{x}) \geq R_{t_i}^n(\bar{x} \pm \vec{v}_1) \text{ and } R_{t_i}^n(\bar{x}) \geq R_{t_i}^n(\bar{x} \pm \vec{v}_2) \quad (2.18)$$

$$\text{and } R_{t_i}^n(\bar{x}) \geq R_{t_{i+1}}^n(\bar{x})$$

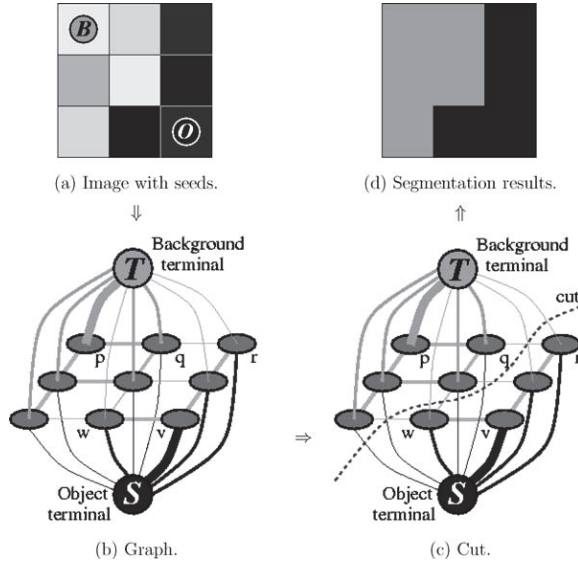


Figure 2.8: A simple 2D segmentation example for a 3×3 image. The seeds are O and B . The cost of each edge is reflected by the edge's thickness. The boundary term defines the costs of n -links while the regional term defines the costs of t -links. Inexpensive edges are attractive choices for the minimum cost cut. Hard constraints are implemented via infinity cost t -links. A globally optimal segmentation satisfying hard constraints can be computed efficiently in low-order polynomial time using max-flow/min-cut algorithms on graphs. From [15]

Another medialness based centreline tracking for vessel segmentation is proposed by Fridman *et al.* [55]. The method was built upon the work of Furst [56] and Aylward and Bullitt [6]. The method extends the work of Furst by improving the robustness of his core following and termination, and by augmenting Furst's method with the ability to handle branching objects. It differs from the work of Aylward and Bullitt by relying on only one seed point per tree structure and no post-processing to segment a tubular branching object. Branching is detected by applying an affine-invariant corner detector along with medialness. This consistently gives strong responses at corners of branches, but also gives strong responses in undesirable places such as the inside edge of a sharply bending object or places that have voxel jaggedness due to noise or aliasing. The medial atom spoke that lies on the intersection of the two branches gives a significantly weaker response in medialness. The location of this spoke tip provides an approximate starting location for the core of the new branch and the direction in which it points provides an approximate tangent direction for the new core.

Wesarg and Firlre [120] proposed a corkscrew algorithm, which is a semiautomatic extraction technique requiring the definition of the start and end points of the centreline path to be found. A first estimation of the centreline of the vessel is calculated and then corrected iteratively by detecting the border of the vessel perpendicular to the centreline. The major drawback of this algorithm is the fact that the computed border points neither form a smooth surface in 3D nor a closed curve in planes perpendicular to the centreline.

Wette *et al.* [121] extended the corkscrew algorithm to detect bifurcations by using a ray casting approach. First, rays are spread out within a cone of angle α directing to the first approximation of the centreline. In a subsequent task the different lengths of the rays are evaluated to detect a possible bifurcation.

2.6 Validation

Once, the segmentation is done, the results have to be validated to determine how well the segmentation method has performed. Validation is an important step to understand, whether the proposed method is better than the ones that are currently available in the literature, or how well the proposed method is suited for the particular application. Two important parts of validations are *gold standard models* and *metrics for segmentation comparison*.

2.6.1 Gold Standard Models

Gold standard models are used as approved models for validating the segmentation results from the proposed method. The three types of models that are generally used are synthetic, phantom and manual segmentation.

Synthetic models are the most widely used ground-truth for validating blood vessel segmentation methods. These are created virtually in a computer. For validating blood vessel segmentations, the synthetic data are made to mimic the tubular nature of the blood vessels. Simple tubular models are the most widely used as they are easy to create and validate [6, 9, 11, 12, 37, 49, 73, 80, 118, 123]. The validation is done by testing methods in tubes of varying curvature and radius. The validation can also be performed to understand whether closely located tubes can be differentiated by the method.

Other than simple tubular models, the models can be made in relation to the tree-like structures of medical blood vessels, where the branching can be made similar to blood vessels. These kind of synthetic blood vessels are especially good in validating methods based on tracking the blood vessels to understand its branch detection capability. *VascuSynth* by Hamarneh and Jassi [61], is a widely accepted method for making synthetic blood vessels. Here, the models are generated by iteratively growing a vascular structure based on a user-defined oxygen demand map. The algorithm also makes use of other user-provided parameters like the location of the root of the tree and number of desired terminal nodes. Esneault *et al.* [46] proposed making models based on real coronary artery tree description, where models are constructed from centrelines previously determined, and *ad hoc* vessel diameters are set. Drechsler *et al.* [38] proposed making synthetic blood vessels similar to liver blood vessels. The model is made using physical vascular model to simulate the growth of liver vessels within liver masks extracted from clinical CT datasets.

Galarreta-Valverde *et al.* [57] proposed a method for 3D synthetic blood vessel generation, where the synthetic blood vessels look more like the real blood vessels. The method is an

extension on the work by Zamir [126] and Liu *et al.* [84], which uses stochastic parameter Lindenmayer systems to generate fractal blood vessel structures incorporated with physiological laws of blood vessel branching. Compared to the rigid tubular branching trees made by VascuSynth, the method of Galarreta-Valverde *et al.* produces real blood vessel-like models, as shown in Fig. 2.9.

As alternatives to computer-generated synthetic models, physical models or phantoms are also used for validating blood vessel segmentation methods. Selle *et al.* [108] used vascular corrosion casts of the human liver for their validation. For making the casts, the portal and hepatic veins of cadavers were injected *in situ* with resin, and left to harden. Then, the liver is removed from the body and corroded, leaving behind only the detailed branching structure of the vessel systems. Bauer *et al.* [10] produced a plastic phantom of a vessel tree with known digital ground-truth for their validations. Biesdorf *et al.* [12] validated using a 3D aorta phantom, which was made with acrylic glass based on a real patient image with a severe aneurysm. Conversano *et al.* [28] in their paper, explained a method for making a liver phantom using stereolithography. Here, the phantom is bonded layer by layer, where the complex shapes are tailor-made using a 3D-CAD drawing of the object.

The final form of gold standard models are made by manual segmentation. The manual segmentation is usually made by drawing the contours of the blood vessels, by an expert (radiologist, medical personnel or medical imaging specialist) [21, 34, 35]. Drawing contours on all the slices is a lot of work. A way around it is to draw only on a few slices with maximum number of vessels and compare their overlap to the segmentation result, as described in Conversano *et al.* [27]. Alhonnoro *et al.* [5] performed a landmark based evaluation, where 1024 landmarks were collected along the vessels. Each landmark consisted of centreline and radius at that location, and a hit or miss of landmark was evaluated.

2.6.2 Metrics for Segmentation Comparison

After obtaining the segmentation results from a proposed new method, the results have to be compared qualitatively and quantitatively to gold standard models to understand the effectiveness of the segmentation method. A qualitative evaluation is usually performed visually by an expert by comparing the results with the gold standard models. In contrast to qualitative evaluation that introduces a degree of subjectivity, quantitative evaluation provides objectivity.

For all comparisons, the gold standard models are considered as the ground-truth. As illustrated in Fig. 2.10, on performing a binary classification, the metrics of segmentation can be obtained from the following basic terms: *true positive* (TP), *false negative* (FN), *false positive* (FP), *true negative* (TN). Here, TP + FP is the obtained result and TP + FN is the ground-truth. TP is the region correctly segmented as part of the result and TN is the region correctly segmented as not part of the result. Whereas FP is the region incorrectly segmented as part of result (also termed over-segmentation) and FN is the region incorrectly segmented as not part of the result (also termed under-segmentation). The main aim of a segmentation method is to have as little FN and FP as possible in the result.

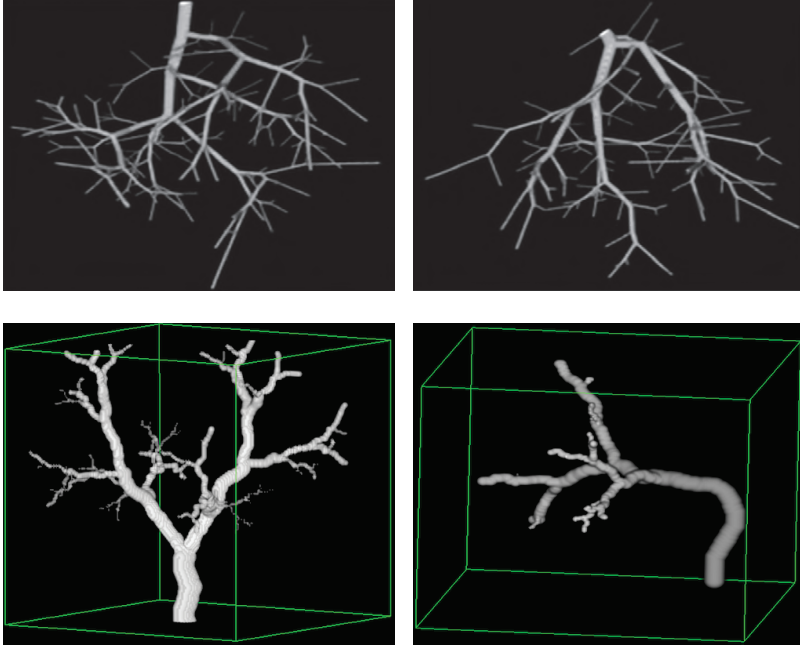


Figure 2.9: Top row: 3D synthetic blood vessels generated using VascuSynth [61]; Bottom row: 3D synthetic blood vessels generated using method of Galarreta-Valverde et al. [57].

The most used metrics of segmentation validation are sensitivity or true positive rate or recall as in [21, 31, 33, 34, 49, 94, 107], and specificity or true negative rate as in [21, 33], which is also used as 1–specificity or false positive rate as in [28, 31, 49, 94, 107].

$$\text{Sensitivity} = \frac{TP}{TP + FN} \quad (2.19)$$

$$\text{Specificity} = \frac{TN}{FP + TN} \quad (2.20)$$

$$\text{False Positive Rate} = \frac{FP}{FP + TN} \quad (2.21)$$

$$\text{False Negative Rate} = \frac{FN}{FN + TP} \quad (2.22)$$

Mostly along with sensitivity and specificity, accuracy as in [8, 21, 31, 33, 94] and precision as in [8, 118, 123] are also calculated to add more information into the evaluation of the validation.

$$\text{Accuracy} = \frac{TP + TN}{TP + TN + FP + FN} \quad (2.23)$$

$$\text{Precision} = \frac{TP}{TP + FP} \quad (2.24)$$

The measure of similarity between two segmentation are mainly provided by the *Dice coefficient* as in [11, 12, 28, 34, 40, 46] and the *Jaccard similarity coefficient* as in [21]. Here, the Dice

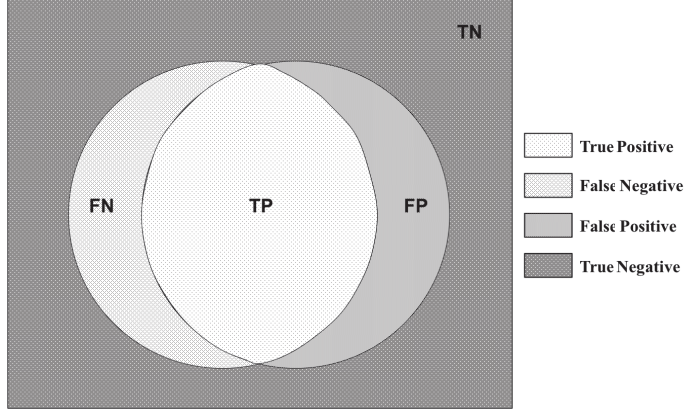


Figure 2.10: A binary classification showing true positive, false negative, false positive and true negative.

coefficient, which is the same as F1 score, is the most commonly used measure for comparison.

$$Jaccard\ coefficient = \frac{TP}{TP + FP + FN} \quad (2.25)$$

$$Dice\ coefficient = \frac{2TP}{2TP + FP + FN} \quad (2.26)$$

The metrics of segmentation validation could also be calculated by measuring the distance between the models, or the distance between the centrelines of the models. The most commonly used distance measurement is maximal distance or Hausdorff distance as in [11, 40, 54].

$$Hausdorff = \max_{a \in A} \{ \min_{b \in B} d(a, b) \} \quad (2.27)$$

where a is an element of set A , b is an element of set B , and $d(a, b)$ is the Euclidian distance between the points a and b . A modified symmetric Hausdorff distance (MSHD) was also proposed by Dubuisson and Jain [41], given by

$$MSHD = \max \left\{ \frac{1}{N_a} \sum_{a \in A} \min_{b \in B} d(a, b), \frac{1}{N_b} \sum_{b \in B} \min_{a \in A} d(b, a) \right\} \quad (2.28)$$

The advantages of using a MSHD is that it is robust to outliers that might result from segmentation errors and also it increases with an increase in the amount of difference between the set of points.

Apart from metrics of evaluation based on binary classification or distances between surfaces is vessel branch detection based validation. For many medical images, it is hard to obtain a completely manually segmented 3D image as ground-truth, and medically, it might be more relevant to understand hit and miss of branches. Thus, some work by Conversano *et al.* [27, 28], Bauer *et al.* [10] and Fridman *et al.* [55] describes methods of evaluation, where they have used branch detection rate according to the radius of the brach as a major criterion for validation.

Chapter 3

Vessel Segmentation in Clinical Practice

The human body contains several different types of blood vessels that constitute a network of arteries and veins. Visualisation of these blood vessels is important for improving the planning and navigation in several interventional procedures. It is specially relevant in catheter-based procedures and liver resection planning.

3.1 Catheter Navigation

3.1.1 Stent Grafting

An aneurysm is a balloon-like bulge in an artery. It occurs when the blood vessel is damaged or there is a weakness in the wall of the blood vessel. As the aneurysm grows there is a greater risk of rupture, which can lead to severe haemorrhage and other complications including sudden death. The two main types of aneurysm are aortic aneurysm (can be abdominal or thoracic) and cerebral aneurysm.

Endovascular stent grafting is a treatment for aneurysm. It does not require surgical opening of chest or abdomen. In this procedure an endovascular stent graft is used to reinforce the vessel wall and to prevent the damaged area from rupturing. An endovascular stent grafting is done by inserting a catheter into an artery (using groin) and it is threaded to the site of the aneurysm using angiography. A guide wire is used to pass the detachable coils (stent) through the catheter and it is released at the site of the aneurysm. The coil fills the aneurysm, block it from circulation and cause the blood to clot, which effectively destroys the aneurysm. Fig. 3.1 illustrates the procedure. The use of vessel segmentation in stent grafting is explained in Section 3.1.3.

3.1.2 Valve Replacement

There are four valves within the heart; the mitral, aortic, pulmonary and tricuspid. These valves ensure that the blood flows in only one direction through the heart. Valvular heart diseases occur when there is a damage or defect to these valves. The mitral and tricuspid valves control the flow of blood between the atria and the ventricles (the upper and lower chambers of the heart).

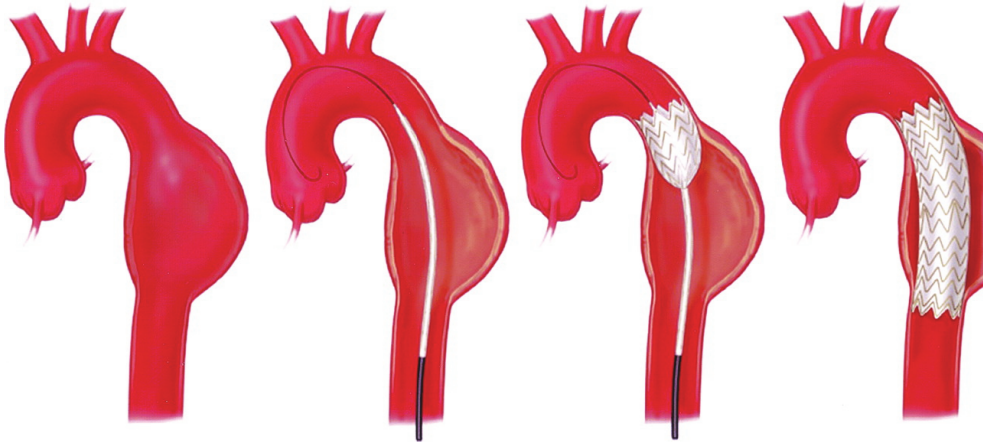


Figure 3.1: Stent grafting. From [62]

The pulmonary valve controls the flow of blood from the heart to the lungs, and the aortic valve governs blood flow between the heart and the aorta, and thereby the blood vessels to the rest of the body. Mitral and aortic valves are the most commonly affected by valvular heart disease.

Normally functioning valves ensure that blood flows with proper force in the proper direction at the proper time. In valvular heart disease, the valves may become too narrow and hardened (stenotic) or are unable to close completely (incompetent), leading to poor pumping action. To compensate for this, the heart muscle enlarges and thickens, thereby losing elasticity and efficiency. In addition, in some cases, there is greater chance of clot formation, increasing the risk of stroke or pulmonary embolism.

A transcatheter valve replacement is a minimally invasive surgical procedure for the treatment of valvular heart diseases. This procedure is done without removing the old damaged valve. Instead of that, it wedges a replacement valve into the valve's place as shown in Fig. 3.2. Earlier valve replacement required an open heart procedure, whereas nowadays transcatheter valve replacement procedures can be done through very small openings.

The transcatheter valve replacement is performed either by the transfemoral approach or the transapical approach. In a transfemoral approach, a catheter is placed in the femoral artery (in the groin) and guided into the heart chamber. A compressed heart valve is placed on a balloon catheter and is positioned directly onto the diseased valve. Once it reaches the position, the balloon is inflated and the valve is secured in place. During the transapical approach, a small incision is made between the ribs. A compressed heart valve is placed on a balloon catheter, inserted through the ribs into the apex of left ventricle and positioned inside the diseased valve. Once in position, the balloon is inflated to secure the valve in place. The use of vessel segmentation in valve replacement is explained in Section 3.1.3.

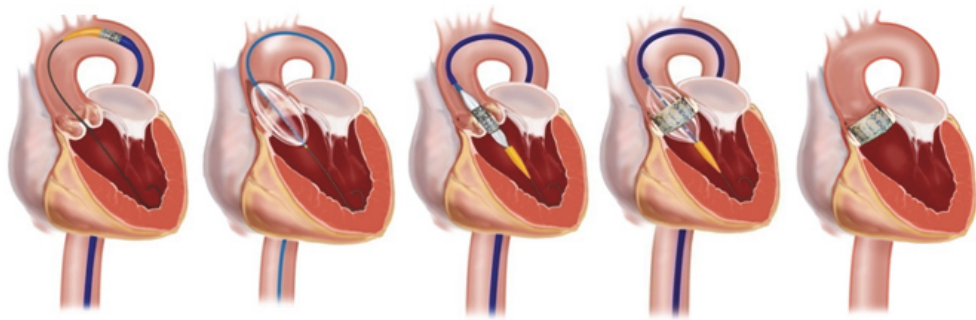


Figure 3.2: Transcatheter valve replacement. From [2]

3.1.3 Interventional Imaging

The catheter navigation procedures are commonly performed using X-ray fluoroscopy imaging. During a fluoroscopy procedure, an X-ray beam is passed through the body. The image is transmitted to a monitor so the movement of a body part or of an instrument or contrast agent through the body can be seen.

The major disadvantage of fluoroscopy is the radiation. The radiation dose the patient receives varies depending on the individual procedure. Fluoroscopy can result in relatively high radiation doses, especially for complex interventional procedures which require fluoroscopy to be administered for a long period of time. Radiation-related risks associated with fluoroscopy include: radiation-induced injuries to the skin and underlying tissues, which occur shortly after the exposure, and radiation-induced cancers, which may occur some time later in life.

Magnetic Resonance Imaging (MRI) has recently become a possible imaging modality in guiding this type of interventions [23, 64, 86, 102]. MRI can remarkably discriminate soft tissue contrast. In addition, the use of ionising radiation is avoided. MR guidance can also give close to real time imaging with satisfactory resolution.

One of the major challenges of using MR-guided interventions was the guide wire. The metallic part of the guide wires get heated up in the MR. However, MR-compatible guide wires are now developed with improved manoeuvrability [24, 25]. With the availability of the new MR-compatible and safe guide wire, certain percutaneous cardiac interventions will become feasible to perform solely under MR guidance in the future [119].

Regardless of the imaging modality used, blood vessel visualisation is important for all catheter based navigation procedures. An accurate segmentation and visualisation of the blood vessels help in better placement of valves and stents, for planning the size of stent and valve to be used with the information on radius of cross-section of the blood vessel, and also for 3D navigation of the catheter through the blood vessel. Recently catheter tip tracking methods were also implemented for use in MR-guided intervention [44]. The tracking methods will be greatly favoured with a pre-segmented model of blood vessels in which the tracked tip of the catheter could be shown during intervention.

3.2 Liver Resection Planning and Navigation

3.2.1 Liver

The liver is the largest organ in the body. It occupies a substantial portion of the upper abdominal cavity. It is a wedge shaped organ and its size varies according to age, sex and body size. The liver performs a wide variety of functions. It removes toxic substances, regulates blood glucose and lipids, breaks down amino acids, produces plasma proteins and immune factors and stores certain vitamins and minerals.

The liver is divided into eight (nine) independent functional segments according to Couinaud's division [29], as shown in Fig. 3.3. Each segment has its own vascular inflow, outflow and biliary drainage. The classification is based on the vascular supply in the liver. The right hepatic vein divides the right lobe into anterior and posterior segments. The left hepatic vein divides the left lobe into a medial and lateral part. The portal vein divides the liver into an upper and a lower segment. The left and right portal veins branch superior and inferior to project into the centre of each segment. Each segment can be resected without damaging the others because each one is a self-contained unit [122].

The liver receives its blood supply from two sources. The hepatic artery delivers 25% of the arterial blood to the liver. The portal vein delivers 75% of venous blood to the liver returning from the small intestine, stomach, pancreas and spleen. The terminal branches of the hepatic artery and hepatic portal vein empty together and mix as they enter into sinusoids in the liver. Blood flows through the sinusoids and empties into the central vein of each lobule. The hepatic vein arises from the central vein and carries out blood from the liver and empties into the vena-cava.

3.2.2 Resection

Primary liver cancer, which consists predominantly of Hepatocellular Carcinoma (HCC), is the fifth most common cancer worldwide and the third most common cause of cancer mortality [43]. The incidence of primary liver cancer is increasing in several developed countries and expected to continue increasing [13]. The liver is also a frequent target of metastases from other cancer origins, like colorectal, with an estimated 550,000 cases per year worldwide. In Norway, the most frequent liver neoplasms evaluated for surgical treatment are colorectal metastasis [88]. Liver resection is the treatment of choice with hepatic colorectal metastases [60, 115], even in recurrent cases [112], with 5 year survival rates of up to 40- 58% following resection [113].

Surgical resection of malignant liver tumours is the only curative therapy. Liver resection is also critical for a living donor transplantation programme and other non-oncologic surgical procedures. A successful surgery requires complete removal of the tumour including a safety margin while sparing as much healthy tissue as possible [99]. Safe hepatectomy with adequate tumour-free margins leads to a better prognosis [115]. Traditionally, this has been achieved performing a formal hepatectomy, where the affected lobe of the liver is removed. This is major

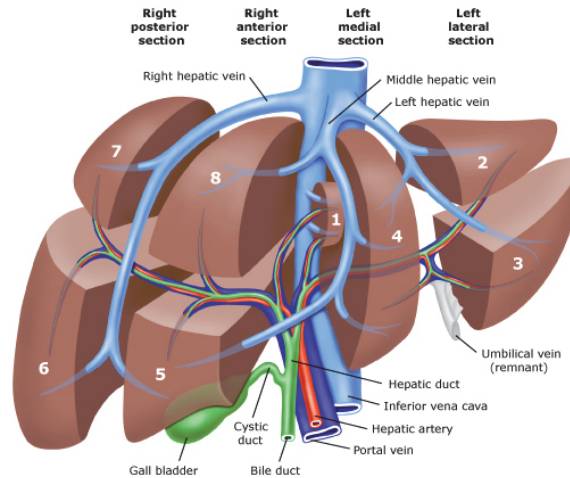


Figure 3.3: Segments of the liver. From [114]

surgery with possibility of serious complications. In addition, the formal liver resection leaves fewer options for repeated liver resections, in case the patients should get new tumours. Tumour recurrence occurs in up to 80% of cases [95]. Finally only 5-15% of the patients are eligible for resection [58, 96, 117].

Parenchyma-sparing liver resection is an alternative to the formal liver resection. With this technique the surgeon only removes the tumour, or sometimes the affected segments, from the liver of the patient. Thus, the patient in most cases will go through a smaller, less traumatising operation, enabling shorter hospital stay and earlier return to daily activities. But most importantly, as a significant part of the liver is spared during the first operation, the patient will have the possibility to go through new liver resections, should recurrence occur. The parenchymal-sparing technique is useful for multiple simultaneous liver resections. Increased use of a parenchymal-sparing approach is associated with decreased mortality without compromise in cancer-related outcome [50]. However, a good visualisation of the liver hepatic segments, blood vessels and tumour are essential for performing parenchymal sparing liver resection in a safer manner.

The main vessels in the liver are potential sources of major bleeding during liver resection, and controlling these is of great importance. 3D visualisation of the blood vessels, especially around the tumour would provide a better planning for liver resection. This minimises the risk of major bleeding, which can be costly both for the patient and the hospital. The introduction of laparoscopic liver resection is also changing many aspects of liver surgery, not least for the patients. Long term survival of laparoscopic resection is better than of open surgery [67]. Also, repeated resections are feasible, safe and oncologically adequate with a laparoscopic approach [111]. However, operating laparoscopically on a solid organ as the liver is very demanding, and necessitates meticulous studies of the anatomy of the patient in order to preoperatively create a safe plan for the operation. 3D visualisation of liver anatomy including blood vessels would be

a giant leap forward for laparoscopic liver surgery.

3.2.3 Planning and Navigation

In order to improve the clinical outcome in terms of surgery time, resectability and safety, a number of surgical planning and navigation systems have been proposed in the past few years. These systems are mainly based on the use of pre-operative images to generate a resection planning from the vascular system of the patient [93]. More recently, interactive visualisation tools, such as the Resection Map [74], PathFinder Explorer (www.pathnav.com), CAS-ONE (www.cascination.com) or others [20, 28, 30], have been proposed to increase the orientation understanding and confidence of the surgeon. During a laparoscopic liver resection, the surgeon sees only the surface of the liver with the laparoscopic camera. With the use of LUS (Laparoscopic Ultrasound) intraoperatively, the surgeons can understand the anatomy of blood vessels or bile ducts and find the precise tumour localisation [76], thus helping in marking the resection margins. When using 3D navigation, LUS helps to orient the pre-planned resection lines with the laparoscopic view.

Among the above mentioned liver resection planning systems, the market leading providers are CAS-ONE and Pathfinder Explorer. Both have in-depth planning systems, where the resection plane could be planned on 3D visualisations of blood vessels, tumour and liver. However, the segmentation and visualisation of blood vessels, tumour and liver, are done externally by MeVis (www.mevis.de) [19, 100, 105]. MeVis is currently the leading provider for distant services such as surgery planning for tumour resection. The Computed Tomography (CT) images taken of the liver are sent to MeVis, and after a few days, a completely segmented model is sent back. The models can then be used in the planning systems for planning appropriate resection plans. Therefore, having a planning platform with in-built segmentation and visualisation system will help in saving a lot of time and resources for liver resections. Fig. 3.4 shows the liver resection planning software, Hepa-Navi, developed at The Intervention Centre, Oslo University Hospital, for planning the liver resection plane and to guide the surgeon with his preplanned resection during the surgery. Currently, the blood vessel segmentation needed for the planning in Hepa-Navi is done externally by technical personnel using whole image vessel enhancement techniques with manual additions of unsegmented regions, which altogether takes a few hours for making the plan. Thus, having a fast and user-friendly blood vessel segmentation method in-built into the planning platform will help the surgeons to interact with the system themselves to make a good pre-operative plan.

A fast blood vessel segmentation will also greatly help in making an intra-operative update of the blood vessels. Though intra-operative updates are currently not performed during liver resections, they are widely used in brain surgery to understand the change in brain structure once the skull is opened [22, 26, 83]. A similar update could also be useful in liver surgery to understand the change in liver, blood vessel and tumour, from the pre-operative images to the time when the operation is to be performed. The two scenarios when the liver changes have to be understood are: when the abdomen is inflated for the laparoscopic surgery, and during

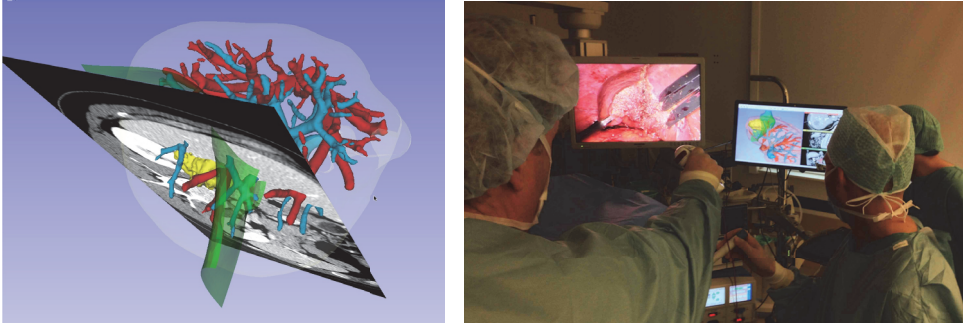


Figure 3.4: Left: 3D visualisation of the segmented blood vessels, liver and tumour, along with the resection plane for planning the liver resection. Right: Laparoscopic liver resection surgery performed with the help of pre-planned liver resections.

surgery when the liver is being moved a lot. The intra-operative images can be taken using MRI or ultrasound (US). Thus, having a fast and user friendly blood segmentation method in-built to the resection planning softwares will not only help the surgeons to make a fast pre-operative planning, but also help in updating the models with new segmentations taken intra-operatively.

Chapter 4

Summary of the Papers

4.1 Overview

In the following sections, we summarise the work done related to each of our thesis papers. The summary will include the aim that we had for each of our paper work, the methods used and the results obtained by applying these new methods. Below is a table highlighting the important points of each of the five thesis papers.

Paper	Aim	Methods	Results
I	Develop a seed initiated blood vessel centreline extraction method.	<ul style="list-style-type: none">- Novel modified multiscale vesselness filtering- Seed initiated localised centreline tracking by peak detection- Bifurcation detection by multiple peak detection	<ul style="list-style-type: none">- 5 times faster than traditional whole image analysis based centreline extraction- Centreline extraction error less than 1 voxel from ground-truth- Time taken for medical image 1 = 111s
II	Test the use of modified multi scale vesselness filter for clinical application, to study the movement of liver during breathing for future motion compensation in HIFU applications.	<ul style="list-style-type: none">- Modified multiscale vesselness filtering from Paper I- Centreline extraction by thinning- Iterative closest point based registration between liver breathholds	Average movement of liver is 3.66mm in left-right direction, 31.17mm in superior-inferior direction and 10.57mm in anterior-posterior direction, calculated with images of resolution 1mmx1mmx1mm
Continued on next page			

– continued from previous page

Paper	Aim	Methods	Results
III	Develop a fast and user-friendly blood vessel segmentation method along with centreline and radius estimation, using 2D cross-section analysis at vessel trunks and 3D volume analysis at vessel bifurcations.	<ul style="list-style-type: none"> - Seed initiated vessel cross-section tracking using eigenvectors - Vessel cross-sectional radius based bifurcation detection - Novel 2D circleness filter for vessel trunk analysis - 3D modified multiscale vesselness for vessel bifurcation analysis 	<ul style="list-style-type: none"> - 7 times faster than our Paper I method - Mean centreline error is 0.62 ± 0.17 voxels - Accuracy in bifurcating vessel detection is 100% detection from a radius of 3.5 voxels, above 90% detection from radii of 2 to 3.5 voxels, and above 70% detection from radii 1 to 2 voxels. - Time taken for medical image 1 = 21s
IV	Develop a fast and user-friendly blood vessel segmentation method along with centreline and radius estimation, using only 2D cross-sectional analysis at both vessel trunk and vessel bifurcation.	<ul style="list-style-type: none"> - Seed initiated vessel cross-section tracking using eigenvectors - Vessel cross-sectional radius, compactness and radius variance based bifurcation detection - Single scale circleness for trunk analysis and multiscale circleness for bifurcation analysis - Optional post-processing time with active contours 	<ul style="list-style-type: none"> - Processing time similar to Paper III. - Dice coefficient for blood vessel segmentation is $80\% \pm 2.7\%$, and $94\% \pm 2.4\%$ with post processing - Mean centreline error is less than 0.8 voxels and decreasing as the radius increases - Time taken for medical image 1 = 28s
V	Test our fast and user-friendly blood vessel segmentation on liver images.	<ul style="list-style-type: none"> - Image preprocessing : remapping, smoothing and resampling - Blood vessel segmentation from Paper III - Additive multiscale analysis for modified multiscale vesselness - Bifurcation restriction based on vessel tracking angle to limit leaking between vessels 	<ul style="list-style-type: none"> - Successfully segmented liver blood vessels with simultaneously showing the hepatic and portal separately labelled. - The time taken for preprocessing is around 11min, and for tracing and segmenting the whole liver vasculature is less than 2min. - Percentage of detection of blood vessels is 100% at $\geq 3\text{mm}$ and 80% at 2.5mm of radius.

4.2 Paper I

Extraction of blood vessel structure is important for improving planning, navigation and tracking in several interventional procedures. It is specifically relevant in catheter based procedures like stent graft positioning and valve replacement, and also in planning and navigation of laparoscopic liver resection. Centreline based registration methods have proven to be fast for clinical applications and an effective way of registering multi-modal images [7, 75, 103].

The most commonly used techniques for centreline extraction depends on extracting centrelines from pre-segmented vascular models. In these cases, the blood vessels are initially segmented through thresholding, model-based approaches, or multi-scale vessel segmentation [53, 101, 107], as explained in Chapter 2. The segmented output is then skeletonised or thinned, ending up with the final centreline [69]. The main disadvantage here is that these approaches are computationally expensive since they must process the whole image space to find a few connected blood vessels.

In this paper, we present a semi-automatic seed point based centreline extraction with local vessel enhancement. Our method lets the user select a single or multiple connected blood vessels of interest, thus reducing the potential noise of uninteresting voxels and also reducing the processing time.

Here, we have implemented a modified multi-scale vessel enhancement filter. Similar to Frangi *et al.*, Sato *et al.* and Erdt *et al.* [45, 53, 107], the proposed filter is also based on a Hessian matrix as in Eq. 2.1. As explained in Section 2.1, we incorporated into our filter advantages of both Erdt *et al.* and Frangi *et al.*, given as

$$V_{\sigma} = \begin{cases} 0 & \lambda_2 > 0, \lambda_3 > 0 \\ (1 - \frac{||\lambda_2| - |\lambda_3||}{|\lambda_2| + |\lambda_3|}) (\frac{2}{3} \lambda_1 - \lambda_2 - \lambda_3) (1 - e^{-\frac{S^2}{2c^2}}) & \end{cases} \quad (4.1)$$

where the eigenvalues are sorted as $|\lambda_1| \leq |\lambda_2| \leq |\lambda_3|$, and S is as shown in Eq. 2.5.

We also found that Eq. 4.1 gives exponentially reduced vessel response peak values as the scale is increased. To normalise this, we multiplied Eq. 4.1 with a scale dependent weighting term,

$$V = V_{\sigma} e^{k\sigma} \quad (4.2)$$

where σ is the current scale used for calculating V_{σ} , and k is a constant set to 0.5 based on initial experiments.

Finally, the multi-scale response is given by taking the maximum across all scales,

$$V_{multi} = \max_{\sigma_{min} \leq \sigma \leq \sigma_{max}} V \quad (4.3)$$

The centreline is extracted using a local computation of modified multi-scale vesselness. Fig. 4.1 *left*, shows a simple flowchart description of the centreline extraction method. The user selects a seed within the interesting connected blood vessel to extract the centreline. From a small 3D volume around the seed, the eigenvectors corresponding to the directions of the vessel are estimated when their corresponding eigenvalues are sorted as $|\lambda_1| \leq |\lambda_2| \leq |\lambda_3|$. Then, the modified multi scale vesselness is applied only

along the cross-section of the vessel using the cross-section eigenvectors, which gives a Gaussian-like profile. The actual centre is then calculated by finding the peak, as illustrated in Fig. 4.1 *Right*. From the centre, the next centre candidate is found by following along the vessel direction, which is the eigenvector along the vessel.

When the tracking reaches the bifurcation, there exists multiple peaks rather than just one as in vessel trunk. Each of these centres are then continued by tracking as before, and the tracking algorithm at any trunk terminates when the new centre candidate is outside the vessel.

The proposed method was evaluated using both synthetic and medical images. The synthetic images were created using VascuSynth software [63] and medical images were downloaded from the freely available DICOM medical image database of OSIRIX [1].

On comparing with a thresholded Frangi's vesselness output combined with Lee's thinning [53, 81], our method is shown to be approximately 5 times faster. The results also show that the proposed method is customised to detect only the desired blood vessels, thereby eliminating the detection of unwanted vessel-like structures. The centreline accuracy was evaluated by comparing with ground-truth data created by finding Hough circle centres at each cross-section of the vessel structure. The modified symmetric Hausdorff distance [41] between our result and the ground-truth was only approximately 1 pixel for both synthetic and medical images.

4.3 Paper II

Liver cancer remains the fifth most common malignancy in men and eight most common in women, with the number of cases estimated to be 550,000 per year worldwide. Surgical resection of the tumours is the main curative therapy. However, only 5-15% of the patients are eligible for resection [50, 96, 117]. Due to this, minimally invasive techniques such as radiofrequency ablation and high intensity focused ultrasound are emerging as potential alternatives [68, 91]. Liver blood vessel breathing movement information is important for improving the accuracy of these minimally invasive therapies. Liver breathing movement information can also show the importance of intra-operative update during a liver resection and thus it can be used for compensation.

In this paper, we presented a method for rigid registration of the centrelines obtained from the vascular structures of vessel-enhanced images of liver to conduct a pilot study on the movement of liver blood vessels during the breathing cycle. The study was conducted using MR images collected from three healthy volunteers and written informed consent was obtained from all the volunteers. The breath-hold scans were obtained at inhale and exhale positions.

As a preprocessing step to the proposed method, a rough liver mask was made to limit the region of interest for later processing. The proposed method starts with the application of our modified multi-scale vesselness, described in Paper I, to the whole image to obtain a vessel enhanced image of the MR liver image. Here we have decided to use the modified vessel enhancement filter, as it has an improved dampening of noise and a good Gaussian profile at the vessel cross-sections.

Following the vessel enhancement, the image was thresholded using the most commonly used automatic Otsu thresholding into a binary image. This gives a good starting point for 3D thinning to be performed on the image for obtaining the centreline [81]. In 3D thinning, the object's surface is eroded iteratively until only the skeleton remains. Erosion has to be performed symmetrically in order to guar-

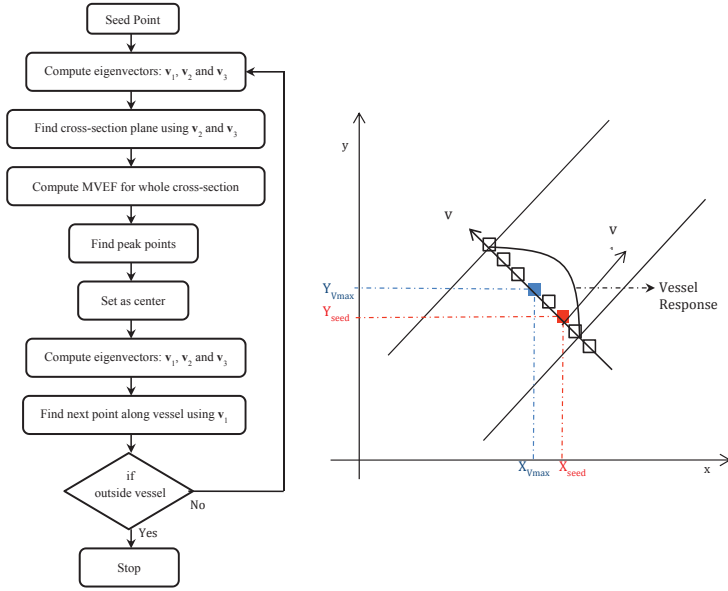


Figure 4.1: Left: Flowchart description of the centreline extraction method of Paper I; Right: 2D representation of the centre point extraction from the seed.

antee a medial position of the skeleton lines and in such a way that the object connectivity is preserved.

To find the centrelines of the blood vessels from the two breath-hold positions, the centrelines are registered to one another to understand their translation or movement. The registration here is performed using iterative closest point based registration. It iteratively revises the transformation (translation, rotation) needed to minimise the distance between the points of the two initial scans. The optimiser used for finding the minimum error in our approach was the Levenberg Marquadt (LM) optimiser. The LM algorithm is an iterative technique that locates a local minimum of a multivariate function that is expressed as the sum of squares of several non-linear, real-valued functions. As the optimiser finds the minimum error, the just found transformation gives the final translation or movement between the liver breath-holds.

The resulting average movement of the liver blood vessels from the inhale to exhale position was thus found to be 3.66mm in the x (left-right) direction, 31.17mm in y (superior-inferior) direction and 10.57mm in z (anterior-posterior) direction. The process of finding centrelines from the vessel thresholded models and their rigid registration took less than 20 seconds. The result gives important information in adjusting the minimally invasive therapies according to the liver movement during breathing. Also, the result proves the importance of having an intra-operative update of liver models during liver resection to account for liver movement.

4.4 Paper III

Results from Paper II have shown the importance of having a fast blood vessel segmentation and centreline extraction for intra-operative update of the models. The planning and navigation of interventional

procedures and catheterisation, requires a good knowledge of the blood vessels, centrelines and diameters at different cross-sections of blood vessels.

In this paper, we propose a novel combined blood vessel segmentation, centreline extraction and radius detection method, with the main aim of reducing the processing time, by processing only the blood vessel regions of the image. The novelty of the method is in performing only 2D cross-sectional analysis at the vessel trunk with our own circleness equation, which reduces the overall computing expense.

The proposed method works by tracing the blood vessel from a user provided initial position seed, direction seed and radius, to the end points of the continuous blood vessel structure. The direction seed, which is also a position, helps in setting the tracking direction by estimating the vector connecting the two positions. Similar to Paper I, eigenvectors are calculated to estimate the vessel directions. The vessel cross-vectors are then used to interpolate a 2D blood vessel cross-section image at the seed. Fig. 4.2 illustrates the overall flowchart of the process.

On determining the cross-section image, the vessel border is extracted by applying a Canny edge detection filter [18]. The radius is then calculated by propagating outwards from the seed towards the border along the vessel cross directions and an average of all the edge intensities is taken as the local adaptive threshold at that blood vessel cross-section.

At the vessel trunk, we formulated a new circle structure enhancement filter or circleness filter to give an output that resembles a Gaussian profile with its peak as the centre of the cross-section. The circleness method is based on 2D Eigen analysis of the 2D Hessian matrix obtained from the cross-section image. The circleness filter is given by,

$$C = (1 - e^{-C_R \alpha^2})(1 - e^{-\frac{s^2}{2\beta^2}}) \quad (4.4)$$

where C_R is circle enhancement ratio that gives a higher value at the center of the cross-section compared to pixels near the border, given by

$$C_R = \frac{|\lambda_{2D1} + \lambda_{2D2}|}{|\lambda_{2D2}| - |\lambda_{2D1}|} \quad (4.5)$$

The seed point for the next cross-section is then calculated along the vessel direction from the 3D position of the centre in the original image, and the new seed is saved into the seed list for further processing.

Our method works on the principle that there is a significant change in radius at the blood vessel bifurcation compared to the neighbouring blood vessel trunks. At a bifurcation, the modified multi-scale vesselness, as explained in Paper I, is performed at the volume around the bifurcation to estimate the different bifurcating vessel tracks. This makes two distinct peaks representing different bifurcating parts of the vessel.

The bifurcating vessel direction is calculated using Eigen analysis at each centre, and then used to find the next possible centre or seed locations at each of the bifurcating vessels. Finally, the new seeds are saved into the seed list, and the algorithm loop continues until seeds go out of the connected blood vessels or the image region.

Our proposed method was evaluated on five contrast enhanced MR angiogram images and three synthetic blood vessel-like images. Three of the medical images were obtained from the publicly available DICOM image database of the OSIRIX software [1] and the other two were obtained from the Institute of Medical Science and Technology, University of Dundee. The synthetic images were made from an

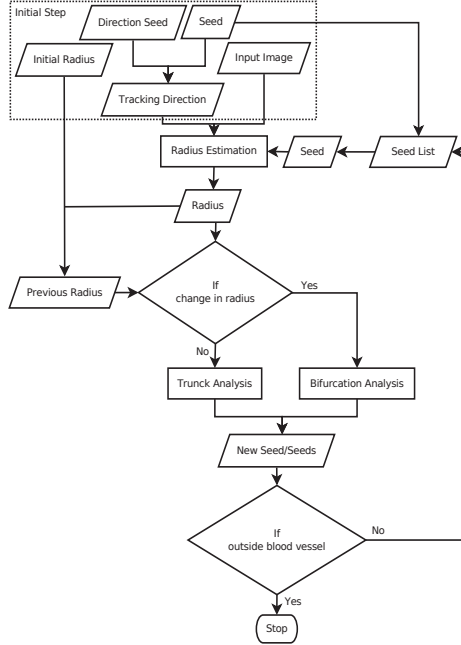


Figure 4.2: Overall process flowchart for Paper III

extension to the traditional Lindenmayer system [57], mentioned in Section 2.6.1.

When comparing the processing time for finding the blood vessel centreline, our proposed method was found to be on average more than 20 times faster than whole image processing by multi-scale vesselness [53] with thresholding and thinning [81] and more than 7 times faster than our own earlier method of blood vessel centreline extraction. Also, the centreline extraction was found to be accurate with a mean error less than 1 voxel in comparison to the corresponding geometric centres. Also, the percentage of bifurcating vessels not detected shows that accuracy in bifurcating vessel detection increases with increasing radius, with 100% detection from a radius of 3.5 voxels, above 90% detection from radii of 2 to 3.5 voxels, and above 70% detection from radii 1 to 2 voxels.

4.5 Paper IV

In this paper, we propose an alternate method of blood vessel segmentation, which is a variation of the method proposed in Paper III. The novelty of this method is in performing only 2D cross-sectional analysis for the whole tracking, including bifurcation analysis.

Similar to Paper III, the user initialises the tracking by setting a seed point, a direction seed point and an approximate blood vessel cross-section radius at the seed point. The cross-section image at the seed point is found using the eigen vectors at the seed. The vessel cross-section boundary is then found by Canny edge detection [18], and an approximate diameter of the cross-section is calculated by taking the maximum of the diameters along the cross-sectional eigenvectors from the seed to the cross-section border.

Here, the bifurcation is detected on the assumption that the contour of a vessel bifurcation cross-section is very different from the contour of a vessel trunk cross-section. The bifurcating vessel cross-section is thus identified by calculating the shape descriptors, such as compactness and radius variance [87]. Fig. 4.3 shows the change in shape descriptor values when the cross-section is a bifurcation.

Compactness is a measure of how circular a given contour is. It can be defined as

$$Compactness = P^2/A \quad (4.6)$$

where P is the perimeter of the vessel cross-section shape and A is the area of vessel cross-section. Here, the perimeter is calculated estimating the number of border pixels for the vessel cross-section and the area found by estimating the number of pixels representing the vessel cross-section. Radius variance is the variance in the distance from the centre candidate to the border points or the vessel cross-section contour.

Compared to Paper III for cross-sectional analysis, the proposed method uses the circleness filter for both vessel trunk analysis and vessel bifurcation analysis. A single-scale approach is used to enhance the cross-section at vessel trunks, while the multi-scale space approach is used to enhance the cross-section at vessel bifurcations. The multi-scale integration of the circleness is performed by taking the maximum across different scales, given as

$$C_{multi} = \max_{\sigma_{min} \leq \sigma \leq \sigma_{max}} C \quad (4.7)$$

where C is the single scale circleness described in Eq. 4.4, and σ_{min} is the minimum radius and σ_{max} is the maximum radius. σ_{max} is set as the radius of the cross-section, and σ_{min} is set as one-third the value of σ_{max} for detecting smaller bifurcations of down to one third the size of the radius. Thus using the circleness for the cross-sectional analysis, the algorithm proceeds in the tracking of the blood vessel cross-sections to the end of the connected blood vessel region.

Once the 3D blood vessel segmentation is obtained, the user is given an option to perform a post-processing, where the initial blood vessel segmentation output is set as a seed volume or contour for an active contour evolution [125], in order to smoothen the surface of the segmented vessel. The user then sets the region of interest, the processing intensity range, and the values for external and internal forces governing the flow of the contour, before starting the evolution. On completing the evolution, the final 3D blood vessel segmentation is well fitted to the original blood vessel.

The proposed method was applied on a set of eight images: four synthetic blood vessel images and four medical images. The synthetic and medical images were obtained in a similar way as in Paper III. Our validation has shown that the centreline error between our centre and the geometric centre of cross-section is below 0.8 pixels and also that the Dice coefficient for the segmentation is found to be $80\% \pm 2.7\%$. On combining our method with an optional active contour post-processing, the Dice coefficient for the resulting segmentation is found to be $94\% \pm 2.4\%$. The results show that the percentage of vessels detected is 100% at and above radius of 2.5 voxels for our proposed. However, the percentage of vessel detection reduces as the radius of vessel falls below 2 voxels for all the methods. Also, by restricting the image analysis to the interesting regions and converting most of the three-dimensional calculations to two-dimensional calculations, the processing of our method was in our experiments found to be more than 18 times faster than whole image multi-scale vesselness with thresholding and thinning, 8 times faster than user-initiated active contour segmentation with thinning and 7 times faster than our own previous method.

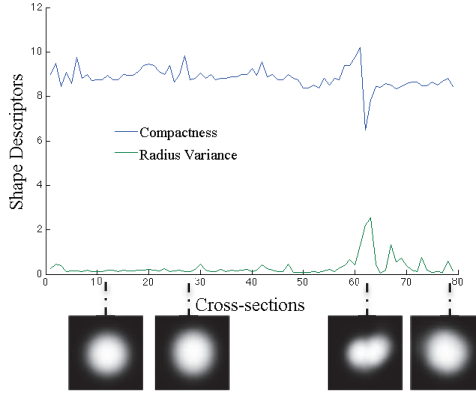


Figure 4.3: Shape descriptor values at various cross-sections of the blood vessel.

4.6 Paper V

Primary liver cancer, which consists predominantly of hepatocellular carcinoma, is the fifth most common cancer worldwide and the third most common cause of cancer mortality [43]. The incidence of primary liver cancer is increasing in several developed countries and expected to continue increasing [13]. Liver resection is the treatment of choice for patients with different types of liver tumours, including metastases of colorectal cancer, hepatocellular carcinoma and some types of another primary and metastatic tumours, with 5-year survival rates of 40-58% following resection [112, 113, 115]. The resection of liver requires extra thorough planning of individual surgical strategy, especially when a non-anatomical parenchyma-sparing technique is concerned. A 3D visualisation of liver blood vessels will greatly help in better planning of liver resection.

We present a simple, user-friendly and fast method for 3D modelling of liver vascular structures. This method can be useful for preoperative planning and intra-operative navigation of liver resection, both with laparoscopic and open access. The work done in the paper is a clinical adaptation of the method in Paper III. The methods used here for liver blood vessel segmentation are divided into preprocessing, blood vessel segmentation and segmentation leak restriction.

The first step in the liver blood vessel segmentation is to pre-process the data to enhance the blood vessel intensity range and smooth out the noises. Within the preprocessing step, the images are first remapped to a CT number or Hounsfield unit (HU) range of the CT image which corresponds to the densities near to contrast-enhanced blood. Followed by curvature flow smoothing of the image to denoise the image, while preserving the blood vessel edges. The preprocessing step concludes by resampling the resulting image to an isotropic 1mm voxel image for later structural analysis.

After the preprocessing of the image, the next step is to segment the blood vessels using the seed based blood vessel tracking method described in Paper III. A change from the method of Paper III is that we have an additive multiscale integration of modified multiscale vesselness compared to the usually used maximum of scales. This helps in reducing the diffusion between nearby tubes and also the filter enhances towards the centre of the vessel cross-section.

The last step in the liver blood vessel segmentation is the vessel direction deviation based leak restriction. Here, the angle between the current branch direction and its grandparent branch is checked to

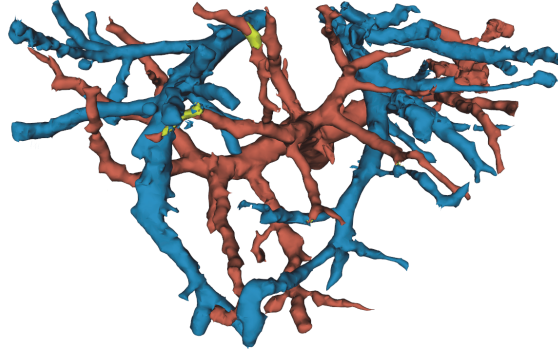


Figure 4.4: Hepatic and portal blood vessels segmented using the proposed method in Paper V. Blue represents the hepatic vein, red represents the portal vein, and the yellow represents the region segmented as both hepatic and portal vein. The yellow region is the leak of our method from hepatic to portal or vice versa.

estimate the deviation in angle. A branch with a huge deviation in angle is considered as a leak branch and the tracking in the branch is stopped. Also measured is the vessel bifurcating angle, which is angle between the vessel tracking vectors before and after the bifurcation. The user is given an option to adjust the vessel bifurcating angle range to limit the abrupt deviations in vessel tracking directions that might be related to leaking.

The data used in the study are CT images of patients acquired with contrast enhanced portal phase. Fig. 4.4 shows a hepatic and portal blood vessel segmentation output by the use of the proposed method. The results show that the processing time taken for the liver blood vessel segmentation is less than 2min. However, the preprocessing time was at an average 11min. Also, the percentage of detection of blood vessels by the proposed method was found to be 100% for all blood vessels of radius at and above 3mm, 80% at 2.5mm, 70% at 2mm and 50% at 1.5mm.

Chapter 5

Discussion

Visualisation of blood vessels is crucial for many clinical procedures for diagnosis, planning and navigation. This is especially important in interventional procedures, such as catheter navigation and liver resection. In the case of catheter navigation a fast intra-operative update of blood vessels with the extra information of their centrelines and radius, will provide a good base for navigation of the catheter, as well as placement and selection of valves or stents according to the size of the blood vessel. In the case of liver resection, fast blood vessel segmentation can help to 3D model the liver vasculature for planning the resection, and provide faster update of the blood vessels during intra-operative procedure.

In our thesis, we have worked on developing a fast and user-friendly method for blood vessel segmentation for interventional planning and navigation. During the period, we developed one method for centreline extraction (Paper I), and two methods for blood vessel segmentation, centreline extraction and radius estimation (Paper III & IV). The methods in Paper III and Paper IV are extensions of Paper I, and are also much faster than Paper I. In Paper II, we studied the movement of liver blood vessels to understand the need for fast intra-operative update of blood vessel models, and in Paper V, we used clinical adaptation of the method described in Paper III for liver resection planning. Fig. 5.1 illustrates the link between the papers.

In Paper I, we developed a semi-automatic seed point based centreline extraction method. For our method, we developed a *modified multiscale vesselness*, which has better dampening of noise and steeper Gaussian-like profiles at the vessel cross-sections compared to commonly used vessel enhancement methods. We used the Hessian-related eigenvectors for tracking the centres along the direction of the blood vessel. The method as such was proven to be faster than methods which would require whole image processing for centreline extraction, such as a vessel enhancement followed by thinning. However, the processing time for the method was seen to increase with increased complexity or increase in the number of bifurcations.

The idea behind the Paper I method was to only detect blood vessels that are of interest to the user, which helped in reducing the processing time. However, the processing was not performed just within the interesting vessel region, as the Hessian analysis was performed for the whole image. Only the calculations related to modified multi-scale vesselness and centreline tracking were performed solely on the voxels within the vessel region. Still, this helped to reduce the processing time, and also eliminated the artefacts caused by vessel-like structures, which would otherwise be created with whole image analysis.

In Paper II, we developed a rigid registration method to register between liver blood vessels of inhale and exhale breath-holds. The method was developed to study the range of movement of the liver blood

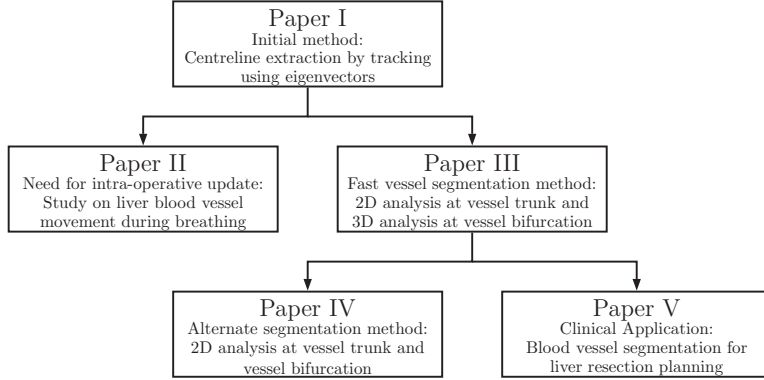


Figure 5.1: Illustration on the link between papers.

vessels to understand the need for an intra-operative update of blood vessels. The study would also give an insight into improving the accuracy of minimally invasive therapies such as high intensity focused ultrasound and radio frequency ablation. Here, we have used our modified multi-scale vesselness from Paper I for vessel enhancement, as our vesselness has the advantage of detecting properly connected vessels from Erdt *et al.* [45] and the strength in suppression of background noise from Frangi *et al.* [53]. Thus this work also provided us with knowledge of how the modified multi-scale vesselness method from Paper I performed on liver images.

After the vessel enhancement, the results were thresholded and then 3D thinned to obtain the centreline. The resulting centrelines were then registered using iterative closest point based registration to understand the movement of liver during the breathing cycle. Since the work was just an initial study of basic understanding, only three volunteers' liver MR images were used. In the translations of the liver blood vessels obtained from the three volunteers, two had more similar translations of liver blood vessels during breathing than the third volunteer. This was a result of increased inhalation and exhalation by the third volunteer to hold the breath for longer periods. Thus, for more accurate understanding of liver movement during breathing, the study has to be performed on a larger group of volunteers. Still, the results from the paper provide a basic understanding of how much the liver moves during breathing, which asserts the need for intra-operative update of blood vessels.

An intra-operative update of blood vessels requires a fast segmentation and visualisation of blood vessels. During the work of Paper II, we realised that our Paper I method was not fast enough in segmenting a number of bifurcations and also that the method failed when the blood vessel structures become very complex. This led us to develop the method in Paper III, which is much faster than the Paper I method. This method processes completely only the voxels of the interesting regions of the blood vessel. However, here it is found that the processing time increases with the increase in percentage of blood vessel volume in the whole image, and with increasing number of bifurcations. This increased processing time is still shown to be less than the processing time taken for methods related to whole image analysis.

The most critical step in the Paper III method is the bifurcation detection, as the bifurcation can be missed if the tracked centre is too far into the vessel. However, our results on the analysis of the accuracy of the bifurcation vessel detection implies that the chance of missing a bifurcation is higher only at very small vessels with radius of around 1 voxel, which are less important for planning and navigation

purposes.

A alternative method of blood vessel segmentation is explained in Paper IV. The Paper IV method is a variation of the method in Paper III; the former uses only 2D cross-sectional analysis for the whole tracking, but the latter uses 2D cross-sectional analysis at the vessel trunks and 3D volume analysis at the bifurcations. Also, the bifurcation detection in Paper IV is based on the knowledge that the contour of a vessel bifurcation cross-section is very different from the contour of a vessel trunk cross-section, whereas in Paper III, the bifurcation detection is based on the knowledge that there is significant change in radius at the vessel bifurcation compared to the neighbouring vessel trunks.

In Paper IV for the centreline validation, the centre calculated at each vessel cross-section was compared to its geometric centre. One pixel is the minimum centre error that can occur at each vessel cross-section. The centre error decreases with increasing radius, where the centre error is the highest at 1 pixel radius with 0.75 pixels error and least at 7 pixels radius with 0.09 pixels error.

The segmentation output of the Paper IV method without post-processing differ from the segmentation output of whole image analysis method, as our method has more false positives and less false negatives than the whole image analysis method. This is proven by higher precision and lower sensitivity for the proposed method without post-processing compared to Frangi's vesselness method. Lower sensitivity for the proposed method without post-processing is due to the gaps in vessel segmentation, particularly at areas where there is a sudden change in the vessel-tracking angle and also at bifurcations where there is a bigger shift in seed positions. These gaps could later be filled with the use of the post-processing step, which is an optional step for the user to smooth surface of the segmented blood vessel and fit well to the original blood vessel. In synthetic images, the measurements show that the segmentation from the user-initiated active contour segmentation is similar to the proposed method with the post-processing step. However, on visual evaluation of medical images, active contour segmentation detects less bifurcations than the proposed method without post-processing.

A drawback for both our blood vessel segmentation methods discussed in Paper III and Paper IV, is that the algorithm might stop tracking at vessel abnormalities (e.g. aneurysms) and vessel gaps. The reason behind this is that our method works by analysing the tubular or circular structural information during vessel tracking. Still, a deeper analysis has to be done to estimate to what extent our methods might fail in these situations. To overcome this drawback, in the future work we propose to detect small gaps in the connected blood vessels with an angle based search at the end points and on detecting abnormalities such as aneurysms in blood vessels, to incorporate spherical structure detection when the tracking reaches an abnormal structure.

Although the alternate blood vessel segmentation method by tracking solely by 2D cross-sectional analysis in Paper IV was made to reduce the processing time, the processing time for Paper III and Paper IV are almost the same. This is due to the need of extra cross-sectional contour analysis for Paper IV. In Paper V for liver blood vessel segmentation, we use the method from Paper III, as 3D bifurcation analysis would give better vessel direction calculation corresponding to new bifurcation seed. Also, the Paper III when compared to Paper IV will not need any extra pre-processing step, as no gaps are formed at bifurcations with 3D analysis at the bifurcation.

The results from the liver blood vessel segmentation were validated by measuring the percentage of detection of blood vessels. The validation results show that our proposed method detects 100% of the blood vessels from 3mm radius and above, 80% at 2.5mm radius and reduces further as the radius reduces. The most important vessels for resection planning are from a diameter of 5mm (radius of

2.5mm), because small vessels can be coagulated with many modern devices. Also the processing time for tracking and segmenting hepatic-portal blood vessels was less than 2min. The preprocessing step required for the liver blood vessel segmentation takes around 11min of processing, making the present method not suitable for intra-operative blood vessel segmentation. However, blood vessel segmentation could be used intra-operatively in the future, by GPU processing of the preprocessing step as it can be parallelised.

In Paper V, we also implemented a leak restriction of the blood vessel segmentation tracking into overlapped blood vessels, using vessel direction based procedure. However, results show that there are still some leaks that occur with our algorithm. In the segmentation result we have given the leaked region a different label than hepatic and portal veins, to leave the final decision making of where the leaked region belongs to the user. It is to be noted that though leaks occur with our algorithm, these leaks are minimised by the vessel direction based leak restriction procedure. Otherwise, the leaks could have easily spread into the whole of the non-connected vessel.

Our liver blood vessel segmentation does not always provide smooth hepatic or portal vessel, as the local segmentation output depends solely on how the contrast enhanced blood vessel is represented in the CT image. In the future work, we would like to make 3D models of the blood vessels with the centreline and radius information that we gather during segmentation, which would greatly help in obtaining smooth 3D visualisation of blood vessels.

Chapter 6

Conclusion and Future Work

A correct segmentation of blood vessels is of major importance in many medical applications, e.g. diagnosis, surgical planning, navigation, simulation and training. A good blood vessel segmentation can help in planning and navigation of many interventional procedures. It is well accepted that there is no general purpose segmentation method suitable for all applications and imaging modalities. As such, the problem has been approached from many disciplines using many different methods, as shown in Chapter 2.

In this thesis work, we have developed fast and user-friendly methods for blood vessel segmentation, which could be applied for multiple contrast enhanced images of imaging modalities. During the process of its development, we implemented novel filters that helped in enhancing the structures. A modified multiscale vessel enhancement was developed, incorporating the advantages of both Frangi *et al.* [53] and Erdt *et al.* [45]. The new enhancement filter gave better dampening of noise and steeper Gaussian-like profiles at the vessel cross-sections. Also, a circle enhancement filter was developed using the eigenvalue analysis, that outputs a centre enhanced circle detection. The circle enhancement filter or circleness filter is applied on 2D vessel cross-sections to provide a single peak at the centre of vessel cross-section with single-scale analysis and multiple peaks at the bifurcation with multi-scale analysis.

The methods developed in this thesis work, is a centreline based tracking of blood vessels using eigenvectors calculated at the centre of the blood vessel cross-section. We have also proposed two bifurcation detection methods, by either detecting a significant change in radius at adjacent cross-sections, or by detecting the change in vessel contour from a vessel trunk to a vessel bifurcation. The final fast blood vessel segmentation methods that we proposed vary in their bifurcation detection and analysis. In one method, the bifurcation analysis is performed using multi-scale modified vesselness at a 3D volume around the bifurcation cross-section, and the other method use multi-scale circleness at the 2D bifurcation cross-section. The results have shown that both the methods work well in segmenting blood vessel structures from synthetic and medical images. However, we have used the method with 3D analysis at the bifurcation for our clinical application, as it might not require a post-processing step to fill the gaps caused by 2D analysis at the bifurcation. Our blood vessel segmentation won the Best Innovative Idea award from Inven2, Oslo, Norway, and it is currently filed for a patent.

Our study on liver blood vessel movement during breathing gave a better understanding of the need of an intra-operative update for interventional procedures. An intra-operative update, which in-turn require a fast blood vessel segmentation method. The study shows that the average movement of liver hepatic and portal vein system from inhale position to exhale position is 3.66mm in x direction (left-right direction), 31.17mm in y direction (superior-inferior direction) and 10.57mm in z direction (anterior-

posterior direction).

Finally, our blood vessel segmentation method was clinically tested to visualise liver blood hepatic-portal system for liver resection planning. The segmentation results validation has shown that the percentage of detection of blood vessels by the proposed method was found to be 100% of all blood vessels at and above 3mm and 80% at 2.5mm of radius. Thus our method finds the important range of blood vessels that are vital for the liver resection planning. Also the processing time was found to be only less than 2min to segment the whole hepatic and portal liver blood vessel system. However, the preprocessing step took around 11min of processing time, which could be improved in the future work by a GPU implementation as the pre-processing step could be easily parallelised.

In the future work, we would work on testing the method for catheter navigation applications, especially with the use of MR as the interventional imaging. The method will also be tested further on liver for more patient datasets, and will be implemented into our liver planning and navigation system, Hepa-Navi. A more in-depth clinical study will also be conducted on a larger dataset of patient data to get further insight into the movement of liver blood vessels during breathing. This information can be valuable for adjusting the HIFU delivery and RFA ablation techniques. Also a branch-wise analysis of liver blood vessels will be conducted to automatically classify liver into its segments. In this thesis, we have not focused on the pre-processing step, but a GPU implementation of mainly the preprocessing for liver blood vessel segmentation will be performed to reduce the whole processing time for the segmentation to just a couple of minutes. We will also work on the possibilities of applying filters locally at the just region of interest and also into other variations of pre-processing filters. Thus making the method fast enough to be used intra-operatively, if the liver blood vessel segmentation models have to be updated from new images taken during the operation.

References

- [1] Osirix dicom database. url <http://www.osirix-viewer.com/datasets/>.
- [2] Transcatheter aortic valve replacement (TAVR) - endovascular - raney zusman medical group.
- [3] Salem Saleh Al-Amri, Namdeo V Kalyankar, et al. Image segmentation by using threshold techniques. *arXiv preprint arXiv:1005.4020*, 2010.
- [4] Fritz Albregtsen. Non-parametric histogram thresholding methods-error versus relative object area. In *Proceedings of the Scandinavian Conference on Image Analysis*, volume 1, pages 273–273, 1993.
- [5] Tuomas Alhonnoro, Mika Pollari, Mikko Lilja, Ronan Flanagan, Bernhard Kainz, Judith Muehl, Ursula Mayrhofer, Horst Portugaller, Philipp Stiegler, and Karlheinz Tscheliessnigg. Vessel segmentation for ablation treatment planning and simulation. In *Medical Image Computing and Computer-Assisted Intervention–MICCAI 2010*, pages 45–52. Springer, 2010.
- [6] Stephen R Aylward and Elizabeth Bullitt. Initialization, noise, singularities, and scale in height ridge traversal for tubular object centerline extraction. *IEEE Transactions on Medical Imaging*, 21(2):61–75, 2002.
- [7] Stephen R Aylward, Julien Jomier, Sue Weeks, and Elizabeth Bullitt. Registration and analysis of vascular images. *International Journal of Computer Vision*, 55(2-3):123–138, 2003.
- [8] Peter Bankhead, C. Norman Scholfield, J. Graham McGeown, and Tim M. Curtis. Fast retinal vessel detection and measurement using wavelets and edge location refinement. *PLoS ONE*, 7(3):e32435, March 2012.
- [9] Christian Bauer and Horst Bischof. A novel approach for detection of tubular objects and its application to medical image analysis. In *Pattern Recognition*, pages 163–172. Springer, 2008.
- [10] Christian Bauer, Thomas Pock, Erich Sorantin, Horst Bischof, and Reinhard Beichel. Segmentation of interwoven 3D tubular tree structures utilizing shape priors and graph cuts. *Medical image analysis*, 14(2):172–184, 2010.
- [11] Fethallah Benmansour and Laurent D Cohen. Tubular structure segmentation based on minimal path method and anisotropic enhancement. *International Journal of Computer Vision*, 92(2):192–210, 2011.

- [12] Andreas Biesdorf, Karl Rohr, Duan Feng, Hendrik von Tengg-Kobligk, Fabian Rengier, Dittmar Böckler, Hans-Ulrich Kauczor, and Stefan Wörz. Segmentation and quantification of the aortic arch using joint 3D model-based segmentation and elastic image registration. *Medical image analysis*, 16(6):1187–1201, 2012.
- [13] F Xavier Bosch, Josepa Ribes, Mireia Díaz, and Ramon Cléries. Primary liver cancer: worldwide incidence and trends. *Gastroenterology*, 127(5):S5–S16, 2004.
- [14] Tobias Boskamp, Daniel Rinck, Florian Link, Bernd Kummerlen, Georg Stamm, and Peter Mildenerger. New vessel analysis tool for morphometric quantification and visualization of vessels in CT and MR imaging data sets 1. *Radiographics*, 24(1):287–297, 2004.
- [15] Yuri Boykov and Gareth Funka-Lea. Graph cuts and efficient nd image segmentation. *International journal of computer vision*, 70(2):109–131, 2006.
- [16] Yuri Boykov and Vladimir Kolmogorov. An experimental comparison of min-cut/max-flow algorithms for energy minimization in vision. *IEEE Transactions on Pattern Analysis and Machine Intelligence*, 26(9):1124–1137, 2004.
- [17] Yuri Boykov, Olga Veksler, and Ramin Zabih. Fast approximate energy minimization via graph cuts. *IEEE Transactions on Pattern Analysis and Machine Intelligence*, 23(11):1222–1239, 2001.
- [18] John Canny. A computational approach to edge detection. *IEEE Transactions on Pattern Analysis and Machine Intelligence*, (6):679–698, 1986.
- [19] David M Cash, Michael I Miga, Sean C Glasgow, Benoit M Dawant, Logan W Clements, Zhujiang Cao, Robert L Galloway, and William C Chapman. Concepts and preliminary data toward the realization of image-guided liver surgery. *Journal of Gastrointestinal Surgery*, 11(7):844–859, 2007.
- [20] Yen-Wei Chen, Masaki Kaibori, Tsukasa Shindo, Kousuke Miyawaki, Amir H Foruzan, Tomoko Tateyama, Xian-Hua Han, Kosuke Matsui, Takumi Tsuda, and A-Hon Kwon. Computer-aided liver surgical planning system using CT volumes. In *2013 35th Annual International Conference of the IEEE Engineering in Medicine and Biology Society (EMBC)*, pages 2360–2363. IEEE, 2013.
- [21] Yanling Chi, Jimin Liu, Sudhakar K. Venkatesh, Su Huang, Jiayin Zhou, Qi Tian, and Wieslaw L. Nowinski. Segmentation of liver vasculature from contrast enhanced CT images using context-based voting. *IEEE Transactions on Biomedical Engineering*, 58(8):2144–2153, August 2011.
- [22] Olivier Clatz, Hervé Delingette, I-F Talos, Alexandra J Golby, Ron Kikinis, Ferenc A Jolesz, Nicholas Ayache, and Simon K Warfield. Robust nonrigid registration to capture brain shift from intraoperative MRI. *IEEE Transactions on Medical Imaging*, 24(11):1417–1427, 2005.
- [23] Kevin Cleary and Terry M Peters. Image-guided interventions: technology review and clinical applications. *Annual review of biomedical engineering*, 12:119–142, 2010.

- [24] Helene Clogenson, John van den Dobbelsteen, and Jenny Dankelman. MRI-compatible guide-wire with improved maneuverability for endovascular interventions. *Journal of Medical Devices*, 6(1):017581, 2012.
- [25] Hélène CM Clogenson, Jenny Dankelman, and John J van den Dobbelsteen. Steerable guidewire for magnetic resonance guided endovascular interventions. *Journal of Medical Devices*, 8(2):021002, 2014.
- [26] Roch M Comeau, Abbas F Sadikot, Aaron Fenster, and Terry M Peters. Intraoperative ultrasound for guidance and tissue shift correction in image-guided neurosurgery. *Medical Physics*, 27(4):787–800, 2000.
- [27] F. Conversano, E. Casciaro, R. Franchini, S. Casciaro, and A Lay-Ekuakille. Fully automatic 3D segmentation measurements of human liver vessels from contrast-enhanced CT. In *2014 IEEE International Symposium on Medical Measurements and Applications (MeMeA)*, pages 1–5, June 2014.
- [28] Francesco Conversano, Roberto Franchini, Christian Demitri, Laurent Massoptier, Francesco Montagna, Alfonso Maffezzoli, Antonio Malvasi, and Sergio Casciaro. Hepatic vessel segmentation for 3D planning of liver surgery: experimental evaluation of a new fully automatic algorithm. *Academic radiology*, 18(4):461–470, 2011.
- [29] Claude Couinaud. *Surgical anatomy of the liver revisited*. C. Couinaud, 1989.
- [30] Henrique G Debarba, Dinamar J Zanchet, Daiane Fracaro, Anderson Maciel, and Antonio N Kalil. Efficient liver surgery planning in 3D based on functional segment classification and volumetric information. In *2010 Annual International Conference of the IEEE Engineering in Medicine and Biology Society (EMBC)*, pages 4797–4800. IEEE, 2010.
- [31] Maryam Taghizadeh Dehkordi, Morteza Jalalat, Saeed Sadri, Alimohamad Doosthoseini, Mohammad Reza Ahmadzadeh, and Rasoul Amirfattahi. Vesselness-guided active contour: A coronary vessel extraction method. *Journal of Medical Signals and Sensors*, 4(2):150–157, 2014.
- [32] Jamshid Dehmeshki, D Amin, Manlio Valdivieso, and Xujiong Ye. Segmentation of pulmonary nodules in thoracic CT scans: a region growing approach. *IEEE Transactions on Medical Imaging*, 27(4):467–480, 2008.
- [33] Konstantinos K. Delibasis, Aristides I. Kechriniotis, C. Tsonos, and Nicholas Assimakis. Automatic model-based tracing algorithm for vessel segmentation and diameter estimation. *Computer Methods and Programs in Biomedicine*, 100(2):108–122, November 2010.
- [34] Maxime Descoteaux, D Louis Collins, and Kaleem Siddiqi. A geometric flow for segmenting vasculature in proton-density weighted MRI. *Medical image analysis*, 12(4):497–513, 2008.
- [35] Klaus Drechsler. *Extraction of Hepatic Veins in Contrast Enhanced CT with Application to Interventional Planning*. PhD thesis, 2012.

- [36] Klaus Drechsler and Cristina Oyarzun Laura. Comparison of vesselness functions for multiscale analysis of the liver vasculature. In *10th IEEE International Conference on Information Technology and Applications in Biomedicine (ITAB)*, pages 1–5. IEEE, 2010.
- [37] Klaus Drechsler and Cristina Oyarzun Laura. A novel multiscale integration approach for vessel enhancement. In *2010 IEEE 23rd International Symposium on Computer-Based Medical Systems (CBMS)*, pages 92–97. IEEE, 2010.
- [38] Klaus Drechsler, Steven Meixner, Cristina Oyarzun Laura, and Stefan Wesarg. A framework for validation of vessel segmentation algorithms. In *2013 IEEE 26th International Symposium on Computer-Based Medical Systems (CBMS)*, pages 518–519. IEEE, 2013.
- [39] Klaus Drechsler, C. Oyarzun Laura, and Stefan Wesarg. Interventional planning of liver resections: An overview. In *Engineering in Medicine and Biology Society (EMBC), 2012 Annual International Conference of the IEEE*, pages 3744–3747. IEEE, 2012.
- [40] Klaus Drechsler, Cristina Oyarzun Laura, and Stefan Wesarg. Hepatic vein segmentation using wavefront propagation and multiscale vessel enhancement. pages 86691A–86691A, March 2013.
- [41] M-P Dubuisson and Anil K Jain. A modified hausdorff distance for object matching. In *Proceedings of the 12th IAPR International Conference on Pattern Recognition, 1994. Vol. 1-Conference A: Computer Vision & Image Processing.*, volume 1, pages 566–568. IEEE, 1994.
- [42] S Eiho, H Sekiguchi, N Sugimoto, T Hanakawa, and S Urayama. Branch-based region growing method for blood vessel segmentation. In *Proceedings of International Society for Photogrammetry and Remote Sensing Congress*, pages 796–801, 2004.
- [43] Hashem B El-Serag and K Lenhard Rudolph. Hepatocellular carcinoma: epidemiology and molecular carcinogenesis. *Gastroenterology*, 132(7):2557–2576, 2007.
- [44] Abubakr Eldirdiri, Frédéric Courivaud, Rafael Palomar, Per Kristian Hol, and Ole Jakob Elle. Catheter tip tracking for MR-guided interventions using discrete kalman filter and mean shift localization. *International journal of computer assisted radiology and surgery*, 9(2):313–322, 2014.
- [45] Marius Erdt, Matthias Raspe, and Michael Suehling. Automatic hepatic vessel segmentation using graphics hardware. In *Medical Imaging and Augmented Reality*, pages 403–412. Springer, 2008.
- [46] Simon Esneault, Cyril Lafon, and J-L Dillenseger. Liver vessels segmentation using a hybrid geometrical moments/graph cuts method. *IEEE Transactions on Biomedical Engineering*, 57(2):276–283, 2010.
- [47] R Fedkiw and S Osher. Level set methods and dynamic implicit surfaces. *Surfaces*, 44:77, 2002.
- [48] Yang Fei and Jong Won Park. Automatic segmentation of liver blood vessels using level set method. In *International Conference on Audio, Language and Image Processing, 2008. ICALIP 2008.*, pages 1718–1720. IEEE, 2008.

- [49] Amir H Foruzan, Reza A Zoroofi, Yoshinobu Sato, and Masatoshi Hori. A hessian-based filter for vascular segmentation of noisy hepatic ct scans. *International journal of computer assisted radiology and surgery*, 7(2):199–205, 2012.
- [50] Dominique Franco, Lorenzo Capussotti, Claude Smadja, Hedayat Bouzari, Jonathan Meakins, Francois Kemeny, Didier Grange, and Mario Dellepiane. Resection of hepatocellular carcinomas. *Gastroenterology*, 98:733–738, 1990.
- [51] Alejandro F Frangi, Wiro J Niessen, Romhild M Hoogeveen, Theo Van Walsum, and Max A Viergever. Model-based quantitation of 3D magnetic resonance angiographic images. *IEEE Transactions on Medical Imaging*, 18(10):946–956, 1999.
- [52] Alejandro F Frangi, Wiro J Niessen, Romhild M Hoogeveen, Theo van Walsum, and Max A Viergever. Quantitation of vessel morphology from 3D MRA. In *Medical Image Computing and Computer-Assisted Intervention—MICCAI’99*, pages 358–367. Springer, 1999.
- [53] Alejandro F Frangi, Wiro J Niessen, Koen L Vincken, and Max A Viergever. Multiscale vessel enhancement filtering. In *Medical Image Computing and Computer-Assisted Intervention—MICCAI’98*, pages 130–137. Springer, 1998.
- [54] Moti Freiman, Noah Broide, Miriam Natanzon, Einav Nammer, Ofek Shilon, Lior Weizman, Leo Joskowicz, and Jacob Sosna. Vessels-cut: a graph based approach to patient-specific carotid arteries modeling. In *Modelling the Physiological Human*, pages 1–12. Springer, 2009.
- [55] Yonatan Fridman, Stephen M Pizer, Stephen Aylward, and Elizabeth Bullitt. Segmenting 3D branching tubular structures using cores. In *Medical Image Computing and Computer-Assisted Intervention-MICCAI 2003*, pages 570–577. Springer, 2003.
- [56] Jacob David Furst. *Height ridges of oriented medialness*. PhD thesis, 1999.
- [57] Miguel A Galarreta-Valverde, Maysa MG Macedo, Choukri Mekkaoui, and Marcel P Jackowski. Three-dimensional synthetic blood vessel generation using stochastic l-systems. In *SPIE Medical Imaging*, pages 86691I–86691I. International Society for Optics and Photonics, 2013.
- [58] Jason S Gold, Chandrakanth Are, Peter Kornprat, William R Jarnagin, Mithat Gönen, Yuman Fong, Ronald P DeMatteo, Leslie H Blumgart, and Michael D’Angelica. Increased use of parenchymal-sparing surgery for bilateral liver metastases from colorectal cancer is associated with improved mortality without change in oncologic outcome: trends in treatment over time in 440 patients. *Annals of surgery*, 247(1):109–117, 2008.
- [59] Gösta H Granlund and Hans Knutsson. *Signal processing for computer vision*, volume 2. Springer, 1995.
- [60] RT Grundmann, P Hermanek, S Merkel, CT Germer, J Hauss, D Henne-Bruns, K Herfarth, UT Hopt, T Junginger, E Klar, et al. Diagnosis and treatment of colorectal liver metastases-workflow. *Zentralblatt für Chirurgie*, 133(3):267–284, 2008.

- [61] Ghassan Hamarneh and Preet Jassi. VascuSynth: Simulating vascular trees for generating volumetric image data with ground-truth segmentation and tree analysis. *Computerized Medical Imaging and Graphics*, 34(8):605–616, December 2010.
- [62] Eric M. Isselbacher. Thoracic and abdominal aortic aneurysms.
- [63] Preet Jassi and Ghassan Hamarneh. Vascusynth: Vascular tree synthesis software. *Insight J.*, 2011.
- [64] Philipp Kahlert, Nina Parohl, Juliane Albert, Lena Schäfer, Renate Reinhardt, Gernot M Kaiser, Ian McDougall, Brad Decker, Björn Plicht, Raimund Erbel, et al. Real-time magnetic resonance imaging–guided transarterial aortic valve implantation in vivo evaluation in swine. *Journal of the American College of Cardiology*, 59(2):192–193, 2012.
- [65] JN Kapur, Prasanna K Sahoo, and Andrew KC Wong. A new method for gray-level picture thresholding using the entropy of the histogram. *Computer vision, graphics, and image processing*, 29(3):273–285, 1985.
- [66] Michael Kass, Andrew Witkin, and Demetri Terzopoulos. Snakes: Active contour models. *International journal of computer vision*, 1(4):321–331, 1988.
- [67] Airazat M Kazaryan, Irina Pavlik Marangos, Bård I Røsok, Arne R Rosseland, Olaug Villanger, Erik Fosse, Øystein Mathisen, and Bjørn Edwin. Laparoscopic resection of colorectal liver metastases: surgical and long-term oncologic outcome. *Annals of surgery*, 252(6):1005–1012, 2010.
- [68] James E Kennedy. High-intensity focused ultrasound in the treatment of solid tumours. *Nature reviews cancer*, 5(4):321–327, 2005.
- [69] Cemil Kirbas and Francis Quek. A review of vessel extraction techniques and algorithms. *ACM Computing Surveys (CSUR)*, 36(2):81–121, 2004.
- [70] Cemil Kirbas and Francis KH Quek. Vessel extraction in medical images by 3D wave propagation and traceback. In *Third IEEE Symposium on Bioinformatics and Bioengineering, 2003. Proceedings.*, pages 174–181. IEEE, 2003.
- [71] Josef Kittler and John Illingworth. Minimum error thresholding. *Pattern recognition*, 19(1):41–47, 1986.
- [72] Karl Krissian, Grégoire Malandain, Nicholas Ayache, Régis Vaillant, and Yves Troussset. Model based multiscale detection of 3D vessels. In *Workshop on Biomedical Image Analysis, 1998. Proceedings.*, pages 202–210. IEEE, 1998.
- [73] Karl Krissian, Grégoire Malandain, Nicholas Ayache, Régis Vaillant, and Yves Troussset. Model-based detection of tubular structures in 3D images. *Computer vision and image understanding*, 80(2):130–171, 2000.
- [74] Pablo Lamata, Félix Lamata, Valentin Sojar, Piotr Makowski, Laurent Massotier, Sergio Casciaro, Wajid Ali, Thomas Stüdeli, Jérôme Declerck, Ole Jackov Elle, et al. Use of the resection map system as guidance during hepatectomy. *Surgical endoscopy*, 24(9):2327–2337, 2010.

- [75] Thomas Lange, Sebastian Eulenstein, Michael Hünnerbein, and Peter-Michael Schlag. Vessel-based non-rigid registration of MR/CT and 3D ultrasound for navigation in liver surgery. *Computer Aided Surgery*, 8(5):228–240, 2003.
- [76] Thomas Langø, Sinara Vijayan, Anna Rethy, Cecilie Våpenstad, Ole Vegard Solberg, Ronald Mårvik, Gjermund Johnsen, and Toril N Hernes. Navigated laparoscopic ultrasound in abdominal soft tissue surgery: technological overview and perspectives. *International journal of computer assisted radiology and surgery*, 7(4):585–599, 2012.
- [77] Gunnar Låthén. *Segmentation Methods for Medical Image Analysis: Blood vessels, multi-scale filtering and level set methods*. PhD thesis, 2010.
- [78] Gunnar Låthén, Jimmy Jonasson, and Magnus Borga. Phase based level set segmentation of blood vessels. In *19th International Conference on Pattern Recognition, 2008. ICPR 2008.*, pages 1–4. IEEE, 2008.
- [79] Gunnar Låthén, Jimmy Jonasson, and Magnus Borga. Blood vessel segmentation using multi-scale quadrature filtering. *Pattern Recognition Letters*, 31(8):762–767, 2010.
- [80] Max WK Law and Albert CS Chung. Three dimensional curvilinear structure detection using optimally oriented flux. In *Computer Vision–ECCV 2008*, pages 368–382. Springer, 2008.
- [81] Ta-Chih Lee, Rangasami L Kashyap, and Chong-Nam Chu. Building skeleton models via 3D medial surface axis thinning algorithms. *CVGIP: Graphical Models and Image Processing*, 56(6):462–478, 1994.
- [82] David Lesage, Elsa D Angelini, Isabelle Bloch, and Gareth Funka-Lea. A review of 3D vessel lumen segmentation techniques: Models, features and extraction schemes. *Medical image analysis*, 13(6):819–845, 2009.
- [83] Marloes Maria Johanna Letteboer, Peter WA Willems, Max A Viergever, and Wiro J Niessen. Brain shift estimation in image-guided neurosurgery using 3D ultrasound. *IEEE Transactions on Biomedical Engineering*, 52(2):268–276, 2005.
- [84] Xuemei Liu, Huan Liu, Aimin Hao, and Qinqing Zhao. Simulation of blood vessels for surgery simulators. In *2010 International Conference on Machine Vision and Human-Machine Interface (MVHI)*, pages 377–380, April 2010.
- [85] Liana M Lorigo, Olivier D Faugeras, W Eric L Grimson, Renaud Keriven, Ron Kikinis, Arya Nabavi, and C-F Westin. Curves: Curve evolution for vessel segmentation. *Medical Image Analysis*, 5(3):195–206, 2001.
- [86] Joachim Lotz. Interventional vascular MRI: moving forward. *European Heart Journal*, 34(5):327–329, 2013.
- [87] Maysa MG Macedo, Miguel A Galarreta-Valverde, Choukri Mekkaoui, and Marcel P Jackowski. A centerline-based estimator of vessel bifurcations in angiography images. In *SPIE Medical Imaging*, pages 86703K–86703K. International Society for Optics and Photonics, 2013.

- [88] Tom Mala, Eigil Samset, Lars Aurdal, Ivar Gladhaug, Bjørn Edwin, and Odd Søreide. Magnetic resonance imaging-estimated three-dimensional temperature distribution in liver cryoleisions: a study of cryolesion characteristics assumed necessary for tumor ablation. *Cryobiology*, 43(3):268–275, 2001.
- [89] M Elena Martínez-Pérez, Alun D Hughes, Alice V Stanton, Simon A Thom, Anil A Bharath, and Kim H Parker. Retinal blood vessel segmentation by means of scale-space analysis and region growing. In *Medical Image Computing and Computer-Assisted Intervention–MICCAI’99*, pages 90–97. Springer, 1999.
- [90] Yoshitaka Masutani, Thomas Schiemann, and Karl-Heinz Höhne. Vascular shape segmentation and structure extraction using a shape-based region-growing model. In *Medical Image Computing and Computer-Assisted Intervention—MICCAI’98*, pages 1242–1249. Springer, 1998.
- [91] John P McGahan and Gerald D Dodd III. Radiofrequency ablation of the liver: current status. *American Journal of Roentgenology*, 176(1):3–16, 2001.
- [92] Tim McInerney and Demetri Terzopoulos. T-snakes: Topology adaptive snakes. *Medical image analysis*, 4(2):73–91, 2000.
- [93] Hans-Peter Meinzer, Matthias Thorn, and Carlos E Cárdenas. Computerized planning of liver surgery—an overview. *Computers & Graphics*, 26(4):569–576, 2002.
- [94] Elahe Moghimirad, Seyed Hamid RezaTofighi, and Hamid Soltanian-Zadeh. Retinal vessel segmentation using a multi-scale medialness function. *Computers in Biology and Medicine*, 42(1):50–60, January 2012.
- [95] Naofumi Nagasue, Hitoshi Kohno, Yu-Chung Chang, Hiroyuki Taniura, Akira Yamanoi, Masaaki Uchida, Takeo Kimoto, Yoshinari Takemoto, Teruhisa Nakamura, and Hirofumi Yukaya. Liver resection for hepatocellular carcinoma. results of 229 consecutive patients during 11 years. *Annals of surgery*, 217(4):375, 1993.
- [96] DM Nagomey, A Van Heerden, DM Ilstrup, and MA Adsoon. Primary hepatic malignancy: surgical management and determinants of survival. *Management*, 106(4), 1989.
- [97] Nobuyuki Otsu. A threshold selection method from gray-level histograms. *Automatica*, 11(285-296):23–27, 1975.
- [98] Alexandru paul Condurache and Til Aach. Vessel segmentation in angiograms using hysteresis thresholding. In *Proceedings of the Ninth IAPR conference on Machine Vision Applications 2005, Tsukuba Science City, Japan*, pages 16–18, 2005.
- [99] Timothy M Pawlik and Jean-Nicolas Vauthey. Surgical margins during hepatic surgery for colorectal liver metastases: complete resection not millimeters defines outcome. *Annals of surgical oncology*, 15(3):677–679, 2008.
- [100] Matthias Peterhans, Daniel Candinas, and Stefan Weber. Soft tissue navigation and liver surgery support. In Ferenc A. Jolesz, editor, *Intraoperative Imaging and Image-Guided Therapy*, pages 789–798. Springer New York, January 2014.

- [101] Thomas Pock, Christian Janko, Reinhard Beichel, and Horst Bischof. Multiscale medialness for robust segmentation of 3D tubular structures. In *Proceedings of the Computer Vision Winter Workshop*, 2005.
- [102] Kanishka Ratnayaka and Robert J Lederman. Interventional cardiovascular MR—the next stage in pediatric cardiology. *Progress in Pediatric cardiology*, 28(1):59–67, 2010.
- [103] Ingerid Reinertsen, Maxime Descoteaux, Kaleem Siddiqi, and D Louis Collins. Validation of vessel-based registration for correction of brain shift. *Medical image analysis*, 11(4):374–388, 2007.
- [104] Patrick Reuzé, Jean-Louis Coatrieux, Limin M Luo, Jean-Louis Dillenseger, et al. A 3D moment based approach for blood vessel detection and quantification in MRA. *Technology and health care: official journal of the European Society for Engineering and Medicine.*, 1(2):181–188, 1993.
- [105] D Ribes, M Peterhans, S Anderegg, D Wallach, V Banz, C Kim-Fuchs, D Candinas, and S Weber. Image guided liver surgery. *Surgery*, 7:7–16, 2012.
- [106] Florence Rossant, Maddalena Badellino, Alexandre Chavillon, Isabelle Bloch, and Michel Paques. A morphological approach for vessel segmentation in eye fundus images, with quantitative evaluation. *Journal of Medical Imaging and Health Informatics*, 1(1):42–49, 2011.
- [107] Yoshinobu Sato, Shin Nakajima, Nobuyuki Shiraga, Hideki Atsumi, Shigeyuki Yoshida, Thomas Koller, Guido Gerig, and Ron Kikinis. Three-dimensional multi-scale line filter for segmentation and visualization of curvilinear structures in medical images. *Medical image analysis*, 2(2):143–168, 1998.
- [108] Dirk Selle, Bernhard Preim, Andrea Schenk, and H-O Peitgen. Analysis of vasculature for liver surgical planning. *IEEE Transactions on Medical Imaging*, 21(11):1344–1357, 2002.
- [109] James Albert Sethian. *Level set methods and fast marching methods: evolving interfaces in computational geometry, fluid mechanics, computer vision, and materials science*, volume 3. Cambridge university press, 1999.
- [110] Mehmet Sezgin and Bülent Sankur. Survey over image thresholding techniques and quantitative performance evaluation. *Journal of Electronic imaging*, 13(1):146–168, 2004.
- [111] Zahra Shafaei, Airazat M Kazaryan, Michael R Marvin, Robert Cannon, Joseph F Buell, Bjørn Edwin, and Brice Gayet. Is laparoscopic repeat hepatectomy feasible? a tri-institutional analysis. *Journal of the American College of Surgeons*, 212(2):171–179, 2011.
- [112] IM Shaw, M Rees, FKS Welsh, S Bygrave, and TG John. Repeat hepatic resection for recurrent colorectal liver metastases is associated with favourable long-term survival. *British journal of surgery*, 93(4):457–464, 2006.
- [113] Risa Small, Nir Lubezky, and Menahem Ben-Haim. Current controversies in the surgical management of colorectal cancer metastases to the liver. *The Israel Medical Association journal: IMAJ*, 9(10):742–747, 2007.

- [114] Richard Swanson and Bhoomi Mehrotra. Gallbladder cancer: Treatment of localized, potentially resectable disease. *UpToDate*, 2010.
- [115] Nobuhiko Taniai, Koho Akimaru, Hiroshi Yoshida, and Takashi Tajiri. Surgical treatment for better prognosis of patients with liver metastases from colorectal cancer. *Hepato-gastroenterology*, 54(78):1805–1809, 2007.
- [116] Ricardo Toledo, Xavier Orriols, Petia Radeva, Xavier Binefa, Jordi Vitria, Cristina Canero, and JJ Villanuev. Eigensnakes for vessel segmentation in angiography. In *15th International Conference on Pattern Recognition, 2000. Proceedings.*, volume 4, pages 340–343. IEEE, 2000.
- [117] T Tsuzuki, A Sugioka, M Ueda, S Iida, T Kanai, H Yoshii, and K Nakayasu. Hepatic resection for hepatocellular carcinoma. *Surgery*, 107(5):511–520, 1990.
- [118] James Alexander Tyrrell, Emmanuelle di Tomaso, Daniel Fuja, Ricky Tong, Kevin Kozak, Rakesh K Jain, and Badrinath Roysam. Robust 3D modeling of vasculature imagery using superellipsoids. *IEEE Transactions on Medical Imaging*, 26(2):223–237, 2007.
- [119] Aphrodite Tzifa, Gabriele A. Krombach, Nils Krämer, Sascha Krüger, Adrian Schütte, Matthias von Walter, Tobias Schaeffter, Shakeel Qureshi, Thomas Krasemann, Eric Rosenthal, Claudia A. Schwartz, Gopal Varma, Alexandra Buhl, Antonia Kohlmeier, Arno Bücker, Rolf W. Günther, and Reza Razavi. Magnetic resonance–guided cardiac interventions using magnetic resonance–compatible devices: A preclinical study and first-in-man congenital interventions. *Circulation: Cardiovascular Interventions*, 3(6):585–592, 2010.
- [120] Stefan Wesarg and Evelyn A Firlé. Segmentation of vessels: the corkscrew algorithm. In *SPIE Medical Imaging 2004*, pages 1609–1620. International Society for Optics and Photonics, 2004.
- [121] Philip Wette, Stephan Arens, Andreas Elsner, and Gitta Domik. Extending the corkscrew algorithm to find bifurcations of vessels. *Proceedings Computer Graphics and Imaging*, pages 317–323, 2010.
- [122] Peter L Williams et al. Gray’s anatomy: The anatomical basis of medicine and surgery. 1995.
- [123] Changyan Xiao, Marius Staring, Denis Shamonin, Johan HC Reiber, Jan Stolk, and Berend C Stoel. A strain energy filter for 3D vessel enhancement with application to pulmonary ct images. *Medical image analysis*, 15(1):112–124, 2011.
- [124] Chenyang Xu and Jerry L Prince. Snakes, shapes, and gradient vector flow. *Image Processing, IEEE Transactions on*, 7(3):359–369, 1998.
- [125] Paul A Yushkevich, Joseph Piven, Heather Cody Hazlett, Rachel Gimpel Smith, Sean Ho, James C Gee, and Guido Gerig. User-guided 3D active contour segmentation of anatomical structures: significantly improved efficiency and reliability. *Neuroimage*, 31(3):1116–1128, 2006.
- [126] M. Zamir. Arterial branching within the confines of fractal l-system formalism. *The Journal of General Physiology*, 118(3):267–276, September 2001.
- [127] Frederic Zana and J-C Klein. Segmentation of vessel-like patterns using mathematical morphology and curvature evaluation. *IEEE Transactions on Image Processing*, 10(7):1010–1019, 2001.

- [128] Huang Zhan-Peng, Yi Fa-Ling, Jiang Shi-Zhong, Jie Zhao, and Bao Su-Su. The segmentation of liver and vessels in CT images using 3D hierarchical seeded region growing. In *2011 IEEE International Conference on Computer Science and Automation Engineering (CSAE)*, volume 2, pages 264–269. IEEE, 2011.

Papers

3D multiscale vessel enhancement based centerline extraction of blood vessels

3D multiscale vessel enhancement based centerline extraction of blood vessels

Rahul Prasanna Kumar^{ab}, Fritz Albregtsen^b, Martin Reimers^b, Thomas Langø^c, Bjørn Edwin^a,
Ole Jakob Elle^{ab}

^aThe Intervention Centre, Oslo University Hospital, Norway

^bDepartment of Informatics, University of Oslo, Norway

^cSINTEF, Department of Medical Technology, Trondheim, Norway

ABSTRACT

Extraction of blood vessel structure is important for improving planning, navigation and tracking in several interventional procedures. Centerline based registration methods have proven to be fast for clinical applications and an effective way of registering multi-modal images. Here, we present a novel blood vessel centerline extraction method in 3D. Our method consists of two parts, namely Multiscale Vessel Enhancement Filtering (MVEF) and Centerline Extraction using Vessel Direction (CEVD). Our proposed MVEF has an improved noise reduction and better Gaussian profile at the vessel cross-sections compared to conventional MVEF. The CEVD is our novel method for tracing the peaks of the Gaussian profile of the local MVEF at the vessel cross-sections. The peak of the Gaussian profile provides the center position of the blood vessels. The novelty of this method is in effectively finding only the connected centerlines of the blood vessels of interest. The proposed method was evaluated using both synthetic and medical images. On comparing with Frangi's vesselness filtering combined with thinning, our method is shown to be approximately 5 times faster. The results also show that our method is customized to detect only the desired blood vessels, thereby eliminating the detection of unwanted vessel-like structures. The centerline accuracy was evaluated by comparing with ground truth data created by finding Hough circle centers at each cross-section of the vessel structure. The modified symmetric Hausdorff distance between our result and the ground truth was approximately 1 pixel for both synthetic and medical images.

Keywords: Centerline extraction, vessel tracking, blood vessel segmentation, multi-scale analysis.

1. INTRODUCTION

The human body contains several different types of blood vessels that constitute a network of arteries and veins. Visualization of these blood vessels is important for improving the planning and navigation in several interventional procedures. It is specifically relevant in catheter based procedures like stent graft positioning and valve replacement and also, in planning and navigation of laparoscopic liver resection. Detailed images of these blood vessels are initially formed using computerized tomographic angiography (CTA) and/or magnetic resonance angiography (MRA) depending on the part of the body and equipment available. These blood vessel contrast enhanced images provide a basis for visualizing the blood vessels in three dimensions, which help the interventionists in planning and navigation during procedures.

The interventional procedures of today are going more towards the use of multiple imaging modalities for improving the safety for the patient and, for improving the operational procedures in general. This increases the need for faster blood vessel visualization and registration between multiple modalities, for applications involving navigation using intra-operative image modalities. Though many different methods are available for registration, centerline based registration

methods have proven to be fast enough for clinical applications and an effective way of registering multi-modal images [1,2,3,4].

Many methods for centerline extraction of blood vessels have been presented in the literature. In them, most of the commonly used techniques depend on extracting centerlines from pre-segmented vascular models. For these cases, the blood vessels are initially segmented through thresholding, model-based approaches or multiscale vessel segmentation [5,6,7]. The segmented output is then skeletonised or thinned, ending up with the final centerline [8,9]. The main disadvantage here is that they are computationally expensive since they must process the whole image space to find a few connected blood vessels.

In this paper, we present a novel semi-automatic seed point based centerline extraction with local vessel enhancement. Our method lets the user select a single or multiple connected blood vessels of interest, thus reducing the potential noise of uninteresting voxels and also reducing the processing time.

The paper is organized as follows. Section 2 describes the methods used, which is divided into two parts, namely Multiscale Vessel Enhancement Filtering (MVEF) and Centerline Extraction using Vessel Direction (CEVD). The results are presented in section 3, where the reduction in processing time and the accuracy obtained are shown. We conclude the paper in section 4 by giving details of possible future work.

2. METHODS

2.1. Multiscale Vessel Enhancement Filtering

Our method is based on the eigenvalue analysis of the Hessian matrix, as described in [6], [7] and [10]. The filter detects voxels belonging to blood vessel structures, taking into account that arterial blood vessels resemble tubular structures and venal structures resemble ellipsoidal structures.

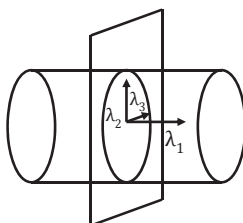


Fig. 1. Eigenvalues along the principal direction of curvature of the cylinder.

The Hessian H of the image I describes the second-order structure of local intensity variations at each voxel. The derivative computation of the Hessian matrix is combined with Gaussian $G(\sigma)$ convolution, for a scale σ that varies accordingly to the width of the blood vessel [7].

$$H(X; \sigma) = \begin{bmatrix} I_{xx}(X; \sigma) & I_{xy}(X; \sigma) & I_{xz}(X; \sigma) \\ I_{yx}(X; \sigma) & I_{yy}(X; \sigma) & I_{yz}(X; \sigma) \\ I_{zx}(X; \sigma) & I_{zy}(X; \sigma) & I_{zz}(X; \sigma) \end{bmatrix} \quad (1)$$

where $X = (x, y, z)$, $I_{xx}(X; \sigma) = \left\{ \frac{\partial^2}{\partial x^2} G(\sigma) \right\} * I(X)$, $I_{xy}(X; \sigma) = \left\{ \frac{\partial^2}{\partial x \partial y} G(\sigma) \right\} * I(X)$ and so on.

This approach measures the contrast between the regions inside and outside the range of scale σ in the direction of the derivative.

In Fig.1, λ_1 , λ_2 and λ_3 are the eigenvalues corresponding to the eigenvectors \mathbf{v}_1 , \mathbf{v}_2 and \mathbf{v}_3 , computed by Eigen analysis of Hessian. On sorting $|\lambda_1| \leq |\lambda_2| \leq |\lambda_3|$, eigenvalue λ_1 represent the eigenvalue along the direction of the vessel and eigenvalues λ_2 and λ_3 represent the eigenvalues along the vessel cross-section. A tube detection filter was developed using these eigenvalues in [10].

$$V_\sigma = \left(1 - \frac{|\lambda_2| - |\lambda_3|}{|\lambda_2| + |\lambda_3|}\right) \left(\frac{2}{3} \lambda_1 - \lambda_2 - \lambda_3\right) \quad (2)$$

The tube detection filter output, obtained from the above equation also tends to detect noise voxels with no definite structure. To reduce this noise, we made use of the *structureness term* described in [6], which is the Forbenius norm of the Hessian.

$$S = \sqrt{\lambda_1^2 + \lambda_2^2 + \lambda_3^2} \quad (3)$$

Thus, our modified Equation 2 for a single scale is,

$$V_\sigma = \left(1 - \frac{|\lambda_2| - |\lambda_3|}{|\lambda_2| + |\lambda_3|}\right) \left(\frac{2}{3} \lambda_1 - \lambda_2 - \lambda_3\right) \left(1 - e^{-\frac{S^2}{2c^2}}\right) \quad (4)$$

where c is a constant which depends on the grey scale range of the initial image [6].

We found Equation 4 to give exponentially reduced vessel response peak values as the scale is increased. To normalise it, we multiplied Equation 4 with a scale dependent weighting term

$$V = \begin{cases} 0 & \text{if } V_\sigma \leq 0 \\ V_\sigma e^{k\sigma} & \end{cases} \quad (5)$$

where k is a constant set to 0.5, based on initial experiments.

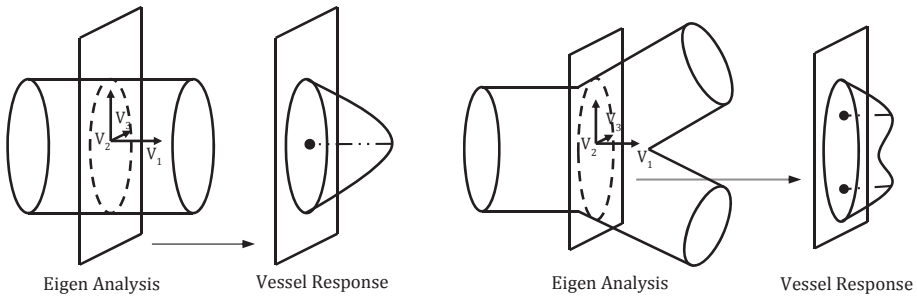


Fig. 2. Left: Description of vessel response at vessel trunk. Right: Description of vessel response at vessel bifurcation.

The response of the vessel enhancement filter is highest at the scale that best fits the vessel. A multiscale response for detecting vessels of varying width is obtained by selecting the maximum response for a range of scales between σ_{\min} and σ_{\max} as described in [6].

$$V_{multi} = \max_{\sigma_{min} \leq \sigma \leq \sigma_{max}} V(\sigma) \quad (6)$$

The Fig.2. left, describes the final MVEF output at the vessel truck cross-section along eigenvectors of the blood vessel and the Fig.2. right, describes the final MVEF output at the vessel bifurcation cross-section along eigenvectors of the blood vessel.

2.2. Centerline Extraction using Vessel Direction

The centerline extraction method is based on local computation of MVEF explained in section 2.1. The semi-automatic method is based on an initial seed point set by the user in one of the blood vessels. This seed point allows the user to extract just the centerlines of the blood vessels of interest, thus reducing the noise and processing time. The seed point can be placed anywhere inside the desired blood vessel.

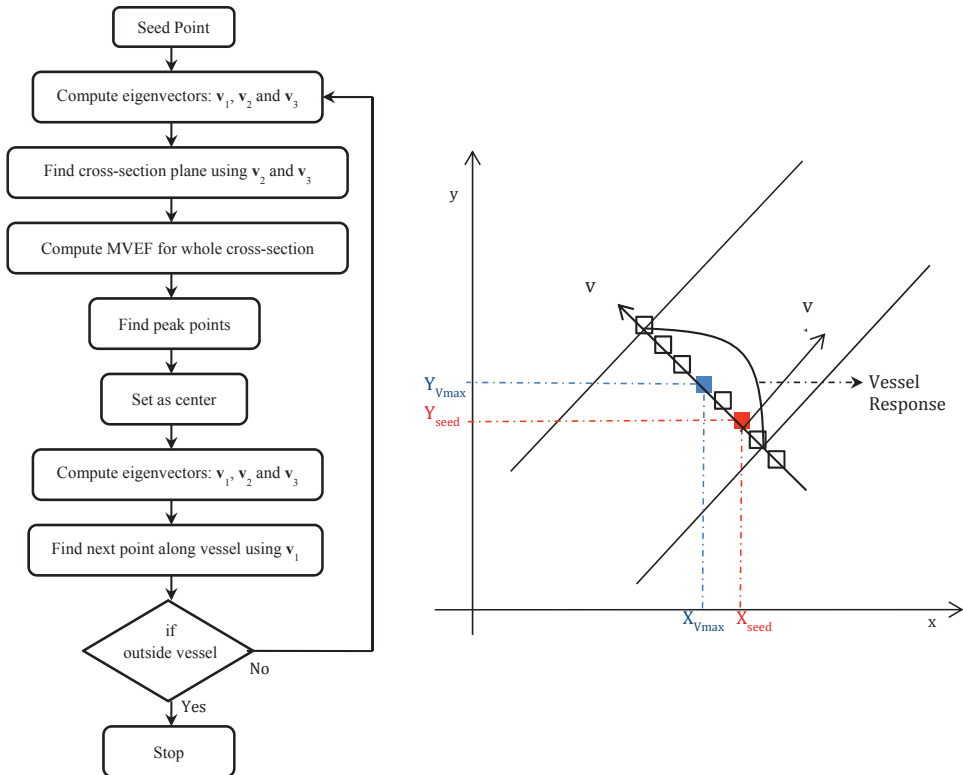


Fig. 3. *Left:* Simple flowchart description of center extraction from seed point. *Right:* 2D representation of center point extraction from the user defined seed point.

In a 3D volume around the seed point, Eigen analysis is performed in order to find the eigenvalues λ_1 , λ_2 and λ_3 and their corresponding eigenvectors \mathbf{v}_1 , \mathbf{v}_2 and \mathbf{v}_3 [7]. These eigenvectors represent the three principal directions of curvature of the vessel at the voxel under observation. Applying the MVEF at the voxels with the limit of σ_{max} along a vessel cross-section plane results in a vessel response of which the profile is similar to a Gaussian. The position of the peak of the Gaussian is set as the center point for the vessel cross-section as shown in Fig.3, right. At the center point, the Eigen

Analysis is again performed to calculate eigenvector \mathbf{v}_1 that corresponds to the direction of the vessel, which is used to find the next cross section plane along the vessel for further centerline extraction. The Fig.3, left shows a simple flowchart explaining the centerline extraction along the vessel trunk.

At the bifurcation, the Gaussian profile of the MVEF is different from that at the vessel trunk. Instead of a single peak, a peak is found for each bifurcation. One of the peaks is set as the center point and the centerline extraction is continued as explained previously. The other peaks are set as new seed points for starting new centerline extractions.

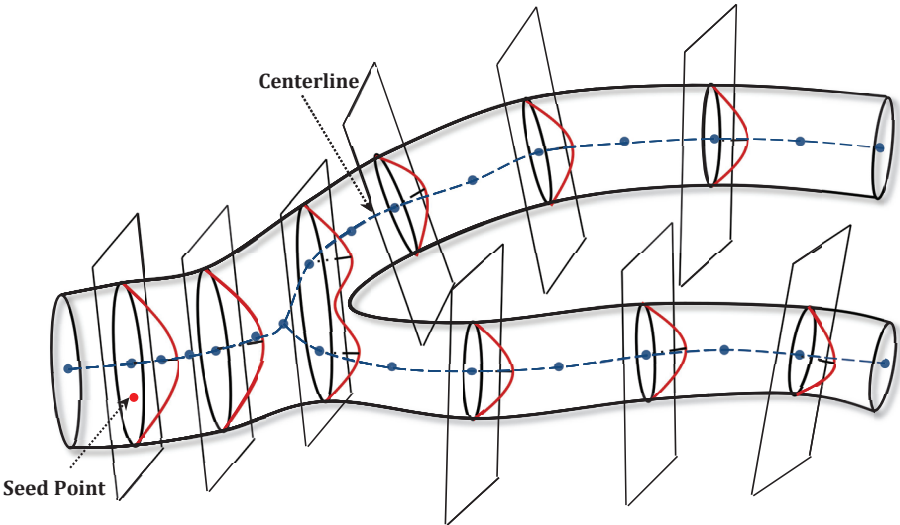


Fig. 4. Representation of 3D centerline extraction from a single seed point

The centerline extraction of the whole blood vessel with all its bifurcations are thus calculated from a single seed point provided by the user as represented in Fig.4.

3. RESULTS

The proposed method was evaluated using both synthetic and medical images. The synthetic data was created through the VascuSyth software implemented in ITK [11]. Multiple varying synthetic data were possible by varying the vascular parameters file and noise parameter file for the software. The parameters mainly used were the number of leaf nodes, pressure at perforation and terminal nodes, image size and noise type. The medical images were downloaded from the freely available DICOM medical image database of OSIRIX [12].

The method is compared with Frangi's vesselness [6] combined with thinning method by Lee [13]. Frangi's vesselness is an automatic blood vessel enhancement filter, where a multiscale vesselness is calculated for every voxel in the image. This is an automatic method where the user has to only select the scales of the blood vessel. Fig. 5 shows six synthetic vessel images of size 100x100x100, of which centerlines were extracted using the proposed method with only a single seed point. Each of these synthetic images has varying number of bifurcations and added Gaussian noise. In Fig. 6 the leftmost column shows the Maximum Intensity Projection (MIP) of the three dimensional medical images. The white circles indicate the seed points used by our method. The images shown are relevant for catheterization procedures. The

middle column shows the MIP results of the centerline extraction using the Frangi's vesselness combined with Lee's thinning and the rightmost column shows the results of centerline extraction using the proposed method. On the medical images of row 2 and 3, two seed points were used to find the centerline of the completely disconnected blood vessels compared to a single seed point used in the medical image of row 1.

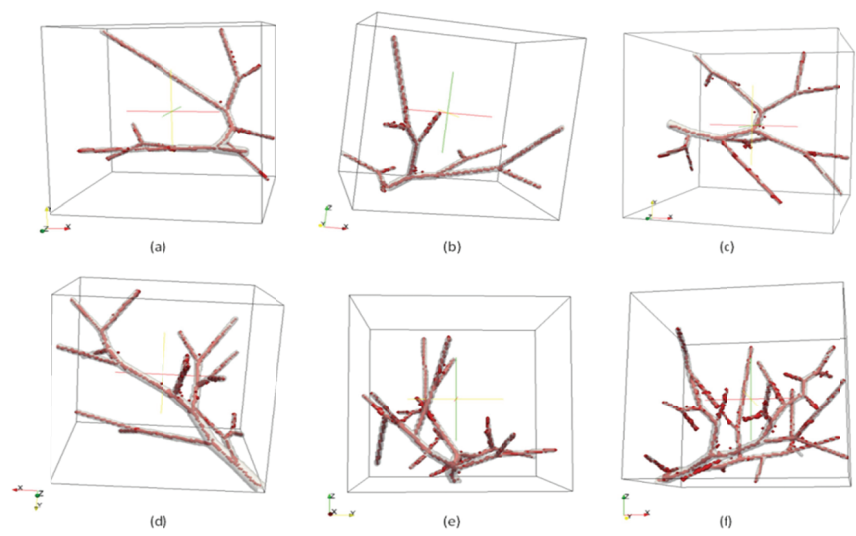


Fig. 5. (a-f)Synthetic images with varying number of bifurcations, overlaid with centerlines extracted using our proposed method

3.1. Processing time

The centerline extractions were performed on an Intel(R) Core(TM) i7CPU @2.93GHz with 8GB RAM. Table 1 below illustrates the processing time for the Frangi and Lee method and the proposed method, for synthetic images in Fig. 5 and medical images in Fig. 6. On an average, the proposed method is about five times faster than the traditional method.

Table 1. Comparison between processing time for Frangi + Lee method and the proposed method on synthetic and medical images

Dataset:	Processing Time	
	Frangi + Lee	Proposed Method
Synthetic Image (a)	42.7s	3.7s
Synthetic Image (b)	43.7s	6.2s
Synthetic Image (c)	41.5s	8.8s
Synthetic Image (d)	44.5s	10.0s
Synthetic Image (e)	44.0s	10.2s
Synthetic Image (f)	43.7s	15.3s
Medical Image (a)	386s	111s
Medical Image (d)	240s	36s
Medical Image (g)	371s	48s

3.2. Centerline accuracy

At each blood vessel cross-section calculated using eigenvectors at the cross-section, a Hough circle is fitted. The center of Hough circle at the blood vessel cross-section is used as the ground truth center and the final combination of all centers give the ground truth centerline. This ground truth centerline is compared with our result by calculating Modified Symmetric Hausdorff Distance (MSHD) between them [14].

$$MSHD(A, B) = \max \left\{ \frac{1}{N_a} \sum_{a \in A} \min_{b \in B} \{d(a, b)\}, \frac{1}{N_b} \sum_{b \in B} \min_{a \in A} \{d(b, a)\} \right\} \quad (7)$$

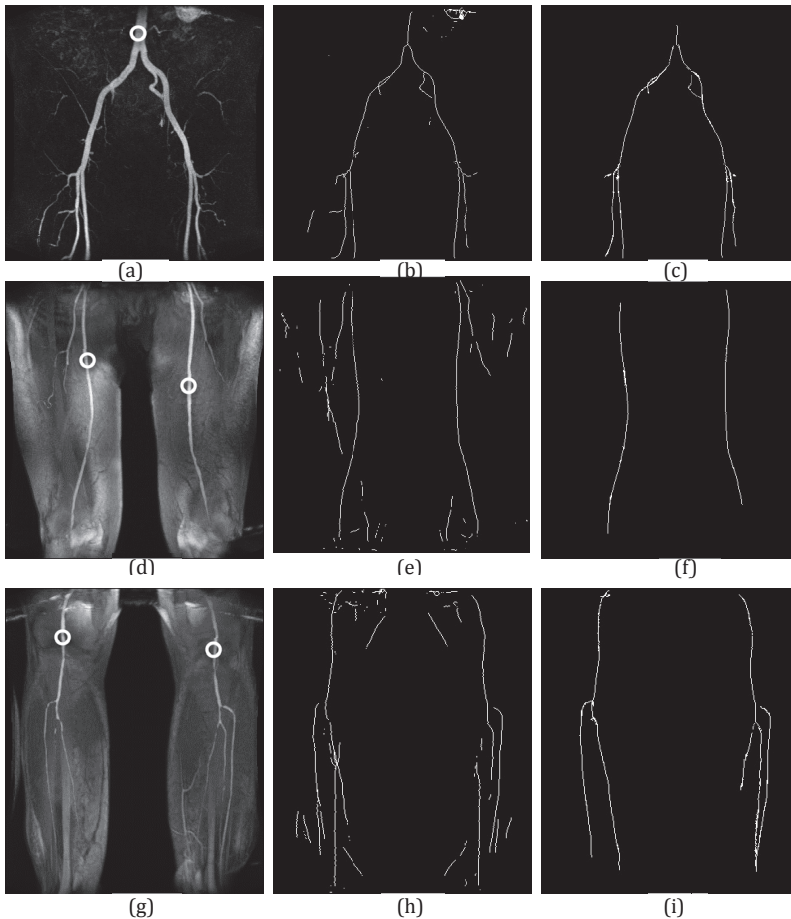


Fig. 6. (a)(d)(g) MIP of 3D Medical Images with the white circles representing the seed points selected (b)(e)(h) MIP of centerlines extracted using Frangi's vesselness combined with Lee's thinning. (c)(f)(i) MIP of centerlines extracted using our proposed method.

We have used MSHD for its desirable features that help in matching two objects based on their edge points. These features include, monotonic increase in its value as the difference between two edge point increases and its robustness to

outlier points. Table 2 gives the MSHD from our centerlines and centerlines from the Frangi and Lee method to the calculated ground truth. It is shown that both methods have good centerline accuracy for all synthetic images with all MSHD of one or less than one pixel. The difference between the Frangi MSHD and our MSHD is ≤ 0.1 pixel for the six synthetic images, and 0.4, 12.0 and 39.4 for the medical images. For the first medical image, both methods again have good accuracy with MSHD less than 2 pixels. But for the second and third medical image there is a huge difference in the accuracy, which is consistent with the increase in undesired centerlines detected by the Frangi and Lee method.

Table 2. Comparison between Modified Symmetric Hausdorff Distance (MSHD) for Frangi + Lee method and the proposed method for all images. MSHD was calculated between the ground truth and results from each of the methods.

Dataset:	Modified Symmetric Hausdorff Distance	
	Frangi + Lee	Proposed Method
Synthetic Image (a)	0.96	0.89
Synthetic Image (b)	1.01	0.89
Synthetic Image (c)	0.92	0.94
Synthetic Image (d)	1.09	0.95
Synthetic Image (e)	1.11	1.09
Synthetic Image (f)	1.70	1.54
Medical Image (a)	1.92	1.56
Medical Image (d)	13.17	1.15
Medical Image (g)	39.81	0.47

4. DISCUSSION AND CONCLUSION

In this paper, we have presented a novel semi-automatic seed point based centerline extraction method. Our proposed MVEF has an improved dampening of noise and better Gaussian profile at the vessel cross-sections compared to conventional MVEF [6]. The CEVD is our novel method for tracing the peaks of the Gaussian profile of the local MVEF at the vessel cross-sections. Though processing time for the proposed method was seen to vary with complexity and the scale range of the blood vessel structures, the proposed method was faster than the conventional method at any given variation. The processing time of our method depends mainly on the total number of voxels belonging to blood vessels rather than the size of the whole image.

Furthermore, our method detects only the blood vessels that are connected to the user's seed point. This is in contrast to automatic and global centerline extraction method such as Frangi's vesselness with thinning, which also detects artefacts that look similar to vessel structures such as bones and muscle edges. This will be very helpful in medical applications such as catheter tracking, liver surgery planning etc., where the surgeon or physician would like to focus only on the blood vessels of interest, i.e. most relevant to the procedure. Since our method depends on the blood vessel connectivity, gaps in the blood vessels could cause abrupt termination of centerline extraction.

In the future work, we will investigate the possibilities of further reducing the processing time as well as increasing the robustness of the method when used for complex medical images. This will include automatic detection of blood vessel width, while the centerline is tracked in order to limit the cross-section analysis to be within the blood vessel and to free the user from selecting the different scales of the blood vessels. This will also improve the effective scale selection and therefore, reduce the need of multiscale analysis. Work will also be done on improving the ability of the method to detect and jump across gaps and to further investigate an extension of the centerline extraction method to a fast vessel segmentation procedure.

ACKNOWLEDGMENTS

The research leading to these results has received funding from the European Community's Seventh Framework Programme (FP7/2007-2013) under grant agreement n° 238802 (IIIOS project).

REFERENCES

- [1] Reinertsen, I., Descoteaux, M., Siddiqi, K., Collins, D.L., "Validation of vessel-based registration for correction of brain shift," *Medical image analysis*, 11, 374-88 (2007).
- [2] Chillet, D., Jomier, J., Cool, D., Aylward, S., "Vascular Atlas Formation Using a Vessel-to-Image Affine Registration Method," *Brain*, 335-342 (2003).
- [3] Lange, T., Eulenstein, S., Hünnerbein, M., Schlag, P.M., "Vessel-based non-rigid registration of MR/CT and 3D ultrasound for navigation in liver surgery," *Computer aided surgery : official journal of the International Society for Computer Aided Surgery*, 8, 228-40 (2003).
- [4] Aylward, S.R., Jomier, J., Weeks, S.U.E., Bullitt, E., "Registration and Analysis of Vascular Images," *International Journal of Computer Vision - Special Issue on Research at the University of North Carolina Medical Image Display Analysis Group (MIDAG)*, 55, 123-138 (2003).
- [5] Pock, T., Beichel, R., Bischof, H., "A Novel Robust Tube Detection Filter for 3D Centerline Extraction," *Image Analysis. Lecture Notes in Computer Science*, 3540, 55-94 (2005).
- [6] Frangi, A.F., Niessen, W.J., Vincken, K.L., Viergever, M.A., "Multiscale vessel enhancement filtering," *MICCAI. Lecture Notes in Computer Science*, 1496, 130-137 (1998).
- [7] Sato, Y., Nakajima, S., Atsumi, H., Gerig, G., Yoshida, S., Kikinis, R., "3D Multi-scale Line Filter for Segmentation and Visualization of Curvilinear Structures in Medical Images," *CVRMED-MRCAS'97, Lecture Notes in Computer Science*, 1205/1997, 213-222 (1997).
- [8] Kirbas, C., Quek, F.K.H., "Vessel extraction techniques and algorithms: a survey," *Bioinformatics and Bioengineering*, 2003. Proceedings. Third IEEE Symposium on, 238-245 (2003).
- [9] Aylward, S.R., Bullitt, E., "Initialization, noise, singularities, and scale in height ridge traversal for tubular object centerline extraction," *IEEE transactions on medical imaging*, 21, 61-75 (2002).
- [10] Erdt, M., Raspe, M., Suehling, M., "Automatic Hepatic Vessel Segmentation Using Graphics Hardware," *Medical Imaging and Augmented Reality*, 5128, 403-412 (2008).
- [11] Jassi, P., Hamarneh, G., "VascuSynth: Vascular Tree Synthesis Software," *Insight Journal*, (2011)
- [12] OsiriX DICOM database, "Advanced Imaging in 3D/4D/5D," <http://pubimage.hcuge.ch:8080/>
- [13] Lee, C., "Building skeleton models via 3-D medial surface/axis thinning algorithms," *Graphical Models and Image Processing*, 56, 462-478 (1994).
- [14] Dubuisson, M.P., Jain, A.K., "A modified Hausdorff distance for object matching," *Proc. of IAPR Int. Conf. on Pattern Recognition (ICPR'94. Jerusalem. IS)*, 566-568 (1994).

Study on liver blood vessel movement during breathing cycle

Blood vessel segmentation and centerline tracking using local structure analysis

Three-dimensional blood vessel segmentation and centerline extraction based on two-dimensional cross-section analysis

Three-Dimensional Blood Vessel Segmentation and Centerline Extraction based on Two-Dimensional Cross-Section Analysis

RAHUL PRASANNA KUMAR^{1,2}, FRITZ ALBREGTSEN^{2,3}, MARTIN REIMERS², BJØRN EDWIN^{1,4}, THOMAS LANGØ⁵, OLE JAKOB ELLE^{1,2}

¹ The Intervention Centre, Oslo University Hospital, Sognsvannsveien 20, 0372 Oslo, Norway

² Department of Informatics, University of Oslo, Gaustadalléen 23 B, 0373 Oslo, Norway

³ Institute for Cancer Genetics and Informatics, Oslo University Hospital, Sognsvannsveien 20, 0372 Oslo, Norway

⁴ Faculty of Medicine, University of Oslo, Klaus Torgårds vei 3, 0372 Oslo, Norway

⁵ Medical Technology, SINTEF, Olav Kyrres gate 9, MTFS, Trondheim, Norway

Abbreviated Title for the Running Head: “Blood vessel segmentation by 2D cross-section analysis”

Corresponding Author:

Rahul Prasanna Kumar, MSc.

The Intervention Centre, Oslo University Hospital

Sognsvannsveien 20, 0372 Oslo, Norway

Phone: +(47) 23 07 01 24

Fax: +(47) 23 07 01 10

Email: rahul.kumar@rr-research.no

Abstract—

The segmentation of tubular tree structures like vessel systems in volumetric datasets is of vital interest for many medical applications. In this paper we present a novel, semi-automatic method for blood vessel segmentation and centerline extraction, by tracking the blood vessel tree from a user-initiated seed point to the ends of the blood vessel tree. The novelty of our method is in performing only two-dimensional cross-section analysis for segmentation of the connected blood vessels. The cross-section analysis is done by our novel single-scale or multi-scale *circle enhancement* filter, used at the blood vessel trunk or bifurcation, respectively. The method was validated for both synthetic and medical images. Our validation has shown that the cross-sectional centerline error for our method is below 0.8 pixels and the Dice coefficient for our segmentation is $80\% \pm 2.7\%$. On combining our method with an optional active contour post-processing, the Dice coefficient for the resulting segmentation is found to be $94\% \pm 2.4\%$. Furthermore, by restricting the image analysis to the regions of interest and converting most of the three-dimensional calculations to two-dimensional calculations, the processing was found to be more than 18 times faster than Frangi *vesselness* with thinning, 8 times faster than user-initiated active contour segmentation with thinning and 7 times faster than our previous method.

Keywords—

Blood vessel segmentation, Centerline extraction, vessel tracking, multi-scale analysis and circle enhancement filter

INTRODUCTION

Many clinical practices rely on angiography in multiple imaging modalities. This leads to an increasing need for visualization and segmentation of blood vessels. Analysis of blood vessel morphology is very important in many clinical applications for diagnosis, planning and navigation. This is especially important for planning liver resections and navigation of catheter-based interventions. Catheter tracking require precise knowledge of the blood vessels for accurate positioning of stents and valves.

Manual segmentation of blood vessels is impractical as they present very complex 3D structures, which makes an automatic or semi-automatic segmentation important. In the literature, many papers are dealing with blood vessel segmentation^{9,15}. Conventional blood vessel segmentation methods can be classified as top-down or bottom-up approaches. In top-down approaches, the process starts from single or multiple user-initiated seed points and iteratively merges nearby structures or regions based on a predefined condition. In bottom-up approaches, a predefined condition for blood vessel segmentation is evaluated at each and every voxel of the input image, not requiring any seed point initializations from the user.

Typical top-down methods include region growing and deformable models. Two major conditions looked for in region growing methods are intensity value similarity and spatial proximity^{22,23}. Region growing methods also include an initial thresholding. Deformable model methods include active contours or snakes, level sets and wave-front propagation^{2,8,10,17,19}. These methods work on iteratively adjusting the initial user set contour to fit to the blood vessel structure. The major disadvantages of these methods are that there is little use of structure information leading to high chance of leakage, and also that iteratively modifying the contour is very time consuming.

Typical bottom-up methods are based on local shape descriptors or tube detection filters^{4,5,11,21}. The radius for tube detection varies, but following the concepts of scale-space theory¹⁶, the response of a tubular filter is maximal if the scale fits the object size. Conventional tube detection filters try to identify the tubular objects at different scales and combine all responses into one multi-scale response. The major disadvantages of such methods are that they are computationally very expensive, due to their processing of each and every voxel and its neighborhood in the image at several scales.

Along with segmentation, a centerline extraction of these blood vessels is also important. An extracted centerline could be used for fast registration of blood vessels and updating blood vessel models obtained intraoperatively^{13,20}. We have earlier proposed a centerline extraction method that uses our *modified multiscale vesselness* equation¹². Our earlier method was faster than the conventional *vesselness* method by performing the modified *vesselness* only within regions of interest; however, this was still not fast enough, as it required prior calculation of whole image Hessian.

In this paper, we present a novel blood vessel segmentation and centerline extraction method incorporating both top-down and bottom up approaches. The main aim of this method is to provide the user with a fast and easy to use blood vessel segmentation method, which has the potential to be used for updating models during intra-operative procedures. The proposed method is semi-automatic and works by processing a single 2D blood vessel cross-section at a time and tracking the connected blood vessel tree to its end points. The final 3D blood vessel segmentation is calculated by combining all the tracked 2D vessel cross-sections.

METHODS

Our proposed method focuses on segmenting the 3D connected blood vessels by tracking their cross-sections from a user-initialized seed to the blood vessel ends. The user initializes the tracking by setting a seed point, a direction seed point and an approximate blood vessel cross-section radius at the seed point.

In this section we describe the proposed method, which is divided into four parts: 1) cross-section image, 2) preprocessing for cross-section image analysis, 3) bifurcation detection, and 4) circle enhancement filter. In the first part, we describe how the cross-section image is calculated at a seed point and its corresponding cross-sections. In the second part, we describe all the preprocessing steps required for further cross-section analysis. In the third part, we describe how a cross-section is classified as a bifurcation. In the fourth, we describe our novel circle enhancement filter, which is used enhancing the blood vessel cross-section and subsequent centerline extraction. Finally, we describe an optional post-processing step that allows the user to modify the output, so that the eventual segmentation gaps are filled properly.

Cross-section Image

At the beginning, the tracking direction of the connected blood vessel of interest is estimated as the vector connecting the seed point and the direction seed point,

$$T = (x_s - x_d)\hat{i} + (y_s - y_d)\hat{j} + (z_s - z_d)\hat{k} \quad (1)$$

$$\hat{t} = \frac{T}{|T|} \quad (2)$$

where T is the tracking direction, (x_s, y_s, z_s) is the seed point, (x_d, y_d, z_d) is the direction seed and \hat{t} is the unit vector along the tracking direction.

The tracking direction is used only at the seed point to initialize the direction of segmentation. At the seed, the tracking direction is set as the vessel direction of flow and its cross vectors are set as the approximate vectors representing the cross-section of the blood vessel. However, an Eigen analysis of the Hessian matrix is calculated for precise information of the vessel cross-section vectors. For the subsequent cross-sections along a trunk, the next possible center pixel or the center candidate is determined by moving along the vessel direction from the previous center position.

Eigen analysis can geometrically interpret the second order derivatives of an image at each point. The second order differential quantity for a volume $I(x, y, z)$ with a Gaussian convolution $g_\sigma(x, y, z)$, is given by the indefinite Hessian matrix^{4,5,21},

$$H(x, y, z; \sigma) = \begin{bmatrix} I * \frac{\partial^2 g_\sigma}{\partial^2 x} & I * \frac{\partial^2 g_\sigma}{\partial x \partial y} & I * \frac{\partial^2 g_\sigma}{\partial x \partial z} \\ I * \frac{\partial^2 g_\sigma}{\partial y \partial x} & I * \frac{\partial^2 g_\sigma}{\partial^2 y} & I * \frac{\partial^2 g_\sigma}{\partial y \partial z} \\ I * \frac{\partial^2 g_\sigma}{\partial z \partial x} & I * \frac{\partial^2 g_\sigma}{\partial z \partial y} & I * \frac{\partial^2 g_\sigma}{\partial^2 z} \end{bmatrix} \quad (3)$$

where,

$$g_\sigma(x, y, z) = \frac{1}{(\sigma\sqrt{2\pi})^3} e^{-(x^2+y^2+z^2)/2\sigma^2} \quad (4)$$

and σ is the scale parameter set according to the radius of the blood vessel. At the initial seed point, the user defined initial radius is set as the σ , and for the subsequent cross-sections analysis, the previous cross-section radius is set as the σ .

Let the eigenvalues of the Hessian matrix H , be λ_1, λ_2 and λ_3 , and their respective normalized eigenvectors be represented by \vec{v}_1, \vec{v}_2 and \vec{v}_3 . On sorting the eigenvalues as $|\lambda_1| \leq |\lambda_2| \leq |\lambda_3|$, the eigenvector \vec{v}_1 represents the vessel direction and the eigenvectors \vec{v}_2 and \vec{v}_3 represent the vessel cross-section vectors. These vessel cross-section vectors are used to create the vessel cross-

section image, as shown in Fig. 1. The vessel cross-section image is found by interpolating at a discrete set of points along the 2D plane represented by the two cross vectors, \vec{v}_2 and \vec{v}_3 .

Preprocessing for Cross-Section Image Analysis

Before moving into the cross-section analysis, some preprocessing steps have to be performed for calculating the vessel cross-section border, radius and local threshold. These preprocessing steps help understanding the structure at the cross-section and thus in segmenting the blood vessel itself.

The border of the vessel cross-section is found by applying a Canny edge detection filter on the cross-section image, as the blood vessel intensity is different from that of its surroundings³. 2D Gaussian smoothing filter is applied at the beginning of the Canny filter to smooth out noise. The variance of the Gaussian is proportional to the square of previous radius or the initial user-set radius. Fig. 2 shows the border of the blood vessel cross-section after applying the Canny edge detection method. Each border pixel obtained represents the discrete border contour of the vessel cross-section.

An approximate diameter of the cross-section is calculated by taking the maximum of the diameters along the perpendicular vectors \vec{v}_2 and \vec{v}_3 , from the seed to the cross-section border, as shown in Fig. 2. Finally, the local threshold at the vessel cross-section is also found by averaging all the blood vessel cross-section intensities along the border of the vessel cross-section.

Bifurcation Detection

After performing the preprocessing steps, each of the vessel cross-section images are checked to determine if it is a bifurcation. The contour of a vessel bifurcation cross-section is very different from the contour of a vessel trunk cross-section. Fig. 3 illustrates difference in the shape of the

vessel cross-sections between trunk and bifurcation. By calculating the shape descriptors: compactness and radius variance, we can identify bifurcating vessel cross-sections¹⁸.

Compactness is a measure of how circular a given contour is. It can be defined as

$$Compactness = \frac{P^2}{A} \quad (5)$$

where P is the perimeter of the vessel cross-section shape and A is the area of vessel cross-section. Radius variance is the variance in distance from the center candidate to the border points or vessel cross-section contour.

Whenever there is a sudden increase above a certain threshold or a sudden change in the shape descriptors (compactness and radius variance), the corresponding cross-sections are analyzed as bifurcation cross-sections. Fig. 3 illustrates how the shape descriptor values change as the cross-section changes from vessel trunk to the vessel bifurcation. The sudden change in the shape descriptors resembles the change in vessel cross-section border, signifying bifurcation.

Circle Enhancement Filter

On determining whether the vessel cross-section is part of a vessel trunk or a vessel bifurcation, the process goes forward in enhancing the structure accordingly and finding the center of the cross-section. We have implemented a novel circle enhancement or “*cirleness*” filter, which enhances circular structures in the image and provides a good Gaussian profile for the output intensity. The filter adopts the scale space approach with the possibility of performing the operation in single or multiscale.

In the proposed method, a single scale approach is used to enhance the cross-section at vessel trunks, while the multiscale space approach is used to enhance the cross-section at vessel bifurcations. This makes the bifurcation detection step a very crucial step.

Our *circleness* filter is based on 2D Eigen analysis on the 2D Hessian matrix computed at each pixel of the vessel cross-section image. Similar to Eq. 3, the 2D Hessian matrix is given by,

$$H_{2D}(x, y; \sigma) = \begin{bmatrix} I_{2D} * \frac{\partial^2 g_{2D\sigma}}{\partial^2 x} & I_{2D} * \frac{\partial^2 g_{2D\sigma}}{\partial x \partial y} \\ I_{2D} * \frac{\partial^2 g_{2D\sigma}}{\partial y \partial x} & I_{2D} * \frac{\partial^2 g_{2D\sigma}}{\partial^2 y} \end{bmatrix} \quad (6)$$

where I_{2D} is the vessel cross-section image, $g_{2D\sigma}$ is the 2D Gaussian filter and σ is the scale parameter set according to the vessel cross-section radius, which is found at the preprocessing step.

Let λ_{2D1} and λ_{2D2} be the eigenvalues from the 2D Hessian matrix. These eigenvalues are used to understand the structural information of at each pixel of the cross-section image. The *circleness* filter is formulated with the knowledge that both the eigenvalues will be high at the center of the cross-section as the cross-section is near circular in nature. After sorting the eigenvalues ($|\lambda_{2D1}| \leq |\lambda_{2D2}|$), we have coined a *circleness* ratio

$$C_R = \frac{|\lambda_{2D1} + \lambda_{2D2}|}{||\lambda_{2D2}| - |\lambda_{2D1}||} \quad (7)$$

Our novel *circleness* equation at a single scale using the *circleness* ratio C_R is

$$C = (1 - e^{-(C_R k)^2}) \left(1 - e^{-\frac{S^2}{2c^2}} \right) \quad (8)$$

where k affects the rate of increase of the Gaussian profile of the *circleness* filter, while S is the Frobenius matrix norm of the Hessian,

$$S = \sqrt{\lambda_{2D1}^2 + \lambda_{2D2}^2} \quad (9)$$

which reduces the effect of noise in the filtered output.

For more efficient processing, we apply our *circleness* filter only inside the vessel cross-section region. The region of interest is determined by applying the local threshold found in the

preprocessing step. Fig. 4(a) shows the single scale *circleness* filter output on a vessel trunk cross-section image. The single peak obtained from the single scale *circleness* filter applied to a vessel trunk cross-section is the center of that cross-section. Moving along the vessel direction \vec{v}_1 from the current center, we find the next possible center or the next center candidate for the next cross-section of the vessel trunk.

At the bifurcation cross-section, we apply the multiscale *circleness* filter. This allows determination of multiple peaks, where each corresponds to a bifurcating vessel. The multiscale *circleness* is formulated as,

$$C_{multi} = \max_{\sigma_{min} \leq \sigma \leq \sigma_{max}} C(\sigma) \quad (10)$$

where σ_{min} is the minimum radius and σ_{max} is the maximum radius. σ_{max} is set as the radius of the cross-section and, σ_{min} is set as one-third the value of σ_{max} for detecting smaller bifurcations of up to one-third the size of the radius.

Fig. 4(b) shows the multiscale *circleness* filter output with multiple centers at the vessel bifurcation cross-section image, where each center corresponds to a different bifurcating vessel. Each center found at the bifurcation cross-section is set as a new seed for the whole process to start again.

At the vessel cross-section, the immediate surrounding 3D neighborhood is also checked and added as part of the vessel, if they fall within the local vessel threshold. This helps in reducing the gaps that might be caused by processing 2D slices along a 3D blood vessel. The vessel cross-section tracking finally stops, when the newly found center candidate falls outside the connected blood vessel region.

While tracking through the blood vessel, the *circleness* filter output at each vessel cross-section is added into its corresponding 3D voxel in the final segmentation output. Thus, when the

whole connected blood vessel tree is tracked, the method simultaneously produces the complete 3D blood vessel segmentation output and the extracted centerline.

Post-processing

The initial 3D blood vessel segmentation result is obtained after the vessel cross-section tracking comes to a stop by reaching all the blood vessel end-points. The user then has an option to perform a post-processing, where the initial blood vessel segmentation output is set as a seed volume or contour for an active contour evolution²⁵. The user has the option to set the region of interest and the processing intensity range. Adjusting lower and upper threshold values sets the intensity range, and the curve within the intensity range can be low-pass filtered for smooth propagation of the contour. Finally, the user also has to set values for external and internal forces governing the flow of the contour, before starting the evolution. On completing the evolution, the final 3D blood vessel segmentation is obtained, which has a smooth surface, well fitted to the original blood vessel.

RESULTS

The proposed method was applied on a set of eight images: four synthetic blood vessel images and four medical images. The synthetic images used for our validation were made by a method proposed by Galarreta-Valverde et al., which is an extension of the traditional Lindenmayer system (L-system) that generates synthetic 3D blood vessels by adding stochastic rules, and they were downloaded from Galarreta-Valverde's web-database of synthetic images⁶. These synthetic images were chosen, as they resemble blood vessels from medical images to a great extent. All

the medical and synthetic images were resampled to $1\text{mm} \times 1\text{mm} \times 1\text{mm}$ voxels to obtain an isotropic image resolution that is good for structural analysis.

Fig. 5 shows the synthetic blood vessel images and various outputs obtained using different methods. The first column shows all the synthetic blood vessel images (Image1-4) used in our study. The second column shows the 3D models made from Frangi *vesselness*⁵. In the third column, the 3D segmented output from the active contour method with a user-initiated seed point is shown²⁵. The fourth column shows the 3D models made from blood vessel segmentation using our proposed method without the optional post-processing step, and the segmentation result with post-processing step is shown on the last column. We did not consider adding noise in the synthetic images as our method expects that a blood vessel with contrast will have higher intensity inside than outside of the vessel. Also, our method works by tracking the blood vessel only from within the blood vessel, without considering the outside noise.

Fig. 6 shows the medical images used in our study and their corresponding outputs. All the medical images (Image5-8) shown in the first column are contrast enhanced magnetic resonance angiogram images. The centerlines extracted using the proposed method are shown in the second column. Lastly in Fig. 6, the 3D model views from the blood vessel segmentation performed using Frangi *vesselness* with thresholding^{5,7}, active contour segmentation²⁵ and the proposed method are shown in the third, fourth and last column, respectively. For medical images, the thresholding for Frangi *vesselness* is done using maximum entropy thresholding⁷. The entropy-based thresholding method is selected as it is shown to give better results when compared to other similar thresholding methods¹. The seed for the active contour segmentation is a sphere with diameter of 5 voxels and center at the same position as that of the corresponding seed for the proposed method.

Processing Time

All blood vessel images, both synthetic and medical, used in our study were segmented on a MacBook Pro with 2GHz Intel Core i7 processor and 8GB 1600 MHz DDR3 RAM. We compared the processing time for segmenting the blood vessels from the 8 images by different methods. Table 1 shows the processing time taken for centerline extraction by Frangi *vesselness* with thinning^{5,7,14}, active contour segmentation with thinning, our own earlier method for centerline extraction¹² and our proposed method. The thinning for both Frangi *vesselness* and active contour segmentation was performed using Lee's method¹⁴, where the 3D neighborhood of each foreground voxel is checked for thinning. Our proposed method is shown to be on average more than 18 times faster than Frangi *vesselness* with thinning, 8 times faster than active contour segmentation and more than 7 times faster than our earlier method¹² for centerline extraction.

Centerline Validation

Centerline validation is performed by finding the error between the ground-truth center and the center, from the proposed method at each vessel cross-section. Making a reliable manual ground-truth center for each and every vessel cross-section is a time consuming task for humans. An alternative is to find the geometric center of the vessel cross-section, which is calculated by performing Hough circle detection, as the blood vessel cross-sections resemble circles. The Hough circle center will correspond to the center of the vessel cross-section even when the cross-section is elliptical in shape.

The center error is calculated by finding the Euclidean distance between the Hough circle center and the center calculated by the proposed method. Fig. 7 shows the mean center error at vessel cross-sections of all synthetic and medical images at various radius, and the standard

deviation between images. The center error decreases with increasing radius, where the center error is the highest at 1 pixel radius with 0.75 pixels error and least at 7 pixels radius with 0.09 pixels error.

Segmentation Validation

Ground-truth data for the images are necessary for validating the segmentation methods. In our study, we only made ground-truth data for synthetic images and the segmentation validation was performed only on these images. A simple thresholding is sufficient to create the ground-truth images for synthetic images, as there is no information outside the vessel regions.

In our study, the validations for segmentation are performed at both the 2D vessel cross-section segmentation and the final, whole 3D blood vessel segmentation. Various measurements taken for validating 2D and 3D segmentation are,

$$Dice\ coefficient = \frac{2TP}{2TP + FN + FP} \quad (11)$$

$$Sensitivity = \frac{TP}{TP + FN} \quad (12)$$

$$Specificity = \frac{TN}{FP + TN} \quad (13)$$

$$Precision = \frac{TP}{TP + FP} \quad (14)$$

where, TP is true positives, FP is false positives, TN is true negatives and FN is false negatives. The Dice coefficient, which is same as the F1 score, is a widely used similarity measurement between two segmentations.

2D ground-truth vessel cross-section images for validation are obtained by interpolating 3D ground-truth at positions corresponding to the positions of 2D cross-section images calculated in our proposed method. Table 2 shows the mean Dice coefficient, sensitivity, specificity and

precision measurements, for all the 2D vessel cross-section segmentations of all four synthetic images; and their average values are $87.9\% \pm 0.9\%$, $89.2\% \pm 3.0\%$, $98.3\% \pm 0.7\%$ and $90.0\% \pm 4.0\%$, respectively.

Fig. 8 shows sensitivity, specificity and precision measurements at Dice coefficients measured for 3D blood vessel segmentation of synthetic images by Frangi *vesselness*, vesselness with post-processing by use of active contour segmentation, our proposed method and our proposed method with post processing. For the proposed method, the measurements are given for vessel segmentation without and with the post-processing step. Our proposed method provides segmentation output with Dice coefficient of $80\% \pm 2.7\%$, without the use of post-processing. While, the validation measurements for the proposed method with post-processing step are, $94\% \pm 2.4\%$ for the Dice coefficient, $88.7\% \pm 4.0\%$ for sensitivity, 99.9% for specificity and 99.9% for precision.

Bifurcating Vessel Detection

Since the segmentation validation is performed only for the synthetic images, a bifurcating vessel detection study is performed for validating the proposed method on medical images. For medical images, it is important to know the percentage of detection of bifurcating vessels to understand how the proposed method performs as the radius of the bifurcating vessel reduces.

Fig. 9 shows the percentage of bifurcating vessels detected as radius of the bifurcating vessels increases from 1mm. The study is performed first by counting the total number of bifurcating vessels, and then by identifying the number of bifurcating vessels that were segmented by active contour segmentation, Frangi *vesselness* method with maximum entropy thresholding, and our proposed method, at different vessel radius. The results show that the percentage of vessels

detected is 100% at and above radius of 2.5 voxels for our proposed. However, the percentage of vessel detection reduces as the radius of vessel falls below 2 voxels for all the methods.

DISCUSSION

We have presented a semi-automatic algorithm for segmentation of blood vessels and extraction of their centerlines. The algorithm segments blood vessels from single user-initialized seed, and works by analyzing vessel cross-sections and tracking them to the ends of the connected blood vessel tree.

The proposed method was tested on eight image datasets, in which four were synthetic images and four were medical images. With the use of these datasets, the proposed method was validated for centerline and segmentation accuracy, as well as for processing time.

For the centerline validation, the center calculated by the proposed method at each vessel cross-section was compared to its geometric center. One pixel is the minimum center error that can occur at each vessel cross-section. Fig. 7 shows that the mean center error found for all the vessel cross-sections is 0.55 pixels, which proves that the mean center error for the proposed method is half of the individual minimum. The figure also shows that the center error is lesser at the odd diameter cross-sections than its adjacent even diameter cross-sections. This is due to the discrete nature of the image pixelization, where the odd diameters give a single specific pixel as its center whereas the even diameters can give multiple center candidates.

We performed segmentation validation for both 2D vessel cross-section segmentation and 3D connected blood vessel segmentation. In the proposed method, the 2D vessel cross-section segmented images are combined to form the final 3D blood vessel segmentation. Thus accurate 2D segmentation of vessel cross-section is important for the final 3D blood vessel segmentation.

Our results in Table 2 confirm a correct 2D segmentation with an average Dice coefficient of $87.9\% \pm 0.9\%$ and precision in segmentation with $90.0\% \pm 4.0\%$.

The segmentation validation for 3D blood vessel segmentation is performed for the proposed method without and with the use of post-processing, and the Frangi *vesselness* method without and with the use of post-processing. Fig. 8 shows that the Dice coefficient is similar for the Frangi *vesselness* method with an average of $83\% \pm 4.0\%$, and our proposed method with an average of $80\% \pm 2.7\%$. However, the segmentations differ as our proposed method has more false positives and less false negatives than the Frangi *vesselness* method. This is proven by the higher precision of $96.8\% \pm 1.9\%$ for the proposed method compared to $78.4\% \pm 6.5\%$ for Frangi *vesselness* method, and lower sensitivity of $68.4\% \pm 4.3\%$ for the proposed method compared to $88.9\% \pm 7.6\%$ for Frangi *vesselness* method. Lower sensitivity for the proposed method is due to the gaps in vessel segmentation, particularly at areas where there is a sudden change in the vessel-tracking angle and also at bifurcations where there is a bigger shift in seed positions. These gaps could later be filled with the use of the post-processing step and our results show that the proposed method with post-processing gives a better segmentation with Dice coefficient of $94\% \pm 2.5\%$. However, similar Dice coefficient of $93.7\% \pm 2.4\%$ can also be obtained by using the post-processing step on Frangi *vesselness* method, which shows that the high similarity measures for the segmentation results are actually obtained by the use of the post-processing step i.e. active contours.

In synthetic images, the measurements show that the segmentation from the user-initiated active contour segmentation alone is similar to the proposed method with the post-processing step. However, on visual evaluation of medical images and from results shown in Fig. 9, segmentation by active contour method detects fewer bifurcations than the proposed method.

Thus the results from synthetic and medical images show that by providing the segmentation result from the proposed method as the starting contour for active contour segmentation will give a fast approximation to original blood vessel image with very minimum iterations.

Fig. 9 also shows that the thresholded Frangi *vesselness* segmentation results detect more vessels than both the other methods. However, the disadvantage of *vesselness* method compared to a local tracking method is that the method is applied to the whole image and it detects even blood vessels that are not connected to blood vessel of interest, as shown in Fig. 6. However, *vesselness* or a whole image analysis method has an advantage of detecting vessels that might be wrongly shown as disconnected in medical images due to contrast variation. It is also to be noted that more vessel detection could be achieved with the Frangi *vesselness* method by manually lowering the threshold, but at the cost of detecting more vessel-like structures that are not of interest.

The proposed algorithm was coded in C++ with the use of ITK libraries and the post-processing step was performed using ITK-Snap. Table 1 clearly shows that our proposed method is faster than all the compared methods for centerline extraction. The post-processing step for the proposed method took on an average only 1 second extra. The final processing time is within reasonable limits for use during intra-operative procedures, where faster update of the blood vessels is required.

A drawback of our method is in not detecting gaps and abnormalities in the blood vessels. The reason behind this is that our method while tracking always analyses the structural information of the blood vessel, which is tubular in nature for blood vessels and circular or ellipsoidal for vessel cross-sections. Another concern is at blood vessel fusion, where the blood vessels overlap due to imaging artifacts. Here, the proposed method might consider the fusion area as a bifurcation.

Fig. 9 shows that the percentage of detection of bifurcating blood vessels for our proposed method falls drastically below vessel radius of 2 mm/voxels. However, for medical applications such as liver resection, blood vessels with a radius below 2 mm are not of interest.

In conclusion, we have presented a fast method for simultaneous blood vessel segmentation and centerline extraction. The novelty of our method is in performing only two-dimensional cross-section analysis for segmentation of connected blood vessels from a single user-initialized seed point. Our method also has the potential to be used for simultaneous blood vessel segmentation and labeling, for example in visualizing liver blood vessels separately as hepatic and portal system. In the future work, we will work on extending our algorithm to segment more complex blood vessel structure like trifurcations, which are particularly useful for blood vessel segmentation in liver. We will also work on detecting small gaps in the connected blood vessels with an angle based search at the end points and on detecting abnormalities such as aneurysms in blood vessels by incorporating blob detection when the tracking reaches an abnormal structure. Our future work will also include detection of overlap and limit the leaking at these areas by including a vessel direction based restriction.

ACKNOWLEDGMENTS

The research leading to these results has received funding from the European Community's Seventh Framework Programme (FP7/2007-2013) under grant agreement number 238802 (IIIOS project) and also, received top-up financing from Norwegian Research Council. The authors thank Mr. Martin Rube and Prof. Andreas Melzer from the Institute of Medical Sciences and Technology, University of Dundee for providing the images necessary for our study. The authors also thank Mr. Rafael Palomar for proofreading the document.

REFERENCES

1. Albregtsen, F. Non-parametric histogram thresholding methods-error versus relative object area. In: Proceedings of the Scandinavian Conference on Image Analysis. 1993, pp. 273–273.
2. Abd-Almageed, W., C. E. Smith, and S. Ramadan. Kernel snakes: non-parametric active contour models. In: IEEE International Conference on Systems, Man and Cybernetics, 2003. 2003, pp. 240–244 vol.1.
3. Canny, J. A Computational Approach to Edge Detection. *IEEE Trans. Pattern Anal. Mach. Intell.* PAMI-8:679–698, 1986.
4. Erdt, M., M. Raspe, and M. Suehling. Automatic Hepatic Vessel Segmentation Using Graphics Hardware. In: Medical Imaging and Augmented Reality. Springer Berlin Heidelberg, 2008, pp. 403–412.
5. Frangi, A. F., W. J. Niessen, K. L. Vincken, and M. A. Viergever. Multiscale vessel enhancement filtering. In: Medical Image Computing and Computer-Assisted Intervention—MICCAI’98. Springer, 1998, pp. 130–137.
6. Galarreta-Valverde, M. A., M. M. Macedo, C. Mekkaoui, and M. P. Jackowski. Three-dimensional synthetic blood vessel generation using stochastic L-systems. In: SPIE Medical Imaging. 2013, p. 86691I–86691I–6.
7. Kapur, J. N., P. K. Sahoo, and A. K. C. Wong. A new method for gray-level picture thresholding using the entropy of the histogram. *Comput. Vis. Graph. Image Process.* 29:273–285, 1985.
8. Kass, M., A. Witkin, and D. Terzopoulos. Snakes: Active contour models. *Int. J. Comput. Vis.* 1:321–331, 1988.

9. Kirbas, C., and F. Quek. A review of vessel extraction techniques and algorithms. *ACM Comput. Surv. CSUR* 36:81–121, 2004.
10. Kirbas, C., and F. K. Quek. Vessel extraction in medical images by 3D wave propagation and traceback. In: *Bioinformatics and Bioengineering, 2003. Proceedings. Third IEEE Symposium on.* 2003, pp. 174–181.
11. Krissian, K., G. Malandain, N. Ayache, R. Vaillant, and Y. Troussel. Model-based detection of tubular structures in 3D images. *Comput. Vis. Image Underst.* 80:130–171, 2000.
12. Kumar, R. P., F. Albrechtsen, M. Reimers, T. Langø, B. Edwin, and O. J. Elle. 3D multiscale vessel enhancement based centerline extraction of blood vessels. In: *SPIE Medical Imaging. International Society for Optics and Photonics*, 2013, p. 86691X–86691X–9.
13. Kumar, R. P., E.-J. Rijkhorst, O. Geier, D. Barratt, and O. J. Elle. Study on liver blood vessel movement during breathing cycle. In: *Colour and Visual Computing Symposium (CVCS)*, 2013. IEEE, 2013, pp. 1–5.
14. Lee, T. C., R. L. Kashyap, and C. N. Chu. Building Skeleton Models via 3-D Medial Surface Axis Thinning Algorithms. *CVGIP Graph. Models Image Process.* 56:462–478, 1994.
15. Lesage, D., E. D. Angelini, I. Bloch, and G. Funka-Lea. A review of 3D vessel lumen segmentation techniques: Models, features and extraction schemes. *Med. Image Anal.* 13:819–845, 2009.
16. Lindeberg, T. Scale-Space. In: *Wiley Encyclopedia of Computer Science and Engineering*. John Wiley & Sons, Inc., 2007.
17. Lorigo, L. M., O. D. Faugeras, W. E. L. Grimson, R. Keriven, R. Kikinis, A. Nabavi, and C.-F. Westin. CURVES: Curve evolution for vessel segmentation. *Med. Image Anal.* 5:195–206, 2001.

18. Macedo, M. M. G., M. A. Galarreta-Valverde, C. Mekkaoui, and M. P. Jackowski. A centerline-based estimator of vessel bifurcations in angiography images. edited by C. L. Novak, and S. Aylward. 2013, p. 86703K.
19. Maksimovic, R., S. Stankovic, and D. Milovanovic. Computed tomography image analyzer: 3D reconstruction and segmentation applying active contour models — “snakes.” *Int. J. Med. Inf.* 58–59:29–37, 2000.
20. Reinertsen, I., M. Descoteaux, K. Siddiqi, and D. L. Collins. Validation of vessel-based registration for correction of brain shift. *Med. Image Anal.* 11:374–388, 2007.
21. Sato, Y., S. Nakajima, N. Shiraga, H. Atsumi, S. Yoshida, T. Koller, G. Gerig, and R. Kikinis. Three-dimensional multi-scale line filter for segmentation and visualization of curvilinear structures in medical images. *Med. Image Anal.* 2:143–168, 1998.
22. Schmitt, H., M. Grass, V. Rasche, O. Schramm, S. Haehnel, and K. Sartor. An X-ray-based method for the determination of the contrast agent propagation in 3-D vessel structures. *IEEE Trans. Med. Imaging* 21:251–262, 2002.
23. Yi, J., and J. B. Ra. A locally adaptive region growing algorithm for vascular segmentation. *Int. J. Imaging Syst. Technol.* 13:208–214, 2003.
24. Yuen, H., J. Princen, J. Illingworth, and J. Kittler. Comparative study of Hough Transform methods for circle finding. *Image Vis. Comput.* 8:71–77, 1990.
25. Yushkevich, P. A., J. Piven, H. C. Hazlett, R. G. Smith, S. Ho, J. C. Gee, and G. Gerig. User-guided 3D active contour segmentation of anatomical structures: Significantly improved efficiency and reliability. *NeuroImage* 31:1116–1128, 2006.

FIGURE CAPTIONS

FIGURE 1. Vessel cross-section image made using the vessel cross vectors \vec{v}_2 and \vec{v}_3 .

FIGURE 2. Right: Vessel cross-section image, and Left: Canny edge of the vessel cross-section and the two diameters, d_1 and d_2 , along the perpendicular vectors \vec{v}_2 and \vec{v}_3 , from the seed.

FIGURE 3. Shape descriptor values at various cross-section images along a blood vessel.

FIGURE 4. (a) *Top row*: Input vessel trunk cross-section image and its 3D intensity plot, *Bottom row*: Single scale *circleness* image of trunk cross-section image and its 3D intensity plot; (b) *Top row*: Input vessel bifurcation cross-section image and its 3D intensity plot, *Bottom row*: Multi-scale *circleness* image of bifurcation cross-section image and its 3D intensity plot.

FIGURE 5. *First column*: Maximum Intensity Projection (MIP) images of input synthetic images (Images1-4); *Second column*: 3D view of blood vessel segmentation obtained using Frangi *vesselness*; *Third column*: 3D view of blood vessel segmentation obtained using semi-automatic active contour segmentation; *Fourth column*: 3D view of blood vessel segmentation obtained using our proposed method without post-processing step; *Last column*: 3D view of blood vessel segmentation obtained using our proposed method with post-processing step.

FIGURE 6. *First column*: Maximum Intensity Projection (MIP) images of input medical images (Images5-8), with red circles indicating the seed points; *Second column* : MIP images of centerlines obtained using our proposed method; *Third column*: 3D volume view of blood vessel segmentation obtained using Frangi *vesselness* and max entropy thresholding; *Fourth column*: 3D volume view of blood vessel segmentation obtained using seed initiated active contour segmentation; *Last column*: 3D volume view of blood vessel segmentation obtained using our proposed method without post-processing step.

FIGURE 7. Mean center error at various radius and its standard deviation between images.

FIGURE 8. Sensitivity, specificity and precision measurements with different Dice coefficients calculated for the whole 3D blood vessel segmentation performed using (a) Frangi *vesselness* method, (b) proposed method, (c) Frangi *vesselness* with post-processing, and (d) proposed method with post-processing.

FIGURE 9. Percentage of bifurcating vessels detected by active contour segmentation, Frangi *vesselness* method with maximum entropy thresholding, and our proposed method at various vessel radius.

TABLE CAPTIONS

TABLE 1. Processing time taken for centerline extraction using, Frangi *vesselness* with 3D thinning ($F.V.+T.$)^{5,14}, seed initiated active contour with 3D thinning ($A.C.+T.$)^{14,25}, our earlier method¹² and our current proposed method.

TABLE 2. Mean of Dice coefficient, sensitivity, specificity and precision, calculated along all the 2D cross-section images of synthetic images.

FIGURES

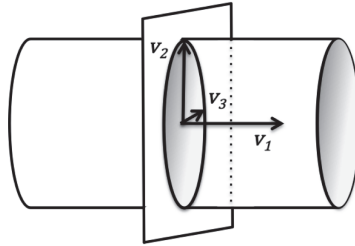


FIGURE 1, RAHUL PRASANNA KUMAR, ABME

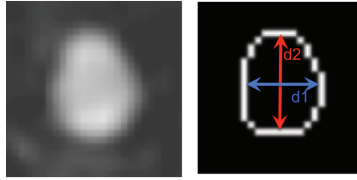


FIGURE 2, RAHUL PRASANNA KUMAR, ABME

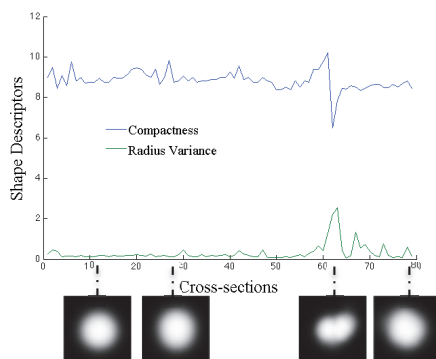


FIGURE 3, RAHUL PRASANNA KUMAR, ABME

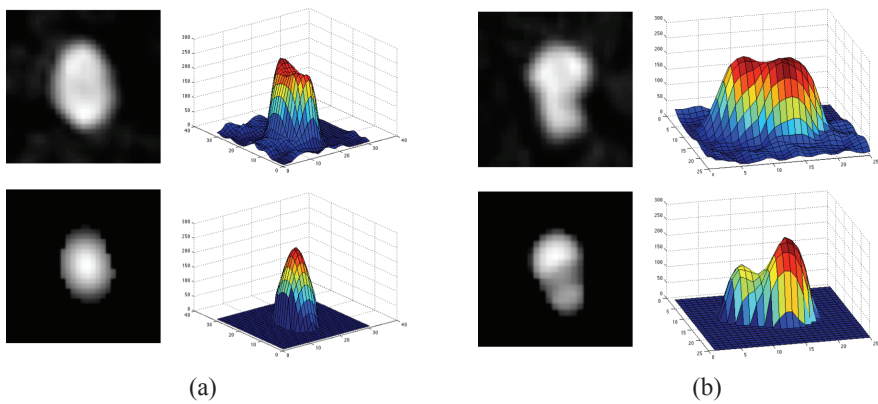


FIGURE 4, RAHUL PRASANNA KUMAR, ABME

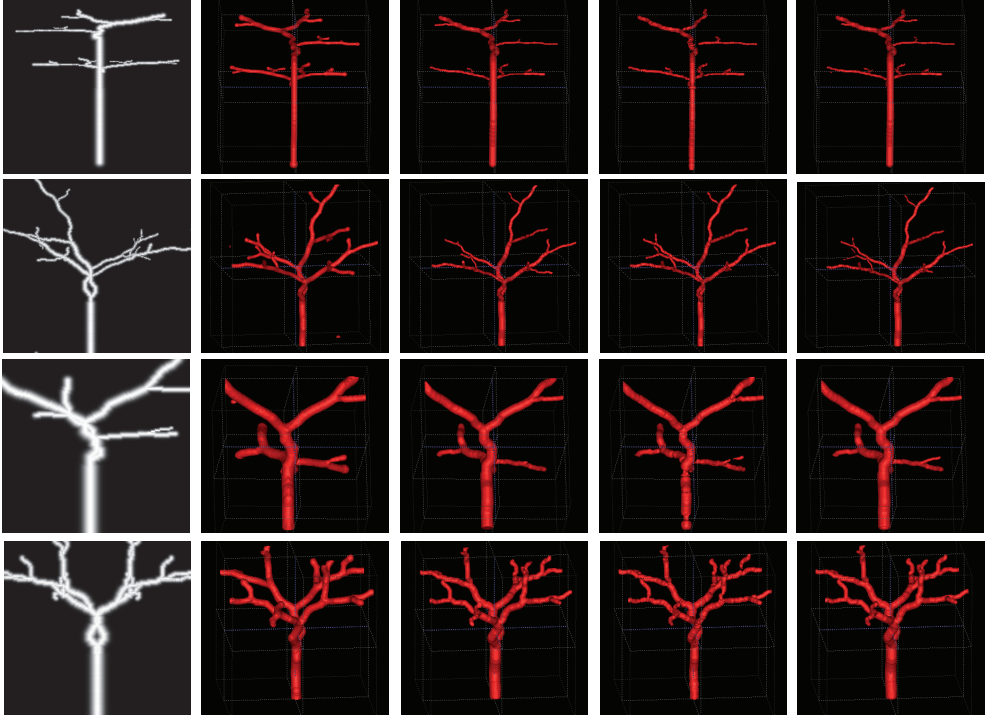


FIGURE 5, RAHUL PRASANNA KUMAR, ABME

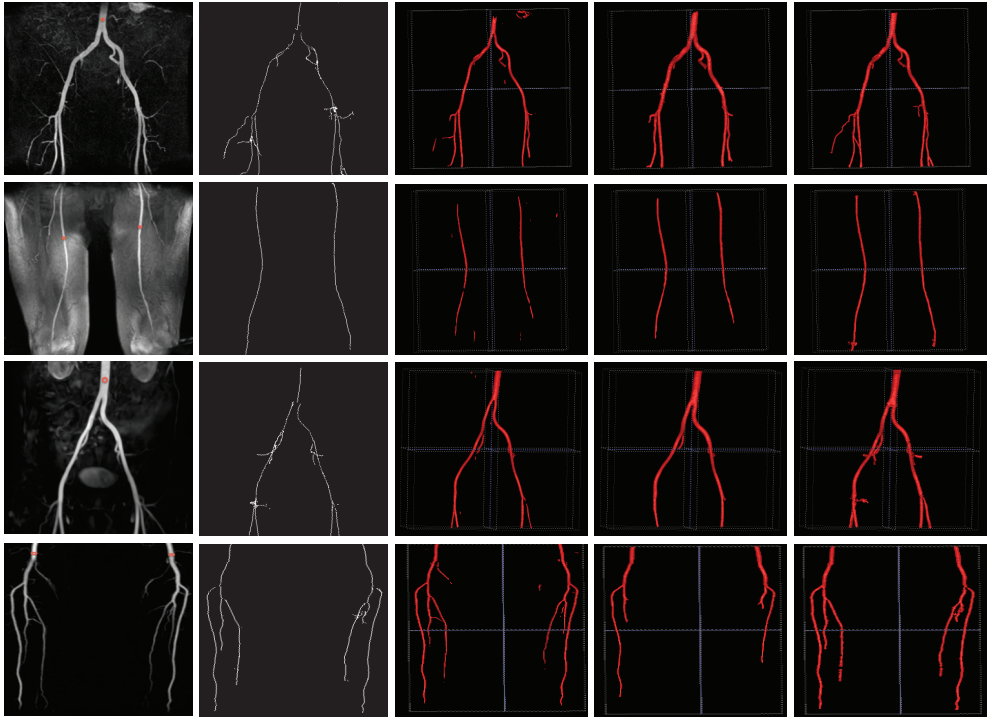


FIGURE 6, RAHUL PRASANNA KUMAR, ABME

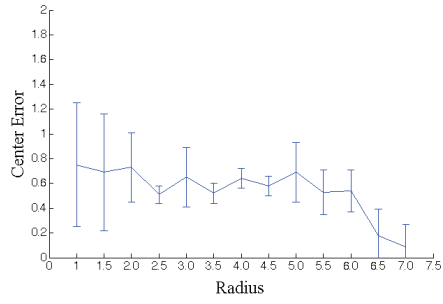
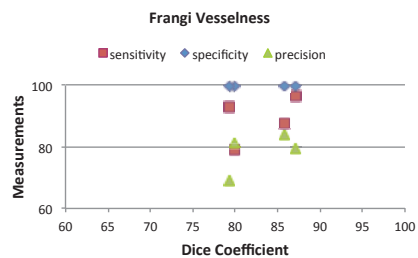
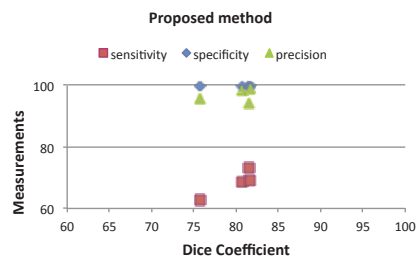


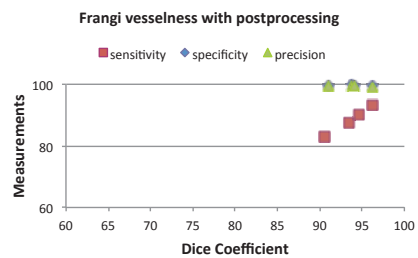
FIGURE 7, RAHUL PRASANNA KUMAR, ABME



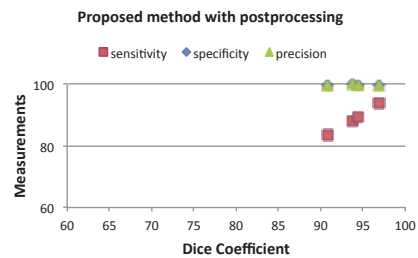
(a)



(b)



(c)



(d)

FIGURE 8, RAHUL PRASANNA KUMAR, ABME

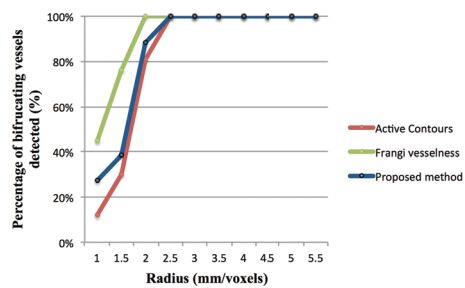


FIGURE 9, RAHUL PRASANNA KUMAR, ABME

TABLES

Data, Size	F.V.+T.	A.C.+T.	Earlier	Curr.
<i>Image1,</i> <i>345×345×345</i>	899s	441s	434s	26s
<i>Image2,</i> <i>300×300×300</i>	604s	225s	270s	19s
<i>Image3,</i> <i>150×150×150</i>	71s	36s	36s	9s
<i>Image4,</i> <i>225×225×225</i>	254s	105s	109s	23s
<i>Image5,</i> <i>384×384×82</i>	321s	132s	96s	28s
<i>Image6,</i> <i>352×384×95</i>	274s	107s	32s	12s
<i>Image7,</i> <i>356×330×124</i>	406s	157s	149s	19s
<i>Image8,</i> <i>272×499×88</i>	198s	151s	88s	26s

TABLE 1, RAHUL PRASANNA KUMAR, ABME

Data	Measurements (%)	2D Cross-section segmentation
<i>Image1</i>	<i>Dice</i>	87.4
	<i>Sensitivity</i>	90.0
	<i>Specificity</i>	98.1
	<i>Precision</i>	88.8
<i>Image2</i>	<i>Dice</i>	87.2
	<i>Sensitivity</i>	92.6
	<i>Specificity</i>	97.4
	<i>Precision</i>	84.9
<i>Image3</i>	<i>Dice</i>	87.9
	<i>Sensitivity</i>	85.2
	<i>Specificity</i>	98.9
	<i>Precision</i>	93.6
<i>Image4</i>	<i>Dice</i>	89.4
	<i>Sensitivity</i>	89.0
	<i>Specificity</i>	98.7
	<i>Precision</i>	92.8

TABLE 2, RAHUL PRASANNA KUMAR, ABME

Hepatic and portal vein segmentation for liver surgery